Gene therapy for Inherited Retinal Diseases

MD(Res) Thesis by Venki Sundaram

Division of Molecular Therapy

Institute of Ophthalmology

University College London

Abstract

Inherited retinal diseases include a number of disorders which typically affect photoreceptor and/or retinal pigment epithelial function, and can often lead to severe visual impairment. Advances in several key disciplines have enabled therapeutic strategies to be developed and applied, in an attempt to provide relief from a range of previously untreatable and debilitating conditions. Specific advances include developments in molecular genetics which have allowed the identification of many of the genes responsible for particular conditions, and progress in viral gene transfer technology which has enabled the transport and replacement of specific genes into targeted regions of the retina.

One of the first human clinical trials of gene therapy for inherited retinal disease was carried out at Moorfields Eye Hospital and UCL Institute of Ophthalmology, just prior to two similar trials conducted in the United States. This trial involved 12 patients with RPE65 deficiency - an early-onset retinal dystrophy, known as Leber Congenital Amaurosis. The results from this trial are described and provide encouraging evidence of the safe administration of viral vectors in the eye, and also demonstrate improvements in retinal function in a number of patients. However, the extent and duration of the response did not match that observed in prior animal studies, suggesting improvements in gene expression level may be required in humans. In addition, careful consideration for future involvement of the foveal region is highlighted, since retinal thinning was observed in a number of patients following subretinal delivery; a finding also observed in the two RPE65 gene replacement trials conducted in the United States.

Achromatopsia is an inherited disorder of congenitally absent cone photoreceptor function resulting in poor visual acuity, absent/markedly reduced colour vision and photophobia. Gene replacement therapy in animal models of achromatopsia has shown evidence of restored cone function, suggesting that this condition may be an appropriate target for gene therapy in humans. Recent studies have suggested that achromatopsia is a progressive condition with deterioration in cone structure with age, implying that the window of opportunity for therapeutic intervention may be narrow. In this study of retinal structure and function (in preparation for a gene therapy trial) in 40 patients with achromatopsia, an age-associated deterioration in cone photoreceptor structure was not identified, suggesting that the age range for potential intervention is wider than recently suggested, and prospective patients should be assessed on an individual basis, irrespective of age.

Contents

Page

Declaration

I, Venki Sundaram, confirm that the work presented in this thesis is my own. Where information has been derived from other sources or where assistance has been sought, this has been acknowledged.

Signed:

Venki Sundaram

Acknowledgements

I would sincerely like to thank my supervisors – Professor James Bainbridge, Professor Robin Ali and Mr Michaelides for their support, encouragement, advice and guidance during my time with them, and in the preparation of the thesis.

I would like to acknowledge the following contributions: Susie Barker for performing the immunological assays for the RPE65 trial; Sarah Kalwarowsky for her help with producing microperimetry and visual mobility figures; Jill Cowing for carrying out achromatopsia genetic screening; and Joe Carroll for his assistance in OCT analysis. In addition, I would like to thank the trial staff at the Institute of Ophthalmology and Moorfields who helped perform numerous investigations that were involved.

I am extremely grateful to the British Retinitis Pigmentosa Society for funding my work.

I also want to thank my wife for supporting me in undertaking this research opportunity, and for her love and encouragement throughout.

I dedicate this work to our son Jay, who was born during this period.

Figures and Tables

Figure Page

Figure — Page

Table Page

Introduction

1.1 Retinal anatomy and function

The retina is the photosensitive tissue within the eye (Fig. 1) that is responsible for receiving and converting light stimulus into neuronal impulses, which then leave the eye via the optic nerve. It is a 10-layer structure (Fig. 2), and can be broadly divided into the inner neurosensory retina, and outer supporting layer of cells - the retinal pigment epithelium (RPE). There are 3 principal cell types that make up the neurosensory retina – photoreceptors, bipolar cells and ganglion cells, and their activity is modulated by other cell types, such as horizontal and amacrine cells. Photoreceptors are the cells that respond to light and there are 2 subtypes in the human retina: rods and cones (Fig. 3). Rods are sensitive to low light levels and are responsible for scotopic (night) and peripheral vision. Cones contribute to fine resolution, visual acuity and colour vision. In the adult retina, there are approximately 90 million rod and 5 million cone cells, and their distribution varies in different regions of the retina. The peripheral retina is mostly rod dominated with approximately 30,000 cells per mm^2, whereas cones are most densely packed (150,000 per mm^2) in the central retina (macula). The macula is approximately 5 mm in diameter and located 3 mm lateral to the optic disc. The central portion of the macula is called the fovea centralis, and in this region, inner retinal cells are laterally displaced, thereby allowing maximum incident light to be absorbed by the underlying photoreceptors.

Photoreceptors consist of an inner and outer segment, a connecting cilium, a cell body that contains the nucleus, and a synaptic region (Fig. 3). The inner segments are densely packed with mitochondria and provide the metabolic requirements required for the conversion of light into electrical impulses. A cilium acts as a conduit for metabolites and lipids between the inner and outer segments. The outer segments of rods and cones are shaped as their names imply, and contain the visual pigments responsible for light absorption. In cones, the outer segments are made up of invaginations known as lamellae that are continuous with the inter-photoreceptor space. In rods, the invaginations undergo further folding to form a column of membranous discs which are surrounded by a plasma membrane. The cell bodies of rod and cone cells are located in the outer nuclear layer (ONL).

Fig. 1 – Structure of the human eye; schematic diagram showing features of the human eye (from www.advancedfunctionalanatomy.com)

Fig. 2 – Schematic of the various retinal layers and cells (from www.advancedfunctionalanatomy.com)

Fig. 3 – Rod and Cone photoreceptor cells; schematic diagram showing rod and cone structure (from www.thebrain.mcgill.ca)

Photoreceptors synapse with bipolar cells, which are located in the inner nuclear layer (INL). Cones make connections with two distinctly different types of bipolar cell: one type is called the ON-bipolar cell because it is depolarised by light, and the other is called the OFF-bipolar because it is hyperpolarized by light. There are further sub-divisions amongst bipolar cells, including the finding that S-cones appear to synapse with different bipolars than the L-/M- cones. Rods are sub served by their own bipolar cells which form connections with as many as 50 rod photoreceptors. Signals are then transmitted to the ganglion cells whose cell bodies are found in the ganglion cell layer (GCL). Ganglion cell axons form the nerve fibre layer which then allows impulses to leave the eye via the optic nerve. Supporting retinal cells include amacrine and horizontal cells, and these have a role in the modulation of signals reaching the ganglion cells. Müller cells are the principal supporting glial cells of the retina and surround blood vessels and cell bodies, providing essential nutrients and survival factors.

The RPE lies posterior to the photoreceptor outer segments and consists of a monolayer of cuboidal cells, whose basal aspect lies on a connective tissue layer known as Bruch's membrane. The apical aspect of the RPE has microvilli that invaginate the photoreceptor outer segments. The RPE provides multiple supportive functions to the neurosensory retina including phagocytosis of photoreceptor outer segments; providing photoreceptor trophic support in the form of various growth factors; synthesis of inter-photoreceptor matrix; providing a selectively permeable barrier between the choroid and neurosensory retina; renewal of retinoids which are an integral part of photoreception; and reduction of light scatter within the eye by light absorption.

The retina has the highest oxygen consumption per weight of any human tissue. It receives a dual blood supply with the inner two-thirds receiving nourishment from branches of the central retinal vessels, and the outer one-third receiving its supply from the choroidal circulation.

1.2 Phototransduction

Phototransduction is the conversion of light into electrical responses, which are then conveyed to the optic nerve, and ultimately to the visual cortex. Rod and cone photoreceptors play an integral part in the phototransduction cascade as they contain visual pigments which are able to absorb light photons. Rhodopsin and cone opsins are the visual pigments in rods and cones, respectively. These are G-protein coupled receptors (GPCR) which consist of seven transmembrane domains, with the peak sensitivity for rhodopsin being approximately 496nm, whilst the cone opsin peaks are about 420nm, 530nm and 560nm for short (blue), middle (green) and long (red) wavelength sensitive pigments respectively. The opsins all contain and utilise the same chromophore, 11-*cis* retinal, which isomerises to all-*trans* retinal when stimulated by photons. This causes a conformational change in the GPCR tertiary structure and an intra-photoreceptor signalling pathway, the phototransduction cascade, is initiated (Fig. 4). The "activated" opsin causes activation of the transducin molecule, which allows the Y subunit of the phosphodiesterase (PDE) enzyme to be released from its αβ complex, which then hydrolyses cyclic guanosine monophosphate (cGMP) to 5'GMP. The lower intracellular concentration of cGMP causes a closure of cGMP-dependent cation channels, preventing the influx of cations and resulting in the closure of voltage-gated Ca^{2+} channels. This leads to photoreceptor hyperpolarisation and prevents the release of the neurotransmitter glutamate (which is normally continually released in non-stimulated conditions). The reduced glutamate level is detected by post-synaptic bipolar cells, which in turn depolarise or hyperpolarise their own synaptic membranes, depending on whether they are ON- or OFF- bipolar cells respectively.

Termination of the phototransduction cascade requires restoration of intracellular cGMP and Ca^{2+} levels including opening of Na^{+}/ Ca^{2+} channels. Reduced intracellular Ca^{2+} following light stimulus causes activation of guanylate cyclase activating proteins (GCAP I and II). GCAP proteins bind to the intracellular domain of retinal guanylate cyclase (RetGC), initiating the resynthesis of cGMP. The increase in cGMP levels allows cGMP to bind to and reopen the cationic channels, restoring the photoreceptor to its initial depolarised dark state. Photorecovery is also facilitated by the deactivation of rhodopsin by rhodopsin kinase (RK) located at the outer segment disc membrane. RK phosphorylates serine residues in the cytoplasmic loops of activated rhodopsin molecules, allowing a second photorecovery protein, Recoverin, to bind. This prevents transducin being bound to phosphorylated rhodopsin and halts downstream signalling in the phototransduction cascade.

A key feature of phototransduction is the amplification of signal that can be achieved at each stage of the cascade. One isomerised rhodopsin molecule is able to activate hundreds of transducin

molecules, and activated transducin then allows PDE to hydrolyse cGMP molecules. This leads to the hyperpolarisation of the photoreceptor by approximately 1mV and therefore only a few light photons are required for photoreceptors to become hyperpolarised.

Fig. 4 – Schematic representation of the phototransduction cascade –from Smith et al. (1). (i) light is absorbed by and activates opsin (ii) activated opsin causes activation of transducin which then activates phosphodiestersae (PDE) by release of its Y subunit (iii) Activated PDE catalyses the hydrolysis of cGMP to 5'GMP and reduced cGMP levels closes cGMP-gated channels and subsequent cell hyperpolarisation (iv) Reduced Ca^{2+} levels stimulates Ca^{2+} release from and activates recoverin, which then activates rhodopsin kinase and in turn phosphorylates (P) opsin. Arrestin then returns opsin to its inactive state. Lower Ca^{2+} also activates retinal guanylate cyclase (RetGC) (v) RetGC increases cGMP concentration which opens cGMP-gated channels, allowing an influx of ions and depolarising the cell.

1.3 The visual cycle

The visual cycle (Fig. 5) is essentially a series of enzymatic reactions that primarily take place in the RPE, and it facilitates the recycling of all-*trans* retinal back to 11-*cis* retinal, therefore allowing photoreceptors to function during many hours of continuous light stimulation. In rod photoreceptors, the visual cycle begins with the release of all-*trans* retinal from activated rhodopsin, and all-*trans* retinal is transported into the cytoplasm by ATP-binding cassette protein in the retina (ABCA4). All-*trans* retinal is then converted to all-*trans* retinol in the photoreceptor cytoplasm by retinol dehydrogenase (RDH). All-*trans* retinol is then bound to inter-photoreceptor retinoid binding protein (IRBP) and transferred to the RPE. Once in the RPE, all-*trans* retinol is bound to the intracellular transporter protein CRBP1, and is esterified to form all-*trans* retinyl ester by lecithin retinol acyltransferase (LRAT). Following this, all-*trans* retinyl ester is converted to 11-*cis* retinol by the isomerohydrolase, RPE65. Finally, 11-*cis* retinol is oxidised to 11-*cis* retinal and transported by IRBP to the photoreceptor, where it can re-associate with rhodopsin.

In addition to the aforementioned visual cycle, cone photoreceptors also utilise an alternative pathway for opsin regeneration which involves Müller cells. In this visual cycle, all-*trans* retinol leaves the cone cell and is absorbed by Müller cells, where it is converted to 11-*cis* retinol by all-*trans* retinol isomerase with the aid of palmitoyl-CoA as an acyl donor. 11-*cis* retinol is transported to the cones by IRBP, where it is oxidised back to 11-*cis* retinal (by a cone specific 11-*cis* RDH) and combines with cone opsin to form the cone pigment (2, 3). Two features of this alternative visual cycle assist in cones remaining responsive at almost any level of illumination, since a degree of their visual pigment is almost always regenerated. Firstly, the alternative pathway is approximately 20-fold faster than the RPE-mediated pathway, and secondly, rods are unable to use the alternative pathway as they are unable to oxidise 11-*cis* retinol to 11-*cis* retinal. This prevents isomerised retinoids from being utilised by rods under daylight conditions when rod vision is less useful (2).

Fig. 5 – Schematic representation of the visual cycle – from Smith et al. (1). Activation of rhodopsin by light occurs through isomerisation of the bound chromophore, 11-*cis*-retinal, to all-*trans* retinal. Whilst the phototransduction cascade continues, all-*trans* retinal is transported to the cytoplasm by ABCA4. After modification by retinol dehydrogenase (RDH) to all-*trans* retinol, it is transported to the RPE and trans-isomerised to 11-*cis*-retinal by the actions of LRAT, RPE65 and 11-cis-RDH. 11-*cis*-retinal is then transported back to the photoreceptor by inter-photoreceptor retinoid binding protein (IRBP), where it binds to rhodopsin, rendering it light sensitive.

1.4 Inherited Retinal Disorders

The inherited retinal disorders are a heterogeneous group of conditions in which an underlying gene defect leads to retinal dysfunction and/or degeneration. They represent a significant cause of blindness (see Table 1). They can be classified according to the mode of inheritance, principal site of retinal dysfunction (rod, cone, RPE, inner retina), extent of dysfunction (isolated macular disorder or generalised retinal dysfunction), typical age of onset, rate of progression, underlying gene defect, and association with systemic syndromes. A hallmark of inherited retinal disorders is the genetic and clinical heterogeneity; with mutations in the same gene known to cause different diseases, and similar phenotypes can be associated with sequence variants in different genes.

Disorders of rod function can be divided into stationary and progressive conditions. Such patients experience difficulties with night vision and peripheral visual field loss. In progressive disease there is subsequent cone system dysfunction resulting in impaired visual acuity, reduced colour vision and central scotomata. The vast majority of progressive retinal disorders (retinal *dystrophies*) have a degree of both rod and cone involvement over time, and are therefore termed rod-cone or cone-rod dystrophies, depending on which photoreceptor type is predominantly affected in the early stages (see Fig. 6).

Retinitis pigmentosa (RP) is the most common inherited retinal disorder, affecting approximately 1 in 3,000 individuals and represents a generalised, progressive group of conditions. Rods are affected initially with cone cells involved later in the disease process. The characteristic fundus appearance is optic pallor, retinal vessel attenuation and retinal pigmentation including “bone spicule” formation, believed to be due to the migration of RPE cells, following photoreceptor death. Over 40 genes have been associated with non-syndromic RP with approximately 50-60% of RP cases showing either autosomal recessive (AR) or sporadic inheritance, 30-40% show autosomal dominant (AD) and 5-20% show X-linked (XL) inheritance (4). An earlier age of onset and more severe disease is typically found in XL and AR cases, compared to ADRP; however there can be considerable variability in fundus appearance, progression and final visual function, both within and between families.

Disorders of cone function can also be divided into stationary and progressive conditions. Stationary disorders such as achromatopsia (ACHM) typically present shortly after birth or in early infancy, with nystagmus, photoaversion, reduced visual acuity and defective colour vision. Whereas, progressive cone dystrophies usually present in childhood or early adult life, with many patients developing rod involvement in later life, therefore leading to considerable overlap between progressive cone

dystrophies (CD) and cone-rod dystrophies (CRD). Approximately 20 genes have been associated with CD or CRD and are inherited in either, AD, AR or XL patterns (5).

Retinal disorders primarily affecting the macula include Stargardt disease and Best disease. Stargardt disease, an AR disorder is the commonest form of childhood macular dystrophy (6). The age of onset is usually in early teens, but there is wide variation, with a later age of onset being associated with a better visual prognosis. Patients present with impaired visual acuity caused by macular atrophy that is usually associated with yellow-white flecks at the level of the RPE. Visual loss may precede any fundus changes and progression is variable, but usually declines to 1.0 logMAR or 1.30 logMAR (7). The causative gene, *ABCA4*, encodes a transporter protein which plays a key role in the visual cycle, with impaired *ABCA4* function leading to an accumulation in the RPE of the toxic metabolite A2E (N-retinylidene-N-retinylethanolamine), a major fluorophore of lipofuscin. Overtime, A2E-associated cytotoxicity is believed to cause RPE dysfunction and cell death, with subsequent photoreceptor cell loss.

Best disease is a highly variable, predominantly AD macular dystrophy that is characterised by a round or oval yellow subretinal macular deposit. The yellow material is due to an accumulation of lipofuscin throughout the RPE (8), which may resorb over time, leaving an area of RPE atrophy that may be complicated by the development of choroidal neovascularisation with acute visual loss and/or subretinal fibrosis. The electro-oculogram (EOG) shows a very reduced or absent light rise, indicating widespread RPE dysfunction whilst the electroretinogram (ERG) is normal. Onset is usually in childhood and visual prognosis is generally good, with most affected individuals retaining reading vision into the fifth decade or beyond. Best disease is associated with missense mutations in the *BEST1* gene (9), encoding the protein bestrophin, which has been localised to the basolateral plasma membrane of the RPE, and is believed to form a calcium-activated chloride channel, responsible for maintaining chloride conductance and regulating fluid transport across the RPE (10).

Although most forms of Best disease show autosomal dominant inheritance, recently there have been reports of autosomal recessive forms of the disease (autosomal recessive bestrophinopathy) in which patients show reduced visual acuity (from 20/60 to 20/200), diffuse irregularity of the RPE with dispersed punctate flecks, and macular oedema or subretinal fluid. In addition to an abnormal EOG, the full-field ERG is also reduced, indicating more widespread photoreceptor impairment (11).

Leber Congenital Amaurosis (LCA) represents a group of early onset, severe retinal dystrophies which can affect both rod and cone function, and is discussed in more detail later (section 1.6).

Disease Category	Total No. of Genes and Loci	No. of Identified Genes
Bardet-Biedl syndrome, autosomal recessive	13	13
Chorioretinal atrophy or degeneration, autosomal dominant	1	1
Cone or cone-rod dystrophy, autosomal dominant	8	5
Cone or cone-rod dystrophy, autosomal recessive	8	7
Cone or cone-rod dystrophy, X-linked	1	0
Congenital stationary night blindness, autosomal dominant	1	1
Congenital stationary night blindness, autosomal recessive	8	8
Congenital stationary night blindness, X-linked	2	2
Leber congenital amaurosis, autosomal dominant	1	1
Leber congenital amaurosis, autosomal recessive	9	8
Macular degeneration, autosomal dominant	13	7
Macular degeneration, autosomal recessive	2	2
Ocular-retinal developmental disease, autosomal dominant	1	1
Optic atrophy, autosomal dominant	5	2
Optic atrophy, autosomal recessive	2	1
Optic atrophy, X-linked	1	0
Retinitis pigmentosa, autosomal dominant	19	18
Retinitis pigmentosa, autosomal recessive	26	23
Retinitis pigmentosa, X-linked	6	2
Syndromic/systemic diseases with retinopathy, autosomal dominant	9	8
Syndromic/systemic diseases with retinopathy, autosomal recessive	34	29
Syndromic/systemic diseases with retinopathy, X-linked	3	2
Usher syndrome, autosomal recessive	11	9
Other retinopathy, autosomal dominant	10	5
Other retinopathy, autosomal recessive	16	13
Other retinopathy, mitochondrial	7	7
Other retinopathy, X-linked	8	7
TOTALS	**225**	**182**

Table 1- Number of genes causing inherited retinal dystrophies according to disease category (RetNet; updated April 19th, 2013)

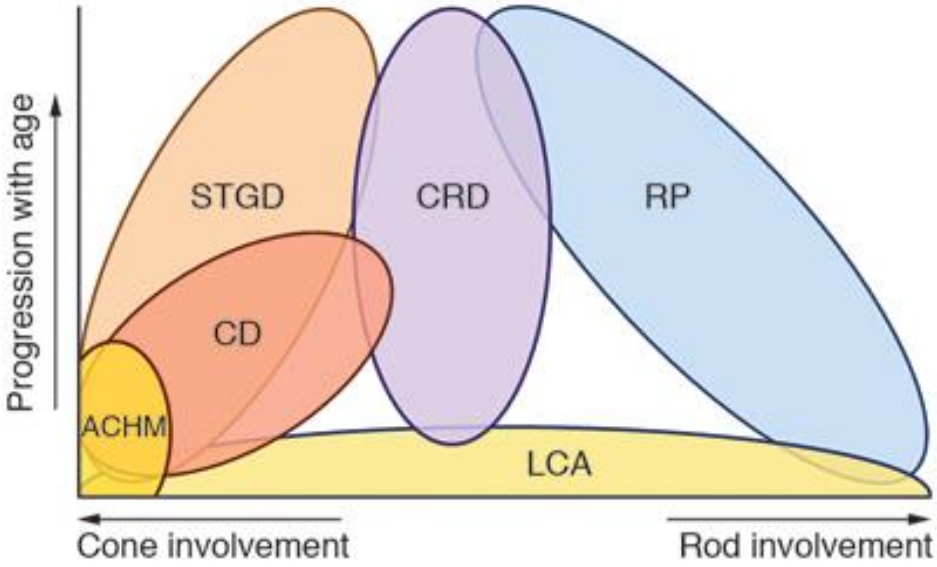

Fig. 6 – Categorisation of various types of retinal dystrophies according to principal photoreceptor type involved – adapted from den Hollander et al.(12). STGD = Stargardt disease, ACHM = achromatopsia, CD = cone dystrophy, CRD = cone rod dystrophy, LCA = Leber Congenital Amaurosis, RP = retinitis pigmentosa.

1.5 Mechanisms of Photoreceptor Cell Death

Although a large number of different gene mutations can result in photoreceptor degeneration, the final pathway leading ultimately to photoreceptor cell death is similar, and involves both caspase-dependent and caspase-independent mechanisms (13). Dysregulation of photoreceptor intracellular calcium concentration is central to the initiation of apoptosis in retinal dystrophies. In the *(rd)* mouse model, a null mutation in the *Pde6b* gene leads to loss of PDE activity, with resulting elevation in intracellular cGMP levels. This causes an influx of calcium ions that resembles an environmental exposure of continuous darkness (so called "equivalent dark" hypothesis) resulting in rapid photoreceptor degeneration and apoptotic cell death (14).

An alternative mechanism of photoreceptor death in retinal dystrophies is the "equivalent light" hypothesis. This proposes that certain mutations lead to an overstimulation of the phototransduction cascade, causing signals to be sent to the inner retina that are equivalent to those sent in response to the detection of incident light (15, 16). Evidence to support the equivalent light hypothesis includes findings from the *Rpe65*$^{-/-}$ mouse, in which rod photoreceptors display behaviour similar to that observed if they were exposed to continuous background light, with reduced circulating current in response to light stimulation and reduced light sensitivity (17). A state of constant hyperpolarisation may lead to cell toxicity and photoreceptor death by either an intrinsic or extrinsic mechanism. An 'equivalent light'signal (and overstimulation of the phototransduction cascade) may result in significant lowering of normally tightly regulated intracellular calcium levels. In addition, an increase in oxidative stress may arise because a decrease in photoreceptor metabolic activity is not matched with a reduced choriocapillaris blood supply (due to the inability of these vessels to constrict); there may thereby be an increase in mitochondrial free radical production in the form of reactive oxygen species.

In contrast, the extrinsic mechanism accounting for photoreceptor cell death involves a disturbance in secondary messenger release from cells in the inner retina. Under normal response circumstances, bipolar cells, Müller cells and ganglion cells secrete neurotrophic factors that promote the survival of photoreceptors following injury. However, following prolonged light stimulation, activated microglia invade the degenerating photoreceptor layer and alter the inner retinal expression of neurotrophic factors, including nerve growth factor (NGF), ciliary neurotrophic factor (CNTF) and glial cell line-derived neurotrophic factor (GDNF) (18).

Progress in the understanding of the mechanisms of photoreceptor cell death in inherited retinal degeneration is ongoing and represents an important avenue of research in the development of therapeutic agents to modify or arrest these common disease pathways.

1.6 Leber Congenital Amaurosis

LCA is a term used to describe a group of recessively inherited, severe, early-onset retinal dystrophies. LCA affects approximately 1/81000 individuals (19), and accounts for approximately 5% of cases of inherited retinal dystrophies and 40% of children who attend schools for the blind (20) (21).

To date, 17 genes have been associated with LCA and a causative gene mutation is found in 60-70% of cases (4), (22). LCA genes are involved in a wide variety of retinal functions including photoreceptor morphogenesis (*CRB1, CRX*), phototransduction (*AIPL1, GUCY2D*), vitamin A recycling (*LRAT, RDH12, RPE65*), guanine synthesis (*IMPDH1*), and photoreceptor ciliary transport processes (*MERTK, CEP290, LCA5, RPGRIP1, TULP1*).

The aforementioned genetic heterogeneity is matched by phenotypic variability; although in certain cases the genetic defect can be associated with a characteristic phenotype e.g. *CRB1* and *RDH12*-associated LCA (Table 2). Affected children typically have poor vision from birth or within the first year, nystagmus, eye rubbing, sluggish pupil reactions and reduced or extinguished scotopic and photopic ERG responses. Fundus appearance is variable, and can be normal at presentation, but there may be typical fundus features associated with particular genotypes (Fig. 7).

GUCY2D is localised to the outer segments of rod and cone photoreceptors. It encodes a membrane guanylate cyclase, RetGC-1, an enzyme involved in the resynthesis of cGMP required for the recovery of the dark state after phototransduction. Patients have very poor vision from birth (from 1.0 logMAR to light perception), photophobia, and high hypermetropia (>+5D) may be present. Fundus appearance is generally normal, although pigmentary changes and macular atrophy may occur. Relatively intact cone photoreceptors at aged 7 years have been detected using optical coherence tomography (OCT) imaging (23).

Aryl hydrocarbon receptor-interacting protein-like 1 *(AIPL1)* is expressed during both rod and cone development and plays a role in photoreceptor viability in the mature retina. More specifically, AIPL1 is necessary for the assembly of the catalytic alpha-subunit of the phototransduction protein phosphodiesterase (24). *AIPL1* mutations cause a severe LCA phenotype with very poor vision (light perception to 1.30 logMAR), variable hypermetropia, and nyctalopia. The fundus may initially be normal but progressive retinal changes occur, including pigmentary changes and macular atrophy. Some patients may also develop keratoconus or cataracts (25).

Lebercillin is expressed in ciliated tissues, and although the exact mechanism is unknown, it is thought to be involved with intra-photoreceptor ciliary transport. *Lebercillin* mutations are a rare cause of LCA and are associated with very poor vision (26). Reported fundus changes have varied from macula coloboma-like lesions, optic nerve head drusen to normal appearing fundi (27, 28).

RP GTPase Regulator interacting protein 1 (*RPGRIP1*) directly binds to the RP GTPase regulator (*RPGR*) and is thought to be involved with ciliary transport, with *RPGRIP1* containing two coiled-coil domains that are homologous to those found in proteins involved in vesicular trafficking (29). Patients have severe loss of vision from early infancy, and although the retina may initially appear normal, most patients develop pigmentary retinopathy with progressive visual loss.

The cone-rod homeobox (*CRX*) gene encodes a homeobox transcription factor that is essential for the differentiation and maintenance of photoreceptor cells. *CRX* acts with the eye-specific transcription factors, neural leucine-zipper (NRL) and homeobox protein RX in the transactivation of photoreceptor specific genes, regulating the high level expression of photoreceptor outer segment proteins such as rhodopsin, IRBP, β-PDE and arrestin (22). CRX mutations have been associated with both AD and AR LCA. Fundus appearances include attenuated retinal vessels, intraretinal pigment deposits and areas of retinal and macular atrophy.

The crumbs homolog 1 (*CRB-1*) gene produces the protein "Crumbs-like protein," which is involved in photoreceptor morphogenesis. Patients may have moderate to high hypermetropia, and although visual acuity is usually poor, it can rarely be as good as 0.3 logMAR. Preservation of the para-arteriolar RPE may be present and some patients develop a Coats'-like exudative retinopathy. OCT characteristically shows significant retinal thickening with disorganisation of normal retinal architecture (30).

CEP290 is a centrosomal protein and is involved in microtubule associated transport across the cilium (31). Mutations lead to a rapid reduction in outer segment length and ONL thickness (32). *CEP290* mutations are one of the most common causes of LCA, and visual acuity is usually very poor, despite relatively well preserved macular structure on OCT. Patients may also have olfactory defects, which may be helpful in identifying families with *CEP290* mutations (33).

The inosine monophosphate dehydrogenase 1 gene (*IMPDH*1) is a rare cause of LCA and is particularly expressed in photoreceptor inner segments and is involved with guanine synthesis, and converts inosine monophosphate into xanthosine monophosphate with the reduction of NAD.

RDH12 is present in photoreceptors and is a component of the visual cycle, catalysing the reduction of all-*trans*-retinal and 11-*cis*-retinal to their corresponding retinols (34). Visual acuity may be moderately reduced in the early stages, but progresses to light perception or worse by the third to fourth decades. Night blindness is the main symptom and progressive retinal pigmentary and macular changes develop (35). OCT imaging has revealed a variation in retinal thickness, with disorganisation of retinal architecture being a consistent finding (36).

LRAT is localised to the membrane of the endoplastic reticulum and catalyses the synthesis of retinal esters. Patients have night blindness and poor vision from early childhood, with severe early loss of peripheral visual field. Fundus examination shows peripheral RPE atrophy with mild retinal pigment migration.

TULP1 is a member of the Tubby-like protein family and is thought to have a role in rhodopsin transport from the inner to outer segment. Affected individuals may retain reading vision in early years, but later can develop pigmentary retinopathy, macular atrophy and optic disc pallor.

Visual acuity in LCA patients usually ranges from 1.0 logMAR to light perception, or even no light perception. However, some cases with a visual acuity of 0.48 logMAR have been reported, usually with *CRB1*, *LRAT* or *RPE65* mutations. Although visual acuity may initially be stable in the majority of LCA patients, there is generally a worsening in vision with increasing age, although there can be considerable variation in rate of decline between genotypes, or even within the same genotype. Patients with *AIPL1* and *RPGRIP1* mutations generally have a progressive course, whereas those with severe, but stable visual loss may have mutations in *CEP290* or *GUCY2D*. Patients with *CRB1*, *LRAT* or *RPE65* mutations may show initial temporary improvements in visual function, but decline thereafter (37).

Post-mortem retinal analysis of LCA patients has been reported in 13 adult specimens, although genotype information is limited. Seven cases showed extensive loss and gliosis of the photoreceptor, inner retina and RPE layer, whereas a normal appearance was found in 6 eyes (22), providing evidence that retinal architecture can remain intact in late stages of the disease in certain genotypes/subjects.

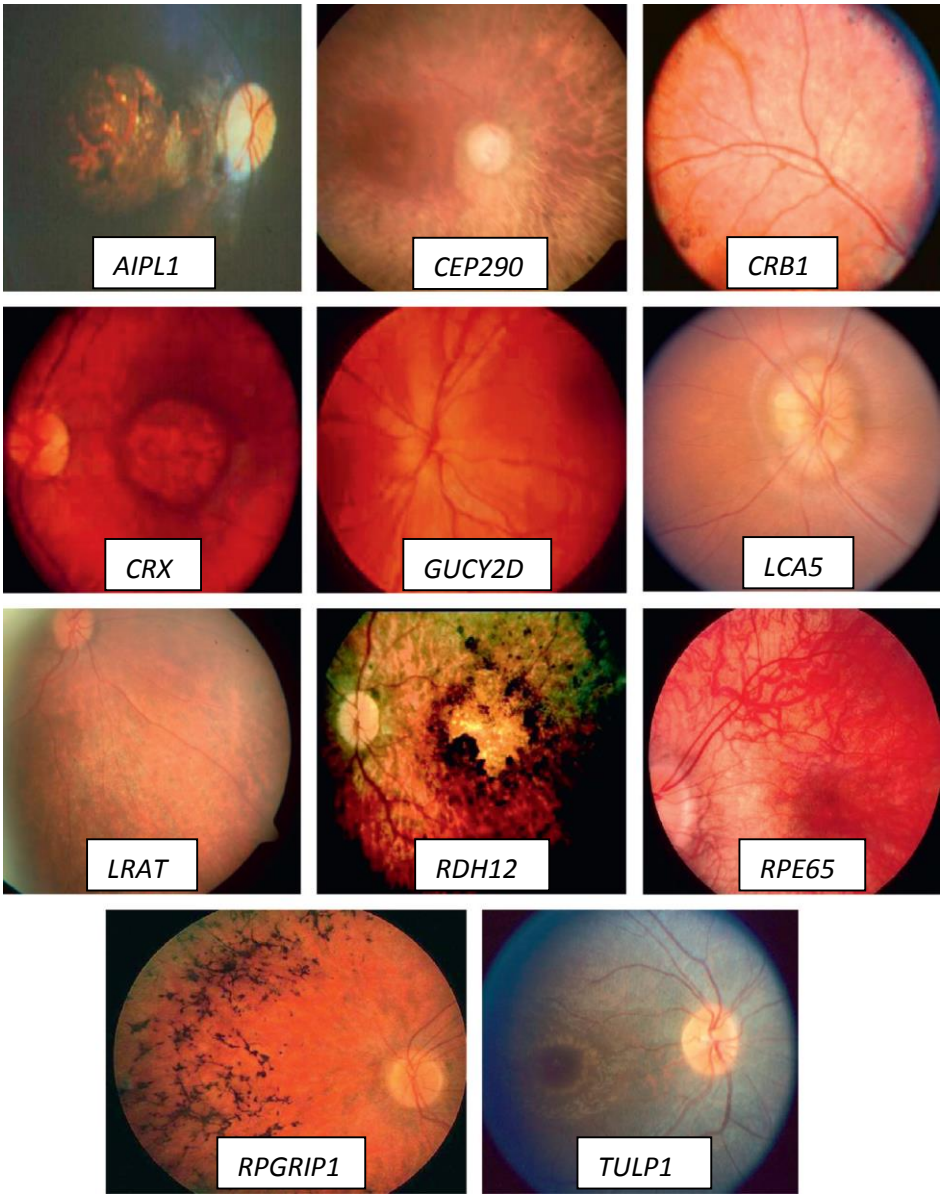

Fig. 7 – Variability in fundus appearance of LCA patients with various genotypes – adapted from den Hollander et al. (22). *AIPL1* – macular coloboma, optic disc pallor and retinal arteriolar narrowing. *CEP290* – optic disc pallor and barely visible retinal vessels. *CRB1* – preservation of para-arteriolar RPE. *CRX* – prominent maculopathy. *GUCY2D* – relatively normal retinal appearance. *LCA5* – optic nerve head drusen. *LRAT* – mild retinal pigmentary changes. *RDH12* – prominent pigmentation and maculopathy. *RPE65* – RPE translucency with normal retinal vessels. *RPGRIP1* – bone spicule pigment changes. *TULP1* – perifoveal yellow annular ring and mild pigmentary changes.

Symbol	Locus	Gene	Mutation frequency (%)	Gene function	Clinical findings
LCA1	17p13.1	GUCY2D	11.7	Hydrolysis cGMP	Very poor vision, normal appearing fundus, photoaversion
LCA2	1p31	RPE65	6	Vitamin A visual cycle	Night blindness, transient visual improvement, relatively good vision in early life
LCA3	14q31.1	SPATA7	Unknown	Unknown	Poor vision, retinal atrophy, attenuated vessels
LCA4	17p13.1	AIPL1	5.3	Rod PDE chaperone	Atrophic maculopathy, poor vision, night blindness
LCA5	6q11-q16	Lebercillin	1.8	Protein transport (cilia)	Severe vision loss, coloboma like macula
LCA6	14q11	RPGRIP1	4.2	Protein transport (cilia)	Severe vision loss, initially normal retinal appearance, progress to pigmentary retinopathy
LCA7	19q13.3	CRX	1	Photoreceptor development	Severe vision loss, infantile nystagmus, some dominant cases
LCA8	1q13.3	CRB1	9.9	Müller cell photoreceptor interaction	Preserved para-arteriolar RPE, Coats like response, thickened and disorganised retina on OCT
LCA9	1p36	Unknown	Unknown	Unknown	Single report of large Pakistani family
LCA10	6q21.3	CEP290	15	Protein transport (cilia)	Most common, extremely poor vision in most patients
LCA11	7q31.3-q32	IMPDH1	8.3	Guanine synthesis	Rare, diffuse RPE mottling, no pigmentary deposits
LCA 12	1q32.3	RD3	0.1	Unknown	Poor vision, atrophic macular lesion, rare
LCA13	14q23.3	RDH12	2.7	Vitamin A visual cycle	Fundus pigmentary fishnet or reticular pattern, Coats like response
LCA14	4q31	LRAT	0.5	Vitamin A visual cycle	Clinically like juvenile retinitis pigmentosa
LCA15	6p21.3	TULP1	0.8	Protein transport (cilia)	Pigmentary retinopathy, reading vision in early stages
Not numbered	3q13.33	IQCB1	2	Protein transport (cilia)	Early ”lobular” pigmentary retinopathy. Renal impairment
LCA16	2q37.1	KCNJ13	Unknown	Potassium regulation	Poor vision, rare

Table 2 – Summary of genotype and phenotype LCA features – adapted from Chung et al. (37)

1.7 RPE65 genotype and phenotype

The visual cycle is the process by which 11-*cis*-retinal is regenerated from all-*trans*-retinal after a photoisomerization event. This cycle takes place in the photoreceptors and RPE, and RPE65 is a key isomerase in this process and is responsible for converting all-*trans*-retinyl ester to 11- *cis*-retinol. Without RPE65, 11-*cis*-retinal levels are substantially reduced and retinyl esters accumulate in the RPE.

The *RPE65* gene was first identified in 1993 (38) and maps to 1p31. It contains 14 coding exons, encoding a 65-kD protein. Over 60 different mutations in *RPE65* (http://www.retina-international.com/sci-news/rpe65mut.htm) have been associated with a variety of overlapping retinal dystrophies ranging from LCA (most severe), to AR early-onset severe retinal dystrophy and juvenile RP, and a recently reported AD choroideremia-like phenotype (39-41).

The role of RPE65 was originally considered to be the binding and mobilization of all-*trans*-retinyl esters for processing by the isomerohydrolase responsible for the critical conversion of all-*trans*- to 11-*cis*- retinoids (42). More recently however, it has been demonstrated that RPE65 is the isomerohydrolase, with RPE65 protein expression correlating linearly with isomerohydrolase activity (43). RPE65 protein is highly preferentially expressed in RPE of all vertebrates, and may be expressed at a low level in cone photoreceptors of some species (44). The role of RPE65 in cones is less well established, but there is evidence that mammalian cones use an alternative retinoid processing cycle (in addition to the traditional one used by rods) that utilises Müller glial cells to regenerate chromophore for the cones (45). This may explain why children have better cone than rod function in the early stages of LCA.

Visual acuity in *RPE65* LCA can vary considerably in the first three decades of life with reports of acuity ranging from 0.16 logMAR to light perception during this period (46). However, after the third decade, most patients have visual acuities of 1.0 logMAR or worse with markedly constricted visual fields (47). Fundus changes can vary from a normal appearance to vessel attenuation, increased peripheral granularity, macular pigmentation, RPE atrophy and peripheral pigment clumping – with changes found to increase with age (46). The ERG is severely affected in *RPE65* LCA, with typically undetectable rod function, but residual cone responses (47). Retinal thickness in *RPE65* LCA within the first three decades shows no simple relationship with age. Retinal thickness can be within normal limits or show a relatively preserved central macular architecture surrounded by peripheral macular thinning, or demonstrate generalised retinal thinning (48). The thickness of the ONL, seen

as a hyporeflective band on OCT scans, is related to the extent of photoreceptor loss. On average, young patients between 6 and 17 years of age show retained ONL thickness centrally and into the superotemporal and temporal retina, however there can be wide inter-individual differences irrespective of age (49). For example, some patients in their early 20s have greater regions of retained photoreceptors compared to patients in the first decade of life. It is encouraging that a significant number of *RPE65* patients have retained photoreceptor architecture, allowing the possibility of effective therapeutic intervention.

Fundus autofluorescence (FAF) imaging measures lipofuscin accumulation in the RPE which is related to shed photoreceptor outer segment discs, allowing for the visualization of disease specific distributions of lipofuscin in the RPE which are often not visible on ophthalmoscopy. Absent or minimal FAF has been reported in *RPE65* LCA (50). The transient pupillary light reflex (TPLR) is a non-invasive method of assessing retinal function, by measuring pupil constriction to a light stimulus. Pupillary responses are typically sluggish in LCA, and in *RPE65* patients, pupillary constriction with high intensity stimuli is similar to normal subjects who receive a dimmer stimulus (51).

Visual pathway and cortical structure and function have also been assessed in *RPE65* LCA patients using MRI and functional MRI (fMRI). No significant differences have been found in optic nerve diameter, cortical grey and white matter, and subcortical structures compared to normal subjects. Visual cortex responses to dimmer light stimuli show decreased responses in *RPE65* patients, however at brighter stimulus intensities, cortical activation is comparable to normal subjects (51). The TPLR and fMRI findings suggest that the visual pathway in these patients remains intact despite years of severe visual impairment, and that improvement in retinal function following therapy may result in significant visual cortical activation at lower light stimuli.

The variation in phenotype amongst *RPE65* mutations may be partly accounted for by the effect of particular gene mutations on RPE65 activity. For example, Y144D and P363T RPE65 mutant proteins are less stable than wild-type RPE65 and have no detectable isomerohydrolase activity, and cause a severe phenotype. Whereas, R91W, P25L and L22P show greater 11-*cis* retinal levels and functional capacity, resulting in a less severe phenotype (52).

1.7.1 Animal models of RPE65 deficiency

Several animal models of *RPE65* associated disease are available. Rpe65$^{-/-}$ mice lack 11-*cis* retinal and 11-*cis*-retinyl esters, and accumulate excessive levels of all-*trans* retinyl esters in the RPE. They have relatively normal retinal anatomy at 7 weeks, but thereafter develop slow rod degeneration with outer segment (OS) length starting to decrease by 15 weeks. Thirty percent of rod photoreceptor nuclei are lost by 1 year, with further loss at 18-24 months (53). In contrast, mouse cones show a fast rate of degeneration with severe degeneration observed by 1 month (54).

Rpe65^{rd12} is a naturally occurring mutant model with a similar phenotype and time course of degeneration to Rpe65$^{-/-}$ mice, and no RPE65, 11-*cis* retinal or rhodopsin expression. An *Rpe65*^{R91W} knock-in mouse model has been generated which has partial expression of mutant RPE65, and 11-*cis* retinal and rhodopsin levels of approximately 10% of normal. Outer nuclear layer thickness of knock-out and knock-in mice is similar with approximately 50% of the thickness of wild-type eyes, suggesting that a low level of rhodopsin production is not sufficient to halt rod degeneration. However, OS organisation is better preserved and cone degeneration is slower in the *Rpe65*^{R91W} knock-in compared to Rpe65$^{-/-}$ mice (55).

The Swedish Briard dog is a naturally occurring RPE65 canine animal model. A 4-nucleotide *RPE65* deletion results in a frameshift and a premature stop codon, truncating the protein (56). Affected dogs have very poor vision and severely abnormal ERG responses after 5 weeks of age. Fundus appearance is normal for the first 3 years, after which there are slowly progressive changes. These include large lipid-like inclusions in the RPE, OS disorganisation, and loss of photoreceptors from the periphery towards the centre. The end stage of the disease involves complete degeneration of the peripheral retina by 5-7 years of age (57).

1.8 Achromatopsia

Achromatopsia (ACHM) is a cone dysfunction syndrome inherited as an AR trait and characterised by an absence of functioning cone photoreceptors. It has an incidence of approximately 1 in 30,000 and presents in infancy with reduced vision (1.0 logMAR to 0.78 logMAR), photophobia, nystagmus and reduced/absent colour vision. ACHM occurs in complete and incomplete forms, with the incomplete form being associated with better visual acuity and some retained colour vision. A hypermetropic refractive error is common and fundus appearance is normal (Fig. 8), although retinal pigment epithelial abnormalities and atrophy may be present in older patients.

Recent high-resolution retinal imaging with OCT has revealed abnormalities in outer retinal structure which have been suggested to progress to photoreceptor loss with advancing age, despite visual symptoms remaining stable in the majority of cases. These macular abnormalities can include, disruption of cone inner segment (IS)/OS junction, loss of cone cells resulting in an optically empty cavity or hyporeflective zone (HRZ), and complete cone and RPE loss (58, 59). In one study involving 40 patients with an age range from 7 to 40 years, cone loss was found to be present in 42% of patients who were under 30 years of age, and in 95% of patients over 30 years (58). In a second study of 13 patients, the presence of a HRZ was significantly associated with increasing age (59). In another study involving 12 patients, an intact IS/OS junction was found in two of the younger patients (mean age 15 years), whereas HRZ presence was found in 7 subjects with a mean age of 32.1 years (60). These findings suggest that although patients are symptomatically stable, ACHM is a slowly progressive condition with loss of cone cells beginning in the second decade and progressing with increasing age thereafter. In a further study of disorders of cone function, the intensity of the IS/OS junction has been found to be reduced in ACHM patients (n=10) who appear to have a normal looking structural integrity of this reflective band (61). Furthermore, studies have indentified that the reflective band visible on OCT which was previously thought to originate from the IS/OS junction, in fact aligns with the ellipsoids of the IS (62, 63), and therefore the IS/OS junction can instead be referred to the IS ellipsoid (ISe) band (61). In addition, multiple ganglion cell layers with lack of formation of a foveal pit, consistent with foveal hypoplasia, has been found in 80% (n=40) of patients with ACHM (58).

To date, mutations in 4 genes have been identified in achromatopsia, *CNGA3*, *CNGB3, GNAT2* and *PDE6C* – all of which encode components of the cone phototransduction cascade (64-66). *CNGA3* and *CNGB3* are located at chromosome positions 2q11 and 8q21 respectively, and encode the α- and β- subunits of the cGMP gated (CNG) cation channel in human cone photoreceptors. In the dark, cGMP levels are high in cone photoreceptors, therefore enabling cGMP to bind to the α- and β-

subunits of CNG channels, resulting in them adopting an open conformation and permitting an influx of cations, with consequent cone depolarisation. However, in light conditions, activated photopigment initiates a cascade culminating in increased cGMP phosphodiesterase activity, thereby lowering the concentration of cGMP in the photoreceptor which results in closure of CNG cation channels and consequent cone hyperpolarisation. Over 50 different disease-causing mutations have been found throughout the *CNGA3* gene, with the majority being missense sequence variants. However, four mutations (Arg277Cys, Arg283Trp, Arg436Trp and Phe547Leu) are found most commonly, and account for approximately 40% of all mutant *CNGA3* alleles (67). The *CNGA3* gene is highly conserved in evolution and it appears that there is little tolerance for substitutions with respect to the function of the channel polypeptide. In contrast, approximately only 15 mutations in the *CNGB3* gene have been identified, with the vast majority being nonsense mutations. The most frequent mutation is a 1 base-pair frameshift deletion 1148delC (Thr383fs), which accounts for 80% of *CNGB3* mutant disease chromosomes (64, 68). Approximately 25-50% of ACHM results from *CNGA3* mutations and 40-50% from *CNGB3* mutations, with less than 1% due to *GNAT2* or *PDE6C* variants (69).

GNAT2 comprises 8 exons and is located on chromosome 1p13, and encodes the α-subunit of cone specific transducin. In cone cells, light activated photopigment interacts with transducin, a three subunit guanine nucleotide binding protein, stimulating the exchange of bound GDP for GTP. The cone α-transducin subunit, which is bound to GTP, is then released from its β- and γ-subunits and activates cGMP phosphodiesterase by removing the inhibitory γ-subunits from the active site of this enzyme. cGMP phosphodiesterase lowers the concentration of cGMP in the photoreceptor which results in closure of cGMP gated cation channels. *GNAT2* mutations result in premature translation termination and in protein truncation, and accounts for under 1% of ACHM (65). Residual colour discrimination and recordable S-cone responses have been reported in patients with *GNAT2* mutations, suggesting that S-cones may express an alternative form of α-transducin (70).

PDE6C encodes the cone α-subunit of cGMP phosphodiesterase, which converts the second messenger cGMP to 5'-GMP during light exposure. This results in closure of the cGMP-gated ion channel in the cone outer segment membrane, leading to hyperpolarization of the cell. Mutations in *PDE6C* have been associated with both complete and incomplete ACHM, and AR progressive cone dystrophy (66).

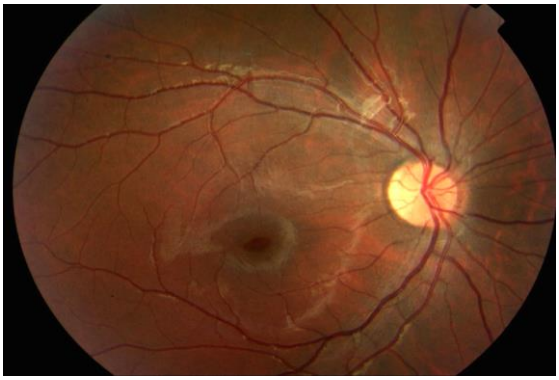

Fig. 8 – Normal fundus appearance in a patient with ACHM

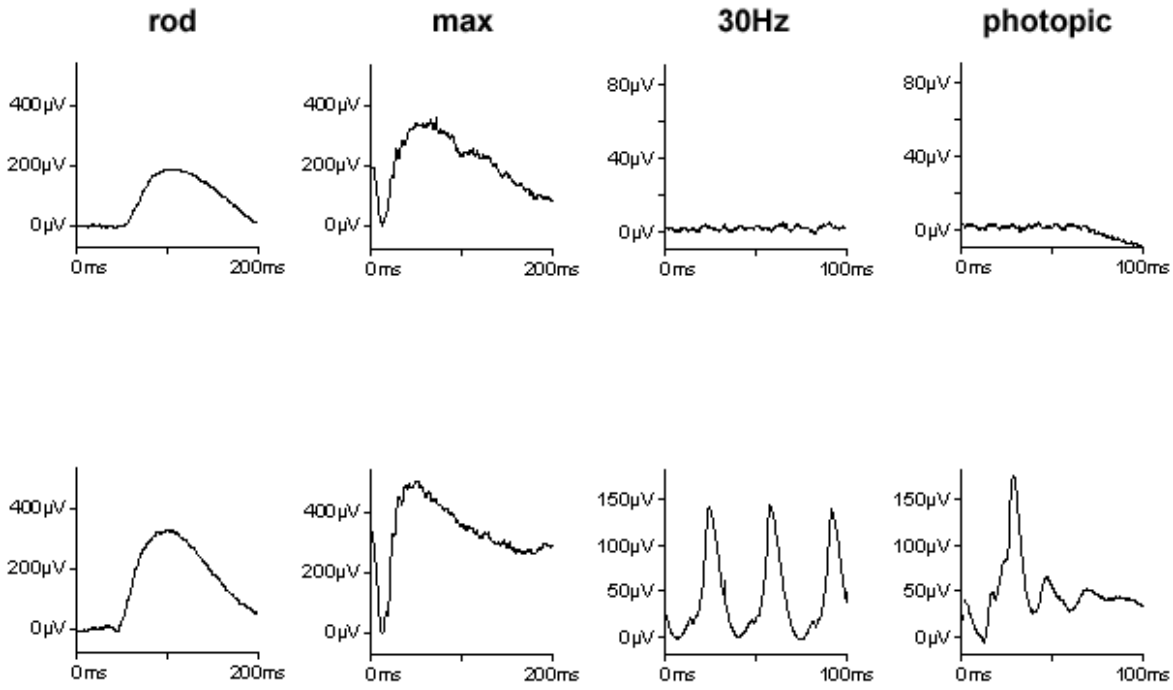

Fig. 9 – Typical ERG recordings in ACHM (top) compared with normal ERG traces (bottom) - The rod-specific and maximal ERGs show no definite abnormality, however the cone-dependent 30Hz flicker and single flash photopic ERGs are undetectable

1.9 Gene therapy techniques

Gene therapy involves therapeutic intervention at a genetic level. The strategy for gene therapy of single-gene defects is broadly dependent on the nature of the mutation and its effect on the function of any protein encoded. For loss-of-function mutations, which typically result in recessively-inherited disorders, the introduction of a normal version of the missing or defective gene can provide cells with normally functioning protein with the aim of restoring normal cell physiology. Mutations resulting in abnormal gain-of-function typically result in dominantly-inherited disorders. For these conditions the therapeutic strategy is likely to require silencing of the mutant allele.

The eye is particularly well suited as a target organ for gene therapy. Ocular tissues are optically accessible and compartmentalised, allowing microsurgical targeting and minimising potential systemic dissemination. Target retinal cells are non-dividing and small in number, facilitating efficient transduction and sustained expression. Relative "immune privilege" conferred by the blood-retinal and blood-aqueous barriers limits the impact of detrimental immune responses. Finally, structural and functional responses to intervention can be measured reliably using a wide range of sensitive imaging, psychophysical and electrophysiological techniques.

Naked plasmid DNA has minimal ability to transfect mammalian cells and therefore successful gene therapy requires a vector to transfer genetic material. The ideal vector should comfortably accommodate the therapeutic gene construct, efficiently transduce the target tissue, and mediate efficient sustained gene expression without a significant inflammatory response. Non-viral vectors include liposomes, in which DNA is complexed with cationic lipids to improve cell membrane penetration, and nanoparticles that usually consist of a peptide or polymer base that condenses or encapsulates the relevant DNA. Non-viral vectors however are typically limited by transient gene expression, and therefore require repeated administration (71).

Viral vectors for ocular application are based on adenoviral, recombinant adeno-associated virus (rAAV) and lentivirus vectors. The AAV genome consists of two open reading frames, *rep*, required for viral genome replication; and *cap*, encoding AAV structural proteins. These are enclosed within two symmetric T shaped palindromic terminal sequences called inverted terminal repeats (ITRs). Recombinant vectors are generated by deleting the *rep* and *cap* sequences from the genome and by inserting the therapeutic gene of interest between the ITRs. rAAV are non-pathogenic, single-stranded DNA viruses that can efficiently transduce photoreceptor and RPE cells, mediating stable expression in the retina for several years (72, 73). Although rAAV vectors are limited by a small packaging capacity (4.7 kb), recent evidence suggests that specific serotypes may be able to

accommodate genomes of up to 8.9 kb, considerably expanding the therapeutic potential of these vectors to carry larger genes such as *ABCA4 (74),* however subsequent studies have been unable to replicate this packaging capacity (75-77). In addition, pseudotyping of AAV vectors can be performed which involves exchanging capsids amongst AAV serotypes (e.g. rAAV2/5 or rAAV2/8 – where the first number denotes the vector genome and the second the capsid) in order to improve transduction efficiency. Another variable is in the use of a promoter, which is a sequence of DNA, upstream from the gene coding region that can have a role in targeting and controlling the location and degree of expression, depending on the type of promoter used.

Lentiviruses are a subgroup of retroviruses, which are single stranded RNA viruses. They have a significantly larger packaging capacity and are capable of mediating highly efficient transduction of RPE. Lentiviral vectors integrate into the host genome, with theoretical potential for insertional mutagenesis (78) but non-integrating versions can also lead to efficient transduction (79). Although adenoviruses are able to transduce a variety of ocular tissues and have a larger packaging capacity than rAAV, their use as a vector is restricted because of the strong immune reaction they elicit, which limits the duration of gene expression (80).

As inherited retinal dystrophies are primarily due to gene defects in photoreceptors and RPE cells, it is essential for vectors to successfully transduce these outer retinal structures. Currently available vectors target the outer retina effectively only following subretinal administration (81). In humans, subretinal delivery is usually performed using a pars-plana transvitreous approach, with injection of vector subretinally through a small retinotomy. Potential complications of this procedure include iatrogenic retinal tears and unplanned retinal detachment, intraocular haemorrhage, infection and cataract.

Features of a condition that potentially make it suitable for ocular gene therapy include the following: (i) visual dysfunction that is severe enough to warrant the risks of any novel therapeutic intervention (ii) a relatively intact photoreceptor and RPE morphology so that treatment can have an effect before irreversible structural and functional loss has occurred (iii) a therapeutic gene that is not too large to be accommodated within an appropriate vector (iv) a sufficient number of patients with the disease, and (v) a relevant pre-clinical animal model to test the therapy. Other considerations include whether the aim of treatment is to improve or preserve visual function. In advanced disease where significant retinal structural damage has already occurred, cell replacement with stem cell therapy or prosthetic retinal implants which are under development, may be better treatment options (82, 83).

1.9.1 Animal models of RPE65 gene therapy

Several animal models have demonstrated the efficacy of *RPE65* gene replacement therapy. Subretinal administration of rAAV containing RPE65 cDNA have been used to treat $Rpe65^{-/-}$ and $Rpe65^{rd12}$ mice at various time points from embryonic day 14, postnatal day 14, 18 and 1-2.5, 6 and 13 months (84-87). Efficient RPE transduction with RPE65 protein expression was achieved at all treatment ages, and was detectable 7 months post-injection. Rhodopsin and retinyl-ester levels were nearly normal and 11-*cis* retinal levels were significantly increased, with retinal morphology resembling a near normal appearance. Functional improvements also occurred with significant improvement in ERG responses to near normal levels at 4-7 months following treatment, and improvements in visual acuity or visual guided behaviour. Importantly, age-dependent effects were found with fewer animals who received treatment at later time points (17-26 months) demonstrating rescue compared to younger animals (48). Also a dose-response effect was established by subretinally injecting 2-5 week old $Rpe65^{rd12}$ mice with a clinical grade AAV2 vector (rAAV2-CB(SB)-hRPE65) and assessing ERG responses at 2 and 4 months. A dose range from 10^8 to 10^{10} vg/µl showed that 10^8 vg/µl was inefficient, 10^9 vg/µl showed increases in photoreceptor and post-receptoral sensitivity, but no increase in amplitude, whereas the 10^{10} vg/µl dose resulted in improvements in both photoreceptor and post-receptoral sensitivity and amplitude (88).

Gene replacement therapy has also been successfully achieved in the Swedish Briard dog model using subretinal rAAV administration in a range of ages from 1 month to 4 years. Significant improvements in ERG function, visual behaviour and 11-*cis* retinal levels were achieved, with functional improvement occurring as early as 2 weeks post-treatment and peak improvement occurring at 3 months post-treatment. In a study of 26 eyes, significant improvement in ERG function was achieved in 23 eyes with restoration of near-normal sensitivity in both rod and cone photoreceptors, and injection at superior sites showed greater ERG responses in the area of retina transduced, than at inferior sites (89). A dose-response effect has also been found in dogs who received AAV2 therapy with a cytomegalovirus/chicken β-actin promoter, with significantly more eyes showing improvement who received a higher dose ($15x10^{10}$ vg/µl) compared to eyes receiving a lower dose ($4.5x10^{10}$ vg/µl) (90). Behavioural studies in treated dogs have shown improvements in TPLR from approximately 0.5 to 4 log units, implying that improvements in retinal function are being transmitted further along the visual pathway. Evaluation of visual cortical activity with fMRI has shown with significant improvements in activity in the lateral gyrus region in treated dogs, to levels of activity approaching that of wildtype controls (51). The immunological effects and biodistribution following subretinal rAAV-*RPE65* defects have shown an increase in neutralising antibodies to AAV2

during the first 12 months (91), but no significant increase in the humoral response to the AAV2 capsid at 3 months post-injection, and studies of brain kidney and bone marrow did not reveal extraocular expression of *RPE65*. Minor surgical complications included mild/moderate conjunctival injection, transient vitritis and lens opacity development (90). Similar to the mouse models, an age-dependent effect has been reported in dogs with functional improvement being greater in dogs treated at 8 versus 30 months of age (92). Long term effects of treatment have been studied and improvements in ERG function have been maintained at 3 years following injection (87).

Safety effects of gene therapy have been assessed in non-human primates. Subretinal injection of rAAV2 carrying green fluorescent protein (EGFP) in monkeys, revealed no long term toxicity and stable and efficient EGFP transgene expression was found localised to retinal cells for over 1 year (93). In another study, subretinal rAAV2-*RPE65* injection (at the highest dose of $4.5x10^{12}$vg/µl) in monkeys showed minimal or no systemic dissemination of vector sequences at 3 months post-injection, and no vector genomes were detected in the gonads of male or female subjects. No toxicity effects were found with ERG testing compared to the untreated eye, however minor anatomical differences were noted at the fovea including subretinal or intraretinal pigmentary disturbances (94).

The safety and efficacy results from these animal studies helped lead the way towards the application of rAAV2-RPE65 gene therapy in humans.

1.9.2 Animal models of gene therapy for ACHM

Several animal models have been used to demonstrate that AAV mediated gene therapy can be effective in restoring cone function in ACHM. *Gnat2*^{cpfl3} homozygous mice (which have a missense mutation in cone α-transducin) at ages day P27 and P29, were given a subretinal injection of AAV5 carrying wild type mouse *Gnat2* cDNA. Cone-specific ERG responses were restored to within the normal amplitude range and visual acuity was restored to normal levels when assessed with optomotor behavioural testing. To investigate the effect of treatment in older mice, 9 month old *Gnat2*^{cpfl3} mice were injected and ERG rescue 1 month later remained feasible, and in one case b-wave amplitude reached wild type levels (95).

A *cnga3*$^{-/-}$ mouse model has received subretinal injection of AAV carrying the *cnga3* cDNA at day P12 to P14, and resulted in restoration of cone ERG responses at 10 weeks post treatment. Functional improvements in visually guided behaviour were also found utilising a water maze under photopic

light conditions, with red and green cues. Immunohistochemistry showed that cnga3 protein was present specifically in cones and localised throughout the cone photoreceptor. In addition, *cnga3* expression lowered cGMP levels, delaying cone death and reducing the inflammatory response of Müller glia cells that typically occurs in retinal degeneration (96). In another model using naturally occurring *cpfl5* mice (who have a missense mutation in exon 5 of the *cnga3* gene) AAV mediated *Cnga3* delivery at day P14 led to restored and stable light adapted ERG responses for at least 2 months after treatment (97).

In a *cngb3*$^{-/-}$ mouse model, subretinal injection of AAV2/8 containing the human *cngb3* transgene gene driven by the human cone arrestin promoter, resulted in both age-dependent and long term restoration of visual function. Mice were treated at day P6, P15, P30, P90 and P180 and underwent ERG testing, visual acuity testing and immunohistochemistry. ERG recordings showed that mice treated at P15 and P30 achieved near normal restoration (>90% of wild-type level) that persisted for at least up to 270 days post injection. However, treatment at P180 only resulted in 60-70% of wild type restoration. Further evidence of an age-dependent effect, was that mice treated at P30 achieved normal visual acuity levels, compared to P180 mice that showed no significant difference in visual acuity between treated and untreated eyes. Improved cone survival was found in treated *Cngb3*$^{-/-}$ eyes, with improvement in cone density, expression of cone proteins and improved structure of cone outer segments (98).

Furthermore, successful restoration of cone function has been achieved in two canine models of *CNGB3* mutations – a missense mutation in exon 6 (CNGB3$^{m/m}$) and a deletion of the entire *CNGB3* gene (CNGB3$^{-/-}$). An age-dependent treatment response was found with only 1 of 3 eyes treated after 54 weeks of age achieved clear restoration of cone ERG function, compared to 11 out of 14 eyes that received treatment before 28 weeks. Improvements in photopic vision were also found when assessed by observing the ability of the dogs to manoeuvre around an obstacle course (99).

These studies have provided encouraging evidence that gene therapy for ACHM can lead to improvements in cone function and structure. In keeping with many other animal models of inherited retinal disease, efficacy has been shown to be age-dependent; this may also prove to be a limiting factor in human clinical trials of achromatopsia gene replacement therapy.

In addition, to optimise the success of a human clinical trial of gene therapy for ACHM, a greater understanding of the relationship between retinal structure and function amongst patients of different ages and genotypes will be important to help identify patients who are most likely to benefit from intervention, and at what time-point.

1.10 Clinical assessments of retinal function and structure

There are various techniques available for investigating visual and retinal function, and retinal structure. These allow an assessment of current disease status and can help identify patients who are potentially most suitable for therapeutic intervention. They also enable monitoring of disease progression and can help detect changes in function following therapy.

Visual acuity

Best-corrected visual acuity (VA) is measured by the smallest letter size a person can read from an acuity chart with any refractive error corrected. Although there are a wide range of VA charts available, the Early Treatment Diabetic Retinopathy Study (ETDRS) chart is commonly used in research studies, and has several advantages. The ETDRS chart is standardised with equal numbers of letters per row; equal spacing of letters on a row; equal spacing between rows; rows are balanced for difficulty; and the chart provides accurate conversion for Snellen and Logarithm of Minimum Angle of Resolution (logMAR) scoring. Testing distance from the chart is determined by the participant's ability to identify the first line of letters correctly. Each eye is measured individually, whilst the fellow eye is occluded.

Contrast sensitivity

Contrast sensitivity (CS) is effectively a measure of the eye's ability to distinguish shades of grey, and can be assessed using the Pelli-Robson (P-R) contrast sensitivity chart. The P-R chart comprises 16 triplets of letters arranged in 8 rows of two triplets, each subtending 2.8 deg at the test distance of 1 metre. The three letters within each triplet have constant contrast, whereas the contrast across triplets, reading from left to right, and continuing on successive lines, decreases by a constant factor. The final triplet at which the patient can read 2 of 3 letters correctly determines the log contrast sensitivity; with the normal range being from 1.68 logCS to 1.84 logCS (100).

Reading acuity

The purpose of taking reading measurements is to evaluate the participant's ability to perform reading as an everyday task and provide a measure of near acuity; with the MN-Read card being commonly used. The MN-Read card comprises 19 sentences of high contrast proportionally spaced text, each containing 60 characters printed as three lines with justified margins. Words used are of a high frequency in 2nd and 3rd grade USA reading material. The sentences have been calibrated to give the correct logMAR sizes, each being 0.1 logMAR units smaller than the previous sentence.

The participant reads the chart at a distance of 40 cm (or 25cm if the visual acuity is worse than 0.76 LogMAR), whilst the researcher records the smallest text size participants can read (reading acuity).

Fundus photography

High-resolution digital colour fundus photography is helpful both in the diagnosis of retinal disease, and documenting and monitoring progression of retinal degeneration. It is also useful when comparing to other forms of retinal imaging.

Optical coherence tomography

Optical coherence tomography (OCT) is a non-invasive imaging modality that enables *in vivo* cross-sectional visualization of the retinal structure, and has become increasingly used in the diagnosis and monitoring of a range of retinal conditions. OCT is based on an optical technique known as Michelson low coherence interferometry, which measures the echo delay and intensity of back reflected or backscattered infrared light (approximately 800 nm) from internal tissue microstructure, to achieve two- or three-dimensional cross-sectional tomographic images of optical reflectivity. The principle of OCT imaging is analogous to B-scan ultrasonography, except that OCT measures light rather than acoustic waves from the tissue boundaries.

Initial OCT images were acquired in a "time domain" fashion which acquire approximately 400 A-scans per second using 6 radial slices oriented 30 degrees apart. However, as the slices are 30 degrees apart it is possible to miss pathology between the slices. More recently, "Spectral domain" OCT (SDOCT) technology has been introduced, which scans approximately 20,000-40,000 A-scans per second. This increased scan rate and number reduces the likelihood of motion artefact, enhances the resolution and decreases the chance of missing lesions. Whereas most time domain OCTs are accurate to 10-15 microns, newer spectral domain devices may approach 3 micron resolution and perform a series of horizontal scans in a predetermined sized area, rather than 6 radial slices.

Electrophysiological testing

Electrophysiological assessment of the retina is useful in establishing the level of any abnormality (e.g. photoreceptor/RPE or inner retina) and also the extent, in terms of macular and or/peripheral dysfunction. The standard electrophysiological tests that are performed include the electro-oculogram (EOG), a full-field electroretinogram (ERG) and pattern ERG (PERG). There are established protocols for each of these assessments, defined by the International Society for Clinical Electrophysiology of Vision (101).

The ERG is the massed electrical response of the retina and allows assessment of generalised retinal function under photopic and scotopic conditions, using a Ganzfeld bowl flash stimulus. Standard ERG traces include (1) Dark-adapted 0.01 ERG (formerly "rod-specific response"); (2) Dark-adapted 3.0 ERG (formerly "maximal mixed rod-cone response"); (3) Dark-adapted 3.0 oscillatory potentials (formerly "oscillatory potentials"); (4) Light-adapted 3.0 ERG (formerly "single-flash cone response") and (5) Light-adapted 3.0 flicker (formerly "30 Hz flicker").

The rod-specific ERG b-wave is generated at the level of the inner nuclear layer. The initial 10-12 ms of the a-wave of the maximal response relates to photoreceptor hyperpolarisation, and is the best measure of photoreceptor function. The slope of the linear portion of the a-wave can be related to the kinetics of phototransduction. The b-wave of the maximal ERG response arises in the mid-retina, principally from the rod ON-bipolar cells and thus defines function that is post-phototransduction or post-receptoral. Photopic (single flash) and 30 Hz flicker allow assessment of cone function. There are mid-retinal contributions to both the a- and b-waves of the photopic (single flash) ERG response, but also a photoreceptor contribution to the photopic a-wave.

The PERG is usually elicited using high contrast checkerboard reversal and mainly reflects central retinal function. There are two major components: the positive P50 - which is driven by macular photoreceptors and can be used as an objective index of macular function, and the N95 – which is considered to arise in the spiking activity of the retinal ganglion cells.

The EOG utilises the standing potential difference between the back of the eye and the electro-positive cornea. It is a mass response of the whole retina and is generated across the RPE. The EOG is assessed by measuring constant eye movements under progressive dark then light adaptation. There is a "dark trough" after 12-15 minutes dark adaptation and a "light peak" after 7-10 minutes light adaptation. The ratio between the light peak and dark trough is expressed as a percentage, and

is the commonly used parameter. The EOG allows assessment of the photoreceptor/RPE interface and its generation depends on the integrity of the photoreceptors. A reduced EOG is generally accompanied by a reduction in the full-field ERG, unless dysfunction is confined to the RPE.

Retinal dystrophies may be classified on the basis of the associated electrophysiological abnormalities. Patients with generalised retinal dysfunction and severe ERG abnormalities can have normal PERGs if the macula is spared. In contrast, patients with disease confined to the macula have normal ERGs, but the PERG P50 may be profoundly abnormal.

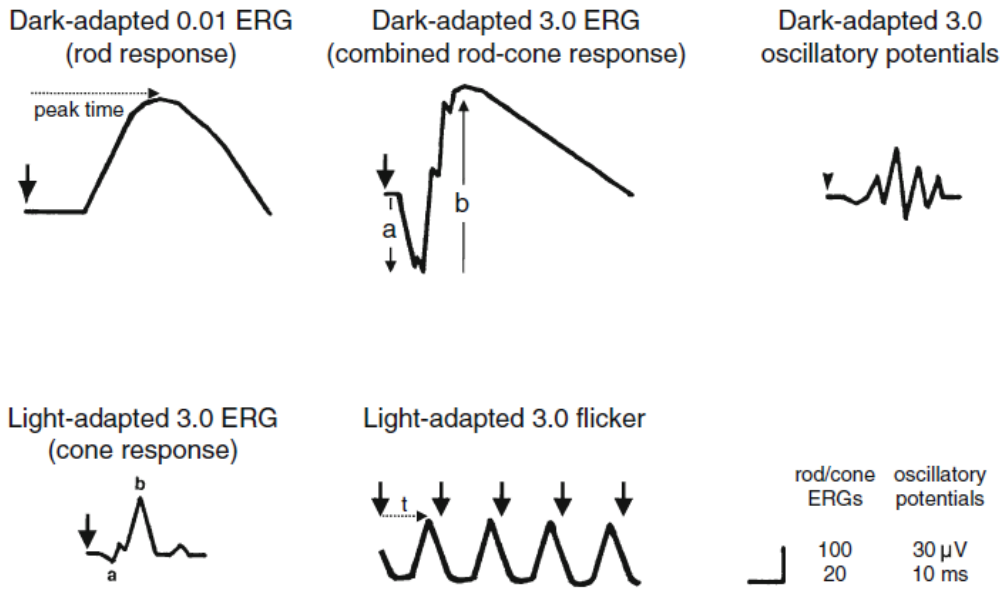

Fig. 10 – Diagram of the five basic ERG responses - adapted from Marmor et al.(101). Large arrows indicate stimulus flash. Dotted arrows illustrate how to measure time to peak (t, implicit time), a-wave amplitude and b-wave amplitude.

Microperimetry

Microperimetry is an assessment method that can reliably measure retinal sensitivity to light at specific locations across the retina. Subjects fixate on a central target while specific retinal locations are presented repeatedly with a Goldmann size I to V stimulus for a duration of typically 200ms. A commonly used microperimeter is the Nidek MP1 microperimeter (NAVIS software version 1.7.1, Nidek Technologies, Padova, Italy). The MP-1 initially takes an infrared photograph and the software package allows the operator to select a biological landmark of high reflectivity under infrared e.g. a bifurcation of a retinal vessel. This image is then digitally registered and matched with the corresponding area on the live video of the patient's retina. An active eye tracking system corrects for fixation errors to ensure accurate stimulus projection in relation to retinal landmarks.

Dark-adapted perimetry

Dark-adapted perimetry using a modified Humphrey Visual Field Analyzer is an established method for quantifying rod and cone sensitivity (102). The standard technique uses a 30-2 Full Threshold Test with optical filters to isolate a narrow range of wavelengths and differentiate between rod and cone function; with near 500 nanometres used to probe rod sensitivity. Measurements are made in the fully dark adapted eye with a Size III or V target. The test is fully automated, thereby markedly reducing potential experimenter bias and the subject's eye position can be continually monitored by an infrared camera.

Visual mobility testing

Visual mobility testing provides a quantitative assessment of a subjects' ability to navigate in a "real life" scenario. One such testing environment is the Pedestrian Accessibility & Movement Environment Laboratory (PAMELA) facility of UCL. PAMELA is a unique mobility research facility (in a specially designed, converted warehouse building) that incorporates a sophisticated set of monitoring and data collection systems including starlight video cameras, laser scanners which can locate objects in the laboratory within 1-2cm, eye tracking systems and heart rate monitors. Visual mobility is tested by subjects negotiating a maze with moveable barriers and the entire platform area is illuminated from overhead to calibrated light levels ranging from 240 lux (moderate office lighting) to 4 lux (UK night time pedestrian lighting standard). Subjects are positioned at one end of the maze and instructed to walk through at a normal comfortable pace without touching the barriers. An experimenter follows along just behind to ensure the subject's safety. Total travel time is recorded with a stopwatch along with mobility errors (touching a barrier, loss of orientation).

Methods

2.1 RPE65 Trial

Aim of trial

The main objective of the trial is to determine the safety and efficacy of subretinal administration of a recombinant adeno-associated viral vector (rAAV 2/2.hRPE65p.hRPE65) at two different dosage levels in 12 subjects with autosomal recessive severe early-onset retinal degeneration (LCA) due to mutations in *RPE65.*

This study was approved by the UK Gene Therapy Advisory Committee, the Medicines and Health Products Regulatory Authority, the Moorfields Research Governance Committee, and the local research ethics committee. All patients gave written informed consent and the study was conducted in compliance with Good Clinical Practice guidelines according to the European Clinical Trials Directive (Directive 2001 EU/20/EC) and the Declaration of Helsinki.

The decision to include 12 patients in this trial was determined after consideration of the likelihood of recruiting patients, and the practical and economical aspects in terms of resources available to provide adequate assessments and support for this trial.

This study involves 2 centres: (1) UCL Institute of Ophthalmology, London, (2) Moorfields Eye Hospital, London.

2.1.1 Inclusion criteria:

The inclusion criteria for this trial were subjects with:

1. Severe early-onset retinal dystrophy (LCA)
2. Homozygous or compound heterozygous for a missense or null mutation(s) in RPE65
3. Aged 5 to 30 years
4. Able to give informed consent or assent, with or without the guidance of their parent/guardian where appropriate

2.1.2 Exclusion criteria:

The exclusion criteria for this trial were:

1. Subjects having contraindications for transient immune-suppression (hypertension, diabetes mellitus, tuberculosis, renal impairment, immunocompromise, osteoporosis, gastric ulceration, severe affective disorder
2. Pregnant or lactating women

2.1.3 Consent

All patients underwent full informed consent with the following issues discussed in particular:

1. The potential for no benefit following treatment
2. The potential for loss of vision due to the following:
    a. Complications of surgery, including retinal detachment and infection
    b. Inflammation due to immune responses to vector or RPE65 protein
3. The theoretical potential for malignancy, spread of vector to other organs and germline transmission
4. The nature and duration of follow-up, including the need for long-term follow up of subjects
5. The decision regarding which of their two eyes was to receive the intervention was determined by the relative degrees of visual impairment and retinal degeneration. The potential benefits and risks of intervention in each eye were discussed with each patient who was fully involved in this decision as part of the consent process.

2.1.4 Preoperative procedure

Subjects were screened to ensure there were no contra-indications for transient immune suppression. A detailed assessment of visual function and imaging was performed on both eyes preoperatively as outlined in schedule of investigations (see 2.1.8). The eye with worse visual impairment was selected to undergo treatment.

Blood was sampled in order to assess baseline levels of circulating antibodies against AAV2 and RPE65 so that following intervention, immunological responses to vector capsid and transgene product might be determined.

For prophylaxis against potential intraocular immune responses to the vector, subjects were prescribed a course of oral prednisolone commencing at a dose of 0.5 mg/kg one week prior to surgery; 1mg/kg for the first week following vector administration, 0.5mg/kg for the second week, 0.25mg/kg for the third week and 0.125/kg for the fourth week.

2.1.5 Recombinant adeno-associated virus details

The virus used to transfer the *RPE65* gene was the tgAAG76 vector - a recombinant adeno-associated virus vector of serotype 2. The vector contains the human *RPE65* coding sequence driven by a 1400-bp fragment of the human *RPE65* promoter and terminated by the bovine growth hormone polyadenylation site. The vector was produced by Targeted Genetics Corporation

according to Good Manufacturing Practice guidelines with the use of a B50 packaging cell line, an adenovirus–adeno associated virus hybrid shuttle vector containing the tgAAG76 vector genome, and an adenovirus 5 helper virus. The vector was filled in a buffered saline solution at a titre of 1×10^{11} vector particles per ml for subjects 1 to 4, and at a titre of 1×10^{12} vector particles per ml for subjects 5 to 12, and frozen in 1ml aliquots at −70°C.

2.1.6 Technique for surgical delivery of vector

The recombinant vector was delivered in the form of a suspension of viral vector particles injected intraocularly (subretinally) under direct observation using an operating microscope. The procedure involved a standard 3-port pars plana vitrectomy with a moderate anterior core vitrectomy performed before inducing (when possible) a posterior vitreous detachment, by aspiration over the optic nerve head.

Intraocular administration of the viral vector suspension (rAAV2/2-hRPE65p-hRPE65) was performed using a de-Juan 41-gauge cannula attached to a 1 ml syringe. The plunger of this syringe is driven by a mechanised device by depression of a foot pedal. The 41-gauge cannula was advanced through the retina at a site pre-determined in each subject according to the area of retina to be targeted. Under direct visualisation the vector suspension was injected mechanically under the neurosensory retina causing a localised retinal detachment with a self-sealing non-expanding retinotomy. The injection of vector suspension was preceded by injection of a small volume of Ringer's solution (0.1 to 0.5 ml) to establish a "bleb", facilitating targeted delivery of vector suspension to the subretinal space and minimising possible exposure of the choroid and vitreous cavity to vector. A sample of uninjected vector suspension was retained for subsequent analysis of bioactivity.

Closure of all sclerotomies was completed with 7/0 vicryl sutures. Standard doses of cefuroxime antibiotic and betamethasone were administered subconjunctivally as prophylaxis against postoperative infection and inflammation respectively.

2.1.7 Early post operative management

The operated eye was examined 2 hours after surgery and any intraocular pressure of greater than 30 mmHg was managed using appropriate ocular antihypertensive therapy.

A standard post-vitrectomy treatment regimen of topical antibiotic (chloramphenicol 0.5% qds for 7 days), steroid (dexamethasone 0.1% qds for 4 weeks) was commenced to minimise inflammation and protect against infection postoperatively. Subjects were maintained on oral prednisolone for 4

weeks following administration of vector suspension as described above. The possible development of steroid-induced adverse effects was monitored regularly - in particular, blood pressure, blood glucose, renal function and liver function tests.

Safety assessments were performed at 1 day, 2 days, 4 days, 7 days, 2 weeks, 3 weeks, 4 weeks and 6 weeks following treatment. These included visual acuity, ocular examination, OCT, fundus photography, systemic review, temperature and blood pressure recording, and serology including immune status.

2.1.8 Assessments of visual function and immune status

Detailed phenotypic assessments were performed at intervals of 2 months for 12 months, then annually until 3 years following administration of the vector. These assessments were scheduled over a period of up to 4 days for each time point. Assessments are listed below. Visual mobility was assessed at baseline and at 6 months following treatment.

List of assessments subjects underwent:

1. Best corrected visual acuity (BCVA)
2. Contrast sensitivity (CS)
3. Reading acuity
4. Microperimetry
5. Dark-adapted perimetry
6. Visual mobility
7. Clinical examination
8. Serology/immune assays
9. Fundus photography
10. Optical coherence tomography (OCT)
11. Electrophysiology
12. Visual mobility

2.1.9 Endpoints

The endpoint for toxicity for each subject is a Grade III adverse event, defined as loss of visual acuity by 15 or more ETDRS letters, or severe unresponsive intraocular inflammation.
The endpoint for efficacy for each subject is defined as any improvement in visual (rod- or cone-derived) function as determined by an array of psychophysical and electrophysiological techniques, that is greater that the test-retest variation for each test.

2.1.10 Methodology of assessments

Visual acuity, contrast sensitivity and reading acuity assessments

Subjects underwent best corrected visual acuity assessment using the ETDRS chart at a distance of 4m or less, according to their visual ability, and logMAR acuity was recorded, with a change in visual acuity of more than 0.3 logMAR considered significant (103). The Pelli-Robson chart was used to measure contrast sensitivity at a distance of 1m with logCS sensitivity recorded. A change in contrast sensitivity of more than 0.2 logCS was considered clinically significant (104). The MN Read acuity chart was used to measure reading acuity in all subjects at 25cm (or 40cm if the visual acuity was better than 0.78 LogMAR), and a change of more than 0.3 logMAR was considered as significant (105).

Immunological assays (undertaken by Dr Susie Barker)

1. Circulating neutralising antibodies against AAV2: Serum was assayed for the ability to block the transduction of 293T cells with AAV2-GFP. Serum was serially diluted in 96 well plates using DMEM. AAV2-GFP was added to each well and plates were incubated at 37°C for 1 h before addition to 293T cells in triplicate. Baseline serum for each subject was assayed alongside each post-gene therapy sample. Green cells were counted in the test wells after 48 h and compared to the number of green cells in the baseline serum sample, and to the no serum positive control sample. The neutralising antibody (NAb) titre was expressed as the serum dilution that resulted in 50% inhibition of transduction of 293T cells by AAV2.GFP.

2. Serum ELISA to detect circulating levels of IgA, IgG and IgM against rRPE65: Microtitre plates were coated overnight with 0.5µg/ml rRPE65 in PBS then blocked with 10% goat in PBS. Serum dilutions in PBS/1%BSA were added to wells (replicates of 4) and incubated for 2 h. Plates were incubated with anti-human IgA, IgG, IgM-HRP, then developed with 3,3',5,5'-tetramethylbenzydine (TMB) substrate. Serum test samples were always compared to the baseline serum that was obtained pre-gene therapy and run alongside in every assay.

3. Serum ELISA to detect circulating levels of IgA, IgG and IgM against AAV2: Microtitre plates were coated overnight with 10^8 vp/well AAV2 in carbonate buffer then blocked with 1% BSA, 5% sucrose in PBS-T. Serum dilutions in PBS/1% dried milk were added to wells (replicates of 4) and incubated for 2 h. Plates were incubated with anti-human IgA, IgG, IgM-HRP, then developed with TMB substrate. Serum test samples were always compared to the baseline serum that was obtained pre-gene therapy and run alongside in every assay.

4. ELISpot assay to detect secretion of the Th1 cytokine IFNγ in response to co-culture with AAV2: PVDF plates were coated with anti-IFNγ antibody (Mabtech, Sweden) and blocked with FCS. PBMC were resuspended in serum-free media (Cellular Technologies Limited, Germany) and 2.5 x 10^5 cells added per well. Positive controls contained anti-CD3 (Mabtech, Sweden) and negative controls were incubated in media only. Triplicate test wells contained 10^7 particles rAAV2/2.hRPE65p.hRPE65. Plates were incubated at 37°C for 48 h. Plates were developed using an avidin-alkaline phosphatase detection system following a biotinylated detection antibody (Mabtech, Sweden). The data shows the average spots per well of triplicate test well. Test wells with more than double the number of spots in the negative controls and more than 15 spots were considered to be a positive response against antigen.

Microperimetry

Microperimetry was performed using a Nidek MP1 microperimeter (NAVIS software version 1.7.1, Nidek Technologies, Padova, Italy). Following 10 minutes of dark adaptation, a white fixation cross (31.8 cd/m^2) was displayed on a dim background (1.27 cd/m2). Goldman V stimuli of 200 ms duration and a maximum luminance of 127 cd/m^2 were presented with a 4-2 adaptive staircase threshold strategy. All testing followed a standardised, detailed protocol, with controlled room lighting, dark adaptation period and a fixed sequence of test patterns. The test is fully automated so there is little opportunity for experimenter bias. The subject's eye position was continually monitored by an infrared camera and the microperimeter tracks the eye movements to compensate for shifts in the direction of gaze. Reliability parameters were determined for each test including fixation losses, false negative and false positive responses. Test reliability was assessed by projecting a light onto a known blind spot (the optic nerve head); positive responses to the light indicated poor reliability. The mean sensitivity in dB was recorded per spot.

Dark-adapted perimetry

In dark-adapted conditions using a short wave length stimulus, sensitivities were measured at 76 locations in the central visual field using a modified Humphrey perimeter. Measurements were made between 60 and 240 minutes dark adaptation using Goldman V stimuli of 200 ms duration. All testing followed a standardised, detailed protocol, with controlled room lighting, dark-adaptation period and a fixed sequence of test patterns. The test is fully automated so there is little opportunity for experimenter bias. The subject's eye position was continually monitored by an infrared camera, therefore allowing fixation to be monitored and controlled for the duration of the test. Reliability parameters were determined for each test including fixation losses, false negative and false positive

responses. Test reliability was assessed by projecting a light onto a known blind spot (the optic nerve head); positive responses to the light indicate poor reliability.

Analysis of dark adapted perimetry was performed using Progressor Software (106, 107). This program applies linear regression analysis to each of the individual test locations to determine whether there is statistically significant progression in sensitivity in that area. The number of locations with a significant ($p<0.05$) change in sensitivity and also the mean sensitivity of the locations with a significant sensitivity change can be identified with Progressor. Each measurement is depicted by a bar; the lengths of the bars represent sensitivity, with the long bars showing loss of sensitivity and the short bars showing normal sensitivity. Yellow indicates a decline in sensitivity that is not significant, red indicates a decline that is significant ($P<0.05$), and green indicates an improvement that is significant ($P<0.05$).

Assessment of visual mobility

Visual mobility was tested with a 10.8m x 7.2m raised platform with concrete paving stones that were configured to simulate an outdoor pavement. Subjects negotiated a 13m long maze with 8 moveable barriers (1.8m x 1.2m) painted in colours matching light or dark blue denim, and the entire platform area was illuminated from overhead to calibrated light levels ranging from 240 lux (moderate office lighting) to 2 lux (less than UK night time pedestrian lighting standard). The subject was positioned at one end of the maze and instructed to walk through at a normal comfortable pace without touching the barriers. The experimenter followed along just behind to ensure the subject's safety. Total travel was recorded with a stopwatch along with mobility errors (touching a barrier, loss of orientation). The barriers were randomly re-positioned before each run and the subject was given 15 minutes to adapt to changes in illumination levels.

OCT imaging

Subjects underwent dilated SDOCT imaging (Heidelberg Engineering, Germany) with line or volume scans at the horizontal meridian. The volume acquisition protocol consisted of 49-B scans (averaging 12 frames per B-scan and 124 micron space between scans) covering an area of 20° by 20°, with the Automatic Real Time (ART) eye tracking software enabled. If a subject's fixation ability did not allow capture of these images, the volume scans were obtained with the ART feature disengaged. Foveal thickness was determined using the automated retinal thickness measurements between the inner limiting membrane (ILM) and the inner border of the line of back-reflection indicating the RPE. The status of the external limiting membrane (ELM) and IS/OS junction were judged for any discontinuity.

Electrophysiological testing

All subjects underwent electrophysiological evaluation including full-field, pattern, and multifocal electroretinography performed to incorporate the standards and guidelines of the International Society for Clinical Electrophysiology of Vision (101).

2.2 Retinal structure and function in Achromatopsia: implications for gene therapy

The aims of this study are to establish a panel of well phenotyped patients with ACHM, by quantatively and qualatively assessing disease status, investigating the relationship between retinal structure and function and correlating phenotypic findings with age and genotype. This information will have implications for a planned gene therapy trial in terms of patient selection, identifying time-points to intervene, and in determining efficacy.

40 patients with a clinical diagnosis of ACHM were included in this study. The number of subjects was decided upon by an estimation of the likelihood of recruiting patients and performing adequate assessments in study time period available. Patients were identified from a genetic database of inherited retinal conditions at Moorfields Eye Hospital. The diagnosis of ACHM was based on patients having a phenotype consistent with ACHM, which included onset from birth/early infancy, reduced visual acuity, photophobia, absent/markedly reduced colour vision, nystagmus in infancy, and absent cone ERG responses, with normal rod function.

All patients underwent a clinical history and complete ocular examination, best-corrected ETDRS visual acuity, reading and contrast sensitivity assessment, colour fundus photography, spectral domain OCT (SDOCT), microperimetry and colour vision testing. If not previously performed, patients underwent full-field ERG and molecular genetic screening of *CNGA3* and *CNGB3* for disease-causing variants.

The study received approval from the local ethics board and was performed in accordance with the tenets of the Declaration of Helsinki, with informed consent obtained from all patients after explanation of the nature of the study.

2.2.1 Visual acuity

All subjects underwent visual acuity assessment using the back-illuminated Early Treatment of Diabetic Retinopathy Study (ETDRS) chart. The chart surface had a luminance of 100-125 cd/m^2 and the test was undertaken at a distance of 4m. If prescribed, the participant used their distance spectacles. Each eye was initially measured individually, followed by assessment with both eyes open. A different chart was used for each patient's right and left eyes and for both eyes together.

2.2.2 Contrast sensitivity

The Pelli-Robson chart was used to measure contrast sensitivity in all subjects. Each eye was tested individually at a distance of 1m.

2.2.3 Reading acuity

The MN Read acuity chart was used to measure reading acuity in all subjects. The chart was read at 25cm (or 40cm if the visual acuity was better than 0.78 logMAR).

2.2.4 Colour vision tests

The colour vision of all subjects was assessed using both the Ishihara and Hardy Rand and Rittler (HRR) pseudoisochromatic plates. With the Ishihara test, if the subject was able to read the first test plate they were then asked to state the numbers on plates 2-25 without more than three seconds delay. If the participant was unable to read numbers, plates 26-38 were used and subjects asked to trace the winding paths. The HRR test comprises of 30 plates which contain one or two coloured symbols. Subjects were asked how many they could see and what symbol they were. Both sets of plates were held at 75cm from the subject and tilted so that the plane of the paper was at 90 degrees to the line of vision.

2.2.5 Fundus examination

On the basis of their fundus appearance on colour fundus photography, each subject was assigned into one of 3 categories (i) no RPE disturbance, (ii) RPE disturbance or (iii) atrophy (58). Images were independently assessed by two observers (VS and MM) and agreement on grading was found in 100% of cases.

2.2.6 Microperimetry

Microperimetry was performed on both eyes of all patients using the MP-1 microperimeter (Nidek technologies, Padova, Italy). Test-retest variability was probed by all patients having 2 tests undertaken on each eye. A customized test grid of 44 retinal locations with an eight degree radius was used to cover the macular and paramacular region. The testing was conducted in a darkened room and all subjects underwent training at the beginning of MP testing, allowing familiarisation and practice with the correct operation of the response trigger and the stimulus target. This was followed immediately by the actual test. All tests were performed after pupil dilatation with tropicamide 1% and phenylephrine 2.5%. Patching of the non-tested eye was performed.

Subjects were instructed to fixate on a 2-degree cross fixation target and background illuminance was set within the mesopic range at 1.27cd/m^2. A Goldmann size III stimulus with an area of 4mm^2 and 200ms duration was used. A 4-2 testing strategy was employed, with the intensity of the stimulus reduced in 4dB steps until it is no longer recognised by the subject. The threshold is then crossed a second time by increasing the stimulus intensity by 2dB steps until it is detected once again. False positive errors were tested for by measuring responses to stimuli projected into the blind spot at 30 second intervals. Fixation stability was assessed using the bivariate contour ellipse area (BCEA) which represents an area in degrees where 68% of fixation points are located (108), and this value can be accessed directly using the Nidek software

Repeat testing was performed on all subjects using the "follow-up" test option, which requires alignment of specific retinal landmarks at each subsequent test, to ensure similar location of stimuli projection.

2.2.7 OCT Imaging

Subjects underwent dilated SDOCT imaging (Heidelberg Engineering, Germany) with line or volume scans at horizontal the meridian. The volume acquisition protocol consisted of 49-B scans (averaging 12 frames per B-scan , and124 micron space between scans) covering an area of 20° by 20°, with the Automatic Real Time (ART) eye tracking software enabled. If a subject's fixation ability did not allow capture of these images, the volume scans were obtained with the ART feature disengaged. Images were assessed and graded into 5 categories: (i) continuous inner segment ellipsoid (ISe) at the fovea; (ii) ISe disruption at fovea; (iii) ISe absence at fovea;(iv) hyporeflective zone (HRZ) presence; and (v) outer retinal atrophy including RPE loss (58). The presence of foveal hypoplasia (defined as the persistence of one or more inner retinal layers (outer plexiform layer, inner nuclear layer, inner plexiform layer or ganglion cell layer) was also assessed. Images were independently assessed by 2 observers (VS and JC) who agreed on OCT categorisation in 36/40 (90%) of cases. In the remaining 4 cases a third observer (MM) made the ultimate decision on OCT grading.

2.2.8 MultiModalMapper Analysis

A custom-made software tool (MultiModalMapper) was used for co-registration of microperimetry and SDOCT datasets (109). The microperimetry data consisted of 2 files that were imported into the software tool. One file contains the actual perimetry data as well as mapping information for the second file, the fundus image. OCT data was exported as a binary volume file containing B-scans, confocal scanning laser ophthalmoscopy (cSLO) and B-scan segmentation data.

Microperimetry data and SDOCT data were aligned from corresponding landmarks set on both fundus images. Landmark selection was done manually using at least 3 landmarks. The result of the co-registration process can be visualized immediately as overlay image to allow for adjustment by moving or adding additional landmarks.
The transformed microperimetry data can then be visualised as an additional layer within the 3D view of the SDOCT. Zoom and rotation of the 3D view as well as scrolling through B-scans and moving the SLO image and SDOCT scan together with the microperimetry layer are supported.
The software also allows for the alignment of B-scans using retinal pigment epithelium segmentation data, which can be loaded from the volume file as well as extracted automatically using a Matlab (The MathWorks, Inc) script that processes the B-scans. Segmentation borders can be altered manually in case of segmentation errors.

2.2.9 Molecular analysis (undertaken by Dr Jill Cowing)

Molecular analysis involved extraction of total genomic DNA from whole blood using the Gentra PureGene kit (Qiagen) following the standard protocol. Coding exons and flanking exon-intron boundaries of *CNGA3* and *CNGB3* were PCR amplified using GoTaq Green Master Mix (Promega) and primer pairs. Bi-directional Sanger sequencing of each exon was carried out using the BigDye® Terminator V3.1 Cycle Sequencing Kit (Applied Biosystems) on an ABI 3730 DNA Analyzer. Resulting sequences were analyzed for mutations by comparison with GenBank sequences using DNASTAR Lasergene SeqMan Pro.

2.2.10 Statistical analysis

Normality of data was assessed by evaluating the shape of histogram plots, with age, visual acuity, contrast sensitivity and reading acuity considered to be normally distributed. Inter-eye correlations for all parameters were assessed using Pearson or Spearman correlation analysis where appropriate and significant correlations were found in all parameters. The left eye was arbitrarily selected for further analysis (as no significant inter-eye difference was found between visual acuity, contrast sensitivity and reading acuity), and differences in parameters between OCT groups, fundus change category and genotype were assessed for using the one-way ANOVA or Kruskal-Wallis test where appropriate. Differences in parameters between patients with or without foveal hypoplasia were assessed using either an independent samples T-test, or Mann-Whitney U test where appropriate.

Results

3.1 RPE65 Trial

3.1.1 Baseline characteristics

12 subjects between ages of 6 and 23 were included in this study. Baseline visual acuity in the study eye ranged from 0.36 logMAR to 1.52 logMAR. Subjects 1 to 4 received the lower dose of vector, with subject 5 to 12 receiving the higher dose. Follow-up length ranged from 8 months in two subjects, 12 months in two subjects, 24 months in four subjects, and 36 months in four subjects (Table 3).

Subject	Age	RPE65 Mutation	Vector Dose	Volume (ml)	Foveal involvement	Baseline Visual Acuity	Follow-Up
1	23	Y368H Y368H	$1x10^{11}$	0.9	Yes	Study eye = 1.16 Control eye = 0.88	36 months
2	17	IVS1+5g>a G40S	$1x10^{11}$	1	Yes	Study eye = 1.52 Control eye = 1.62	36 months
3	18	E6X D167Y	$1x10^{11}$	1	Yes	Study eye = 0.76 Control eye = 0.5	36 months
4	11	K298fs Y368H	$1x10^{11}$	1	Yes	Study eye = 0.91 Control eye = 0.75	36 months
5	23	Y368H Y368H	$1x10^{12}$	1	Yes	Study eye = 0.36 Control eye = 0.31	24 months
6	17	Y368H Y368H	$1x10^{12}$	1	Yes	Study eye = 0.68 Control eye = 0.53	24 months
7	10	IVS1+5g>a IVS12-2a>g	$1x10^{12}$	1	Yes	Study eye = 0.44 Control eye = 0.46	24 months
8	10	R91W R91W	$1x10^{12}$	1	Yes	Study eye = 0.69 Control eye = 0.64	24 months
9	6	IVS1+5g>a IVS1+5g>a	$1x10^{12}$	0.9	No	Study eye = 0.82 Control eye = 0.89	12 months
10	6	IVS1+5g>a Y368H	$1x10^{12}$	1	Yes	Study eye = 0.8 Control eye = 0.7	12 months
11	13	R124X F530fs	$1x10^{12}$	1	No	Study eye = 0.63 Control eye = 0.55	8 months
12	19	G40S G40S	$1x10^{12}$	1	Yes	Study eye = 0.54 Control eye = 0.6	8 months

Table 3 – Baseline characteristics, surgical details and follow-up time of subjects

3.1.2 Surgical details

All subjects underwent three port, pars-plana vitrectomy under general anaesthesia. Up to 1ml of rAAV vector was administered using a 41-gauge subretinal cannula (de Juan Synergistics) into the subretinal space. Foveal involvement was achieved in 10 subjects, with a fluid-air exchange performed in 8 cases to manipulate the location of the induced retinal detachment to involve the fovea. Approximately one third of the total retinal area was involved in all cases. In 2 subjects (9 and 11) foveal involvement did not occur despite fluid-air exchange.

3.1.3 Adverse events

Two subjects (subjects 8 and 9) developed mild, asymptomatic episodes of inflammation, predominantly affecting the posterior segment. In subject 8, mild vitritis, optic disc swelling with retinal vessel tortuosity and sheathing (Fig. 11a) was noted at the 6 week postoperative visit. The subject was recommenced on a course of oral and topical steroid medication and the inflammation significantly improved over the next 2 weeks, and steroid medication was tapered and stopped over the next 2 months. In subject 9, mild vitritis, optic disc swelling with retinal vessel tortuosity and sheathing (Fig. 11b) was noted at 3 weeks postoperatively. The subject's oral prednisolone dose was temporarily increased and the inflammation reduced over the next 3 weeks, with complete resolution at the 2 month visit. Visual acuity was unaffected in both subjects, and no inflammation was noted in the control eyes.

Subject 7 experienced mild anterior uveitis, 2 weeks after stopping the standard postoperative topical steroid course. Topical steroids were recommenced and inflammation resolved with tapering of the steroid regime over the next 6 weeks.

Subject 12 experienced mild distortion of vision in the study eye from 2 weeks postoperatively. This symptom had improved but was still present at the most recent follow-up visit at 8 months.

One subject experienced a rise in intraocular pressure to 34mmHg at 2 weeks postoperatively. Intraocular pressure soon returned to within normal limits following administration of topical ocular antihypertensive medication (G. Timolol 0.25% b.d.).

Mild adverse effects attributed to oral steroid administration included transient glycosuria, lethargy, gastro-oesophageal reflux and facial acne exacerbation.

Fig. 11a and 11b – Transient episodes of mild vitritis, optic disc swelling with retinal vessel tortuosity and sheathing observed in subjects 8 (Fig. 1a) and 9 (Fig. 1b). Resolution of inflammation followed recommencement of oral steroid medication in both subjects and no inflammation was noted after the 4 month visit in subject 8, and inflammation had fully resolved by the 2 month visit in subject 9.

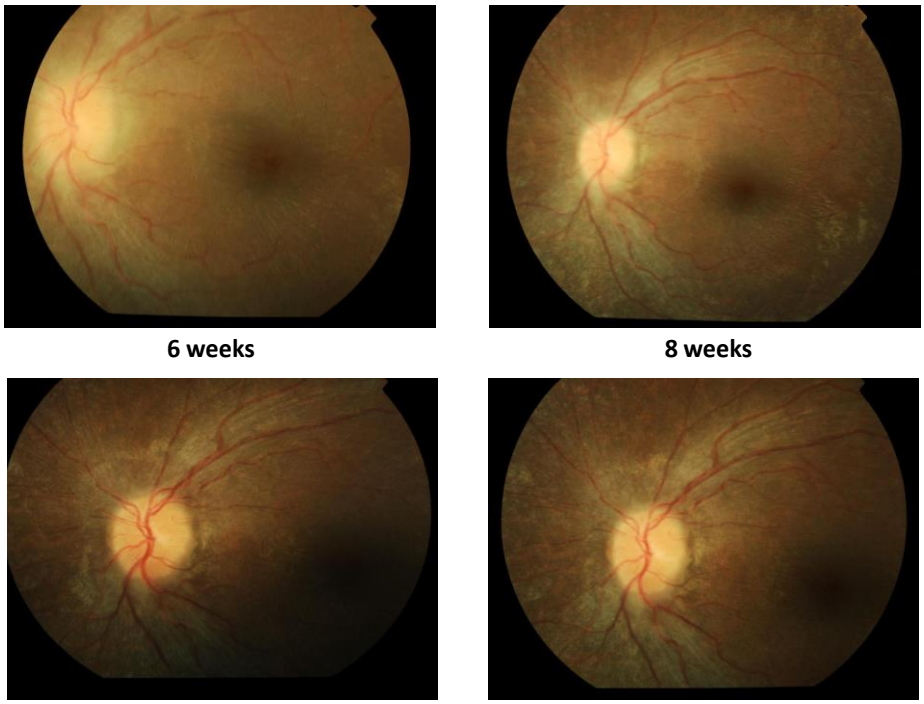

Fig. 11a

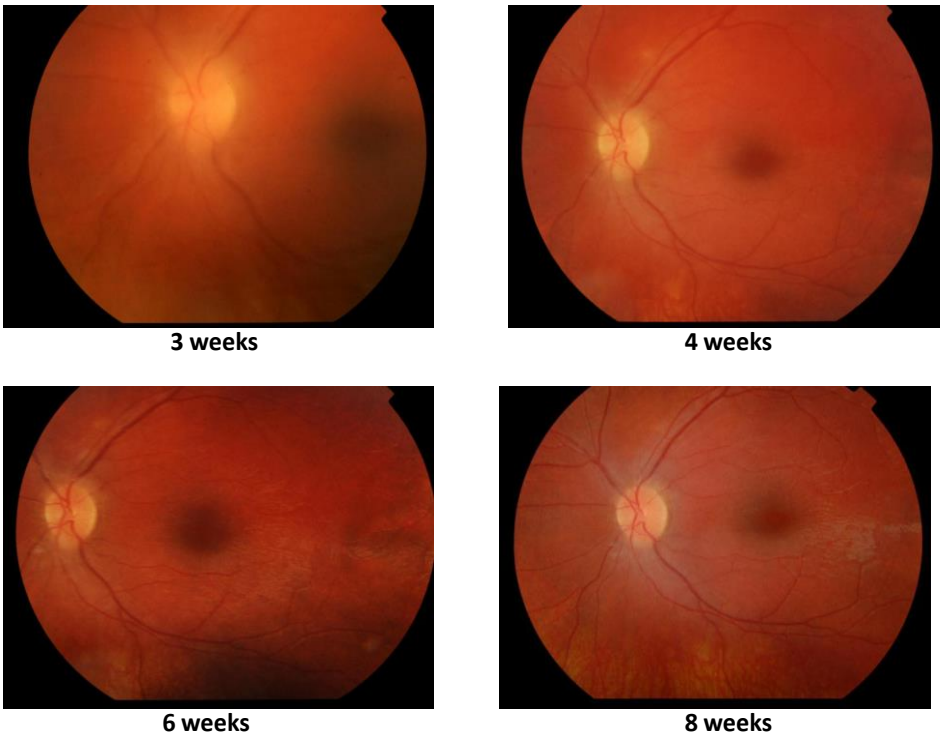

Fig. 11b

3.1.4 Electrophysiological testing

Baseline electrophysiology testing showed severe loss of generalised retinal function affecting rod and cone photoreceptors with severe macular involvement bilaterally, in all subjects. There was no significant change in electrophysiological testing in any of the subjects postoperatively. Multifocal ERGs showed severe widespread reduction pre and post-treatment. Pattern ERGs were undetectable pre and post-treatment in all subjects and the degree of subjects' nystagmus was not an inhibiting factor in performing these tests.

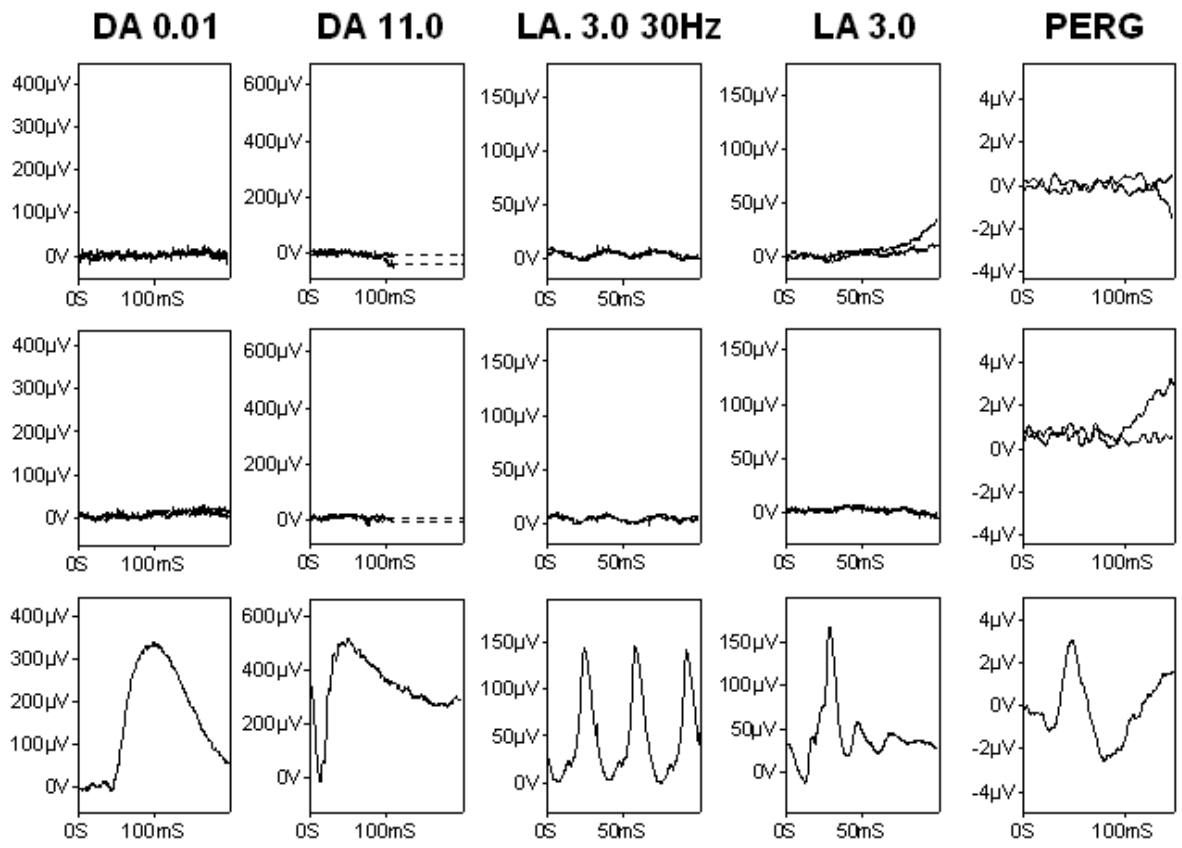

Fig. 12 – Standard ERG traces from subject 3. *Top trace* -preoperative study eye. *Middle trace* – 4 months postoperative in study eye. *Bottom trace* – example of normal ERG.

3.1.5 Immunological Assays

At various time points prior to and post-treatment, subjects' serum was assessed for the presence of immune responses against the AAV2 capsid or the *RPE65* transgene product.

Table 4 shows the results of the neutralising antibody assay (NAb). Patient 7 was the only patient to show a persistent up-regulation of NAb after gene therapy. The increase in their NAb titre is concomitant with the removal of steroid therapy. Patient 7's NAb titre remained elevated for over 2 years but is reducing with time. Patient 8 showed a slight increase in NAb titre at 4 months that has reduced to baseline levels. Patient 9 showed a transient increase in NAb titre but this has greatly reduced with time after gene therapy. Interestingly, even though patient 4 had quite a high NAb titre before gene therapy, this did not increase following administration of the gene therapy vector. No other patients showed any consistent increase in antibody titre for the duration of their follow up, indicating no up-regulation of humoral responses to AAV2 in these patients.

Patient	Base	Day 1	Wk1	Wk2	Wk3	Wk4	Wk8	Mnth4	Mnth8	Yr 1	Yr2	Yr3
1	4	3	4	4	4	6	5	6	…	4	12	16
2	neat	neat	neat	neat	neat	2	neat	neat	…	3	2	3
3	Neat	neat	neat	neat	neat	neat	neat	neat	…	neat	neat	2
4	512	512	1024	512	512	1024	1024	1024	…	512	256	200
5	4	4	2	neat	neat	neat	1.5	neat	3	2	4	…
6	2	neat	1.5	1.5	…	neat	neat	neat	neat	neat	1.5	…
7	2	1.5	2	neat	6	256	600	1024	1024	700	200	…
8	1.5	neat	1.5	1.5	neat	neat	4	16	3	6	3	…
9	4	…	4	…	…	256	200	32	…	…	…	…
10	1.5	neat	neat	neat	neat	2	3	3	3	neat	…	…
11	neat	1.5	1.5	1.5	2	neat	neat	neat	1.5	…	…	…
12	neat	neat	2	1.5	2	1.5	neat	3		…	…	…

Table 4 - **Circulating neutralising antibodies against AAV2**. **Neutralising antibody titre: serum dilution that resulted in 50% inhibition of transduction of 293T cells by AAV2.GFP**

Table 5 shows the results of the ELISA to detect circulating levels of IgA, IgG and IgM against RPE65. No patients showed any increase of greater than 1.5-fold compared to baseline in circulating IgA, IgG or IgM against the transgene product (RPE65) to date, except for patient 5, who had a transient 1.7-fold titre increase at week 4, before dropping back to baseline levels, which could indicate a marginal humoral immune response against RPE65.

Patient	Day 1	Wk1	Wk2	Wk3	Wk4	Wk8	Mnth4	Mnth8	Yr 1	Yr2	Yr3
1	116	95.7	70.3	71.6	97.1	83.7	101.1	…	134.5	92.6	160.0
2	84	97.2	102.2	112.5	124.7	77.1	89.6	…	65.2	109.2	98.4
3	99.3	82.8	90.3	81.5	81.5	100.2	94.5	…	130.6	122.8	130.7
4	100.4	104.4	100	86.6	86.2	101.1	88.4	…	84.9	90.6	148.3
5	111.9	107.7	135.5	129.1	169.1	102.2	93.6	98.4	96.5	99.6	…
6	123.9	143	89.6	…	92.9	94.1	99.7	98.9	87.2	117	…
7	91	105	96	90	103	83	86	127	100	96.3	…
8	104.3	113.9	125.3	126.2	43.6	56.9	59.2	69.9	53.5	87.5	…
9	…	67	…	…	110.2	73	96	…	…	…	…
10	131.3	123	98.4	110.5	116.7	87.8	114	100	102.7	…	…
11	83.3	52.8	110.7	90.8	88.6	96.7	90.4	79.8	…	…	…
12	91.8	94.7	93.3	101.9	96.6	94.5	96.8		…	…	…

Table 5 - Serum ELISA to detect circulating levels of IgA, IgG and IgM against rRPE65. Relative antibody titre (%) compared to the baseline sample

In table 6 the results of the ELISA to detect circulating levels of IgA, IgG and IgM against AAV2 are depicted. Patient 5 showed a transient increase of 2.34-2.03-fold in serum Ig against AAV2 in weeks 3-8, which then resolved back to baseline levels. Patient 7 showed an increase in circulating Ig against AAV2 between wk4-month 8 which is consistent with the increase in NAb titre against AAV2 in this patient over the same time frame. No other patients showed an increase of greater than 1.5 fold within the first year after gene therapy. Patient 1 and 7 had an increase of over 1.5 fold at year 2, but this small spike in anti-AAV2 Ig is not consistent with a humoral response to a single administration of AAV2 vector and is more likely to result from re-exposure to wild type AAV2 within the environment.

Patient	Day 1	Wk1	Wk2	Wk3	Wk4	Wk8	Mnth4	Mnth8	Yr 1	Yr2	Yr3
1	112.5	85.5	88.4	68.2	103	86.1	50.5	…	106.3	156.6	108.1
2	74.0	85.0	110.0	99.3	86.2	85.7	89.6	…	70.3	94.4	74.4
3	95.7	70.1	59.0	73.9	78.2	84.9	95.2	…	143.0	77.3	82.9
4	82.7	90.1	93.0	65.8	70.5	64.8	88.7	…	79.6	185	130
5	85.3	126.6	112.0	234.2	222.6	203.3	143.5	115.4	53.0	79.3	…
6	100.4	96.4	112.2	…	117.5	110.0	123.4	122.5	125.8	139.7	…
7	121.4	111.3	117.5	117.4	182.5	321.0	261.9	174.9	139.2	185.5	…
8	87.2	106.9	98.6	101.8	123.9	106.1	100.5	91.4	72.9	95.4	…
9	…	117.8	…	…	99.9	107.9	116.0	…	…	…	…
10	109.6	105.6	91.6	94.0	95.6	75.1	95.2	116.1	97.3	…	…
11	95.7	71.4	107.6	106.5	101.7	102.2	98.7	90.0	…	…	…
12	113.0	100.8	98.4	97.4	97.4	95.4	113.0		…	…	…

Table 6 - Serum ELISA to detect circulating levels of IgA, IgG and IgM against AAV2. Relative antibody titre (%) compared to the baseline sample

Table 7 shows the result of an ELISpot assay to detect secretion by blood lymphocytes of the Th1 cytokine IFNγ in response to co-culture with AAV2. Patient 1 had a low positive response against AAV2 at baseline, but this positive response was not observed in any samples taken after gene therapy, indicating that administration of AAV2 to the eye did not further activate any AAV2-specific T-cells. Four patients each showed a transient modest positive response at one time point only, which then resolved. One of these was patient 7, who had a high concomitant increase in the NAb titre against AAV2 at the same time point (week 4). However, the T-cell response was not of the same magnitude, being much lower, was not sustained and had dropped back to negative levels by the week 8 time point, so is inconsistent with an effector T-cell response. Patient 9 also had an increase in NAb titre at the same week 8 time point as the modest positive ELISpot result, although the NAb titre was already dropping from its peak at week 4. The other two patients (patients 8 and 10) with single positive ELISpot responses did not have any NAb response to AAV2 and there is no apparent reason for these very modest and transient increases in T-cell responses against AAV2.

Patient	Test	Base	Day 1	Wk1	Wk2	Wk3	Wk4	Wk8	Mnth4	Mnth8	Yr 1	Yr2	Yr3
1	Negative	7	14	14	8	19	13	109	89	…	74	3	305
	Positive	>300	>300	>300	>300	>300	>300	>300	>300	…	500	470	500
	AAV	25	25	6	9	3	21	101	75	…	119	3	271
2	Negative	3.5	0	2	4	1	4	8	1	…	20	20	3
	Positive	>300	374	>300	>300	412	>300	>300	>300	…	500	500	406
	AAV	5.3	1	2	3	0	4	4	3	…	24	24	3
3	Negative	11	13	5	6	6	7	48	89	…	14	11	20
	Positive	>300	>300	>300	>300	>300	>300	>300	>300	…	341	>500	>500
	AAV	15	21	5	13	5	9	27	116	…	0	10	26
4	Negative	143	155	6	6	7	4	41	7	…	6	3	26
	Positive	>300	>300	>300	>300	>300	>300	>300	696	…	147	364	615
	AAV	155	118	5	4	4	7	39	11	…	9	1	7
5	Negative	3	2	6	4	11	6	6	42	0	14	2	Pending
	Positive	568	569	737	455	498	>500	528	500	508	575	744	Pending
	AAV	1	4	8	4	9	10	7	21	2	6	3	Pending
6	Negative	2	0	1	8	…	7	11	3	3	8	7	Pending
	Positive	580	>500	>500	500	…	913	600	419	280	475	649	Pending
	AAV	3	2	1	5	…	5	5	1	2	4	3	Pending
7	Negative	10	3	39	6	11	34	4	13	33	17	6	Pending
	Positive	451	388	501	444	500	500	567	327	409	425	359	Pending
	AAV	12	5	40	8	14	70	8	13	46	12	8	Pending
8	Negative	12	1	11	8	0	5	3	5	11	…	12	Pending
	Positive	400	459	567	555	375	471	514	399	422	…	400	Pending
	AAV	12	6	31	11	0	1	8	3	18	…	12	Pending
9	Negative	66	…	8	…	…	65	10	…	…	…	Pending	Pending
	Positive	471	…	492	…	…	576	632	…	…	…	Pending	Pending
	AAV	56	…	9	…	…	57	26	…	…	…	Pending	Pending
10	Negative	16	9	3	3	5	11	7	8	9	1	Pending	Pending
	Positive	654	573	501	550	574	562	640	494	553	482	Pending	Pending
	AAV	30	9	3	4	5	25	9	5	7	1	Pending	Pending
11	Negative	6	1	6	5	3	5	5	13	40	Pending	Pending	Pending
	Positive	447	461	573	464	498	410	514	613	480	Pending	Pending	Pending
	AAV	13	1	5	6	6	2	4	17	21	Pending	Pending	Pending
12	Negative	19	4	2	2	5	21	8	9		Pending	Pending	Pending
	Positive	500	604	666	496	643	500	500	650		Pending	Pending	Pending
	AAV	13	10	3	1	4	19	12	12		Pending	Pending	Pending

Table 7 - ELISpot assay to detect secretion of the Th1 cytokine IFNγ in response to co-culture with AAV2. Average spot counts from triplicate wells. For positive controls, where spot counts were saturating, the ELISpot reader defined them as greater than 300 spots. A sample with at least twice as many spots in the AAV assay as in the negative control is considered to show a positive response. … = no sample was obtained.

3.1.6 Visual Acuity

At 6 months following treatment, the visual acuity in 1 subject (subject 7) reduced (worsened) by more than 0.3 logMAR in their study eye, compared to baseline (Fig. 13a). No reduction in visual acuity of 0.3 logMAR or more was observed in the control eyes at 6 months. Both the study and control eyes of subject 11 showed an improvement in acuity of 0.3 logMAR or more at 6 months. In the study eye of 10 subjects with at least 12 months follow-up (subjects 1-10), the visual acuity reduced by 0.3 logMAR or more in 2 subjects (subjects 2 and 3) at their final visit (Fig. 13b). No reduction in visual acuity of at least 0.3 logMAR was observed in the control eyes. No subject with more than 12 months follow-up showed an improvement in visual acuity of more than 0.3 logMAR in either eye.

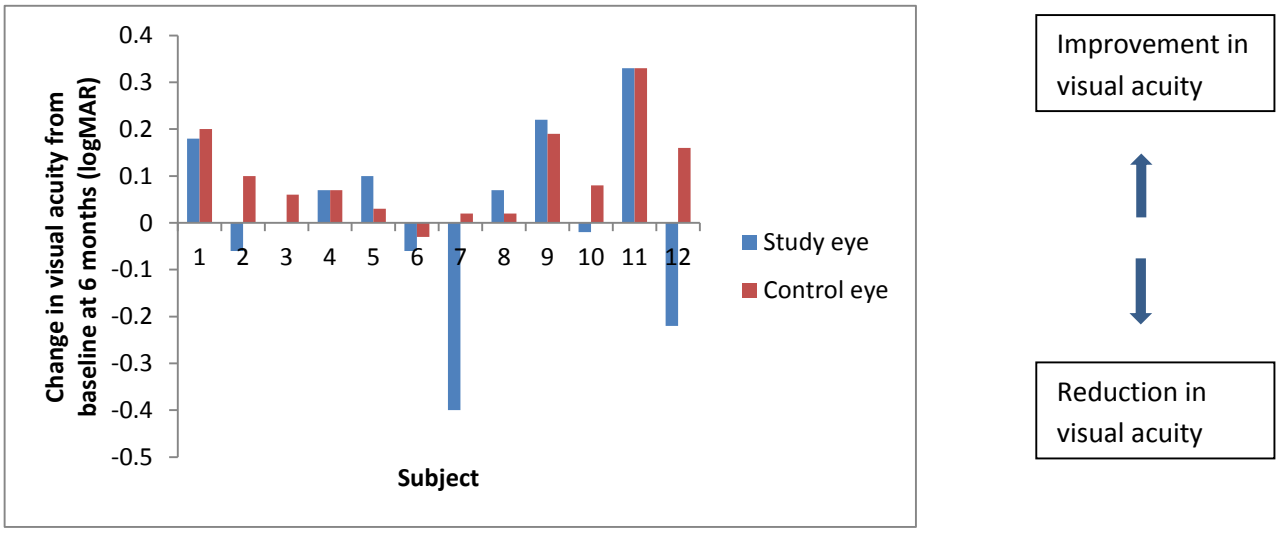

Fig. 13a – Graph showing change in visual acuity from baseline at 6 months

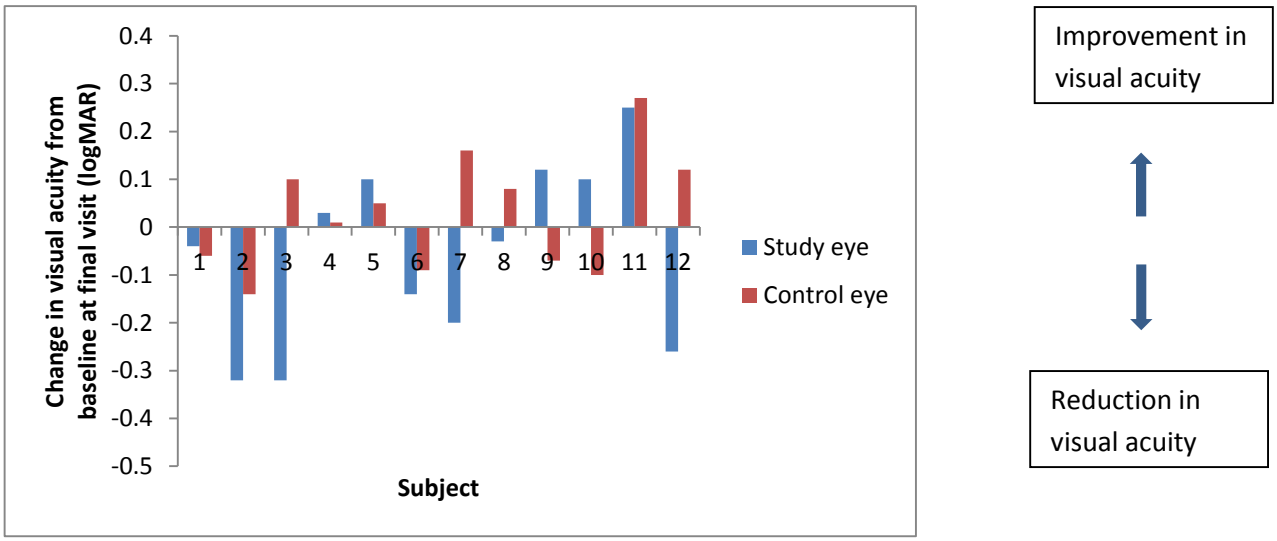

Fig. 13b – Graph showing change in visual acuity from baseline at final visit

3.1.7 Contrast sensitivity

At 6 months following treatment, 2 subjects (subjects 7 and 12) had a reduction (worsening) in contrast sensitivity of at least 0.2 logCS in their study eye, and no control eye showed a reduction to this extent (Fig.14a). Subjects 1, 8 and 9 showed an improvement of more than 0.2 logCS in their study eye, and subject 9 also had more than 0.2 logCS improvement in their control eye. In the study eye of 10 subjects with at least 12 months follow-up, 3 subjects (subjects 3, 6 and 7) had a reduction in contrast sensitivity of at least 0.2 logCS at their final visit (Fig. 14b). No reduction of more than 0.2 logCS was observed in the control eye at similar time points. Subjects 1 and 9 showed an improvement of more than 0.2 logCS in their study at final visit, and subject 9 also had a similar improvement in their control eye.

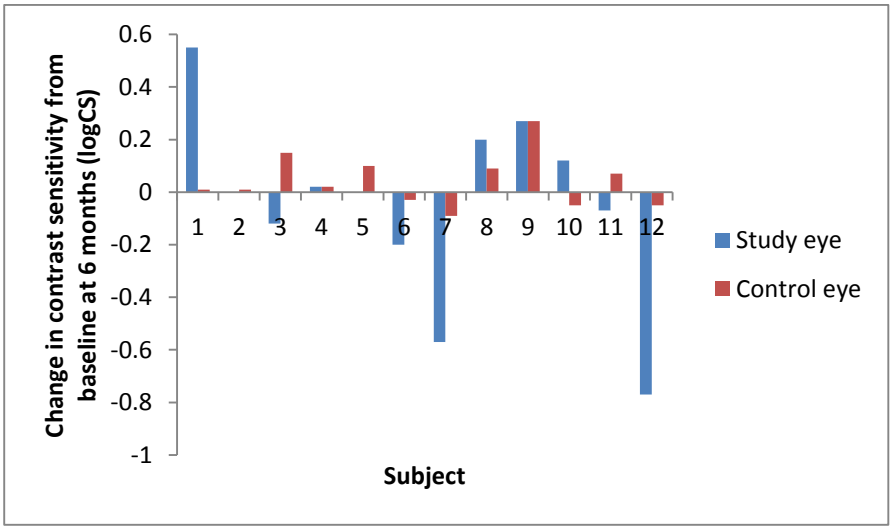

Fig. 14a – Graph showing change in contrast sensitivity from baseline at 6 months

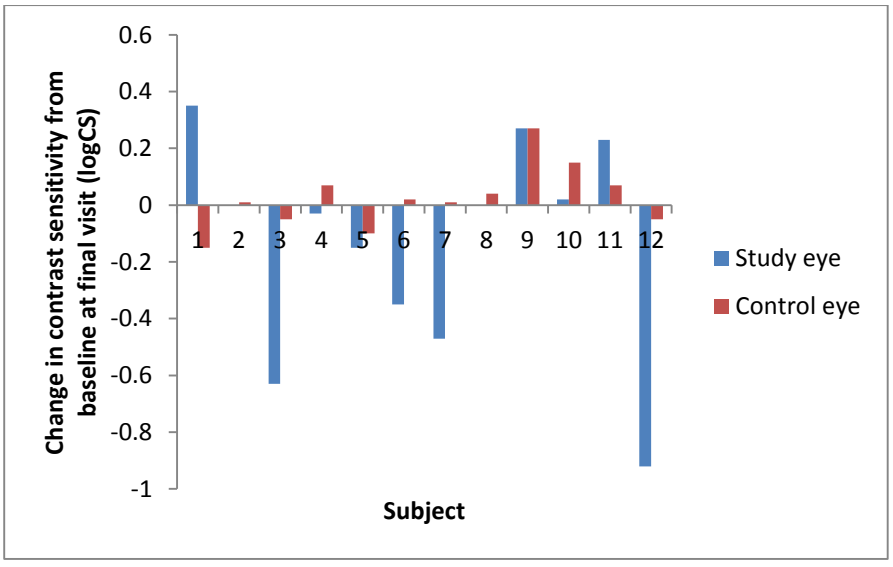

Fig. 14b – Graph showing change in contrast sensitivity from baseline at final visit

3.1.8 Reading Acuity

Reading acuity assessment was performed in 8 subject (4 younger subjects were unable to perform the reading test due to language difficulties), and a reduction (worsening) in reading acuity of at least 0.3 logMAR was observed in the study eye of 3 subjects (subjects 3, 7 and 12) at 6 months, and no control eye showed a reduction in reading acuity of at 0.3 logMAR or more (Fig. 15a). In the 7 subjects with at least 12 months follow-up of reading acuity assessment, reading acuity reduced by at least 0.3 logMAR in 3 subjects (subjects 1, 3 and 7) at their final visit (Fig. 15b). No reduction in reading acuity of at least 0.3 logMAR was found in the control eye, and no eyes showed more than 0.3 logMAR acuity of improvement.

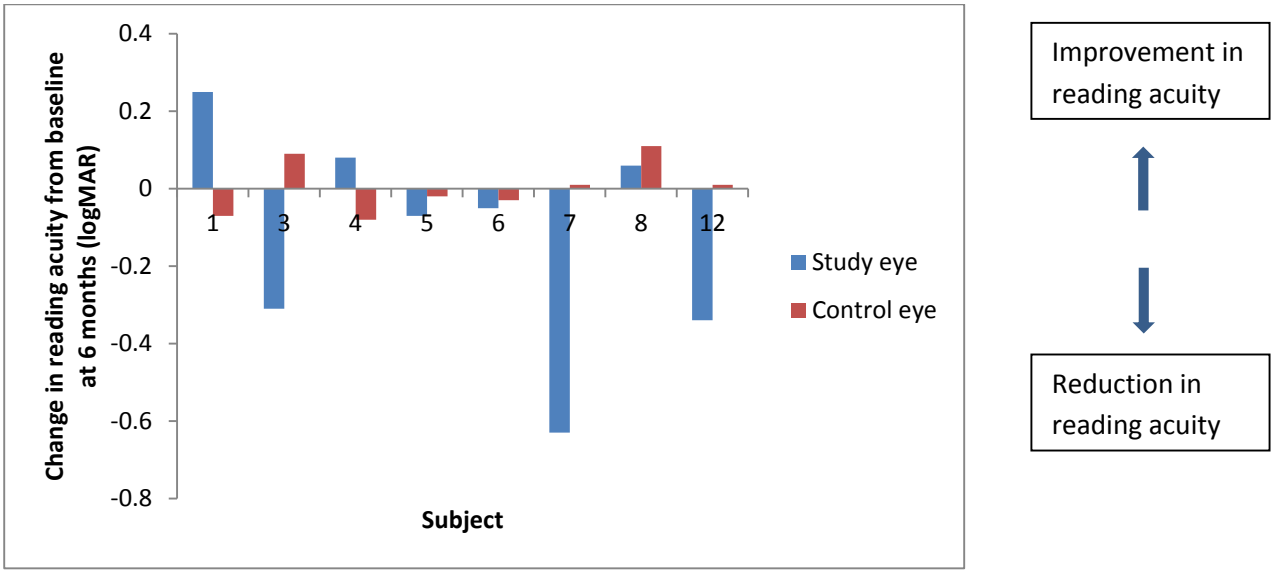

Fig. 15a – Graph showing change in reading acuity from baseline at 6 months

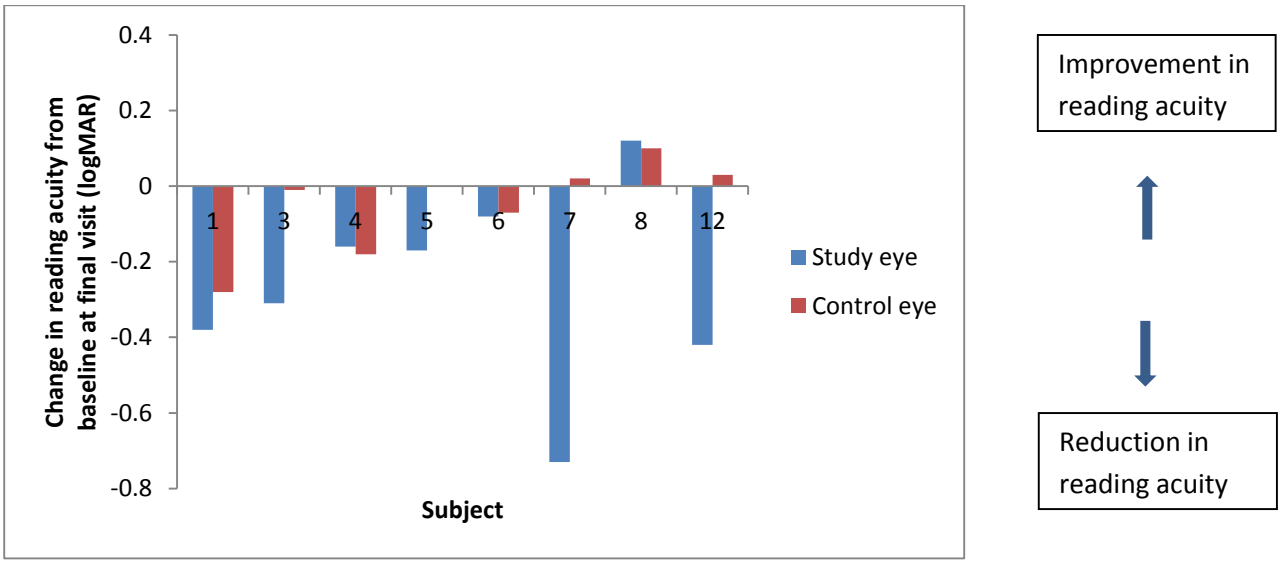

Fig. 15b – Graph showing change in reading acuity from baseline at final visit

3.1.9 Dark-adapted Perimetry

Figure 16 shows the results of the dark-adapted perimetry assessment. Six subjects (subject 3, 5, 6, 8, 10 and 12) showed significant improvement in retinal sensitivity at various loci with dark-adapted perimetry testing using a blue light stimulus in their study eye. Subject 3 displayed the greatest improvement with 54 locations (with mean sensitivity of 17dB- Fig. 17) showing significant improvement in retinal sensitivity at 4 months. The level of peak improvement was not maintained, with retinal sensitivity declining by 12 months. At 36 months, there were 5 remaining locations of improved sensitivity, which however maintained a high mean sensitivity of 21.2dB. In addition, subject 3 displayed numerous loci of reduced retinal sensitivity in their control eye, with 19 and 13 locations showing significant reduction in sensitivity at 24 and 36 months respectively, compared to a reduction at 8 locations at 24 months, and 4 locations at 36 months in their study eye (Fig. 18). Subject 6 showed progressive improvement to a peak of 46 locations (mean sensitivity 10dB) with significant sensitivity improvement at 12 months, with a decline in sensitivity to 21 locations (mean sensitivity 11.6dB) still displaying significantly improved sensitivity at 24 months. Subject 5 had a peak of 26 locations (mean sensitivity 3.9dB) with significant improvement in sensitivity at 8 months, with 11 locations (mean sensitivity 7.5dB) still displaying significantly improved sensitivity at 24 months. Subject 8 had 2 time points of greatest improvement in sensitivity occurring at 6 and 12 months. The numbers of locations showing improvement in sensitivity at these time points were 17 and 20 respectively. In between these time points at 8 and 10 months, retinal sensitivity declined – possibly related to the episode of posterior segment inflammation with optic nerve involvement that this subject experienced. Subject 10 showed a modest degree of improvement with a peak of 10 locations (mean sensitivity 7.4dB) showing improved sensitivity at 8 months, with improvement declining to 5 locations (mean sensitivity 3.6dB) at 12 months. Subject 12 showed an improvement at 3 locations (mean sensitivity 12.3dB) at 8 months. In the control eye, two subjects (subjects 5 and 6) showed significant improvement in retinal sensitivity at a maximum of 8 locations, occurring at 8 months (mean sensitivity 2.8dB) in subject 5, and at 10 months (mean sensitivity 1.6dB) in subject 6 (Fig. 19).

In subject 3 the area of greatest sensitivity improvement occurred in the central 15 degrees, with extension towards 20 degrees inferiorly (Fig. 20). In subject 5, the greatest improvement was seen within the central 10 degrees. In subject 6, the area of greatest improvement occurred centrally and extended 15-20 degrees into the inferior hemifield. In subject 8, the region of most significant improvement was in the superior-nasal field, with improvement also occurring in the periphery of the inferior-nasal field. Similarly, subject 10 showed greatest improvement in the superior-nasal field. Subject 12 showed improvement in the central 15 degrees.

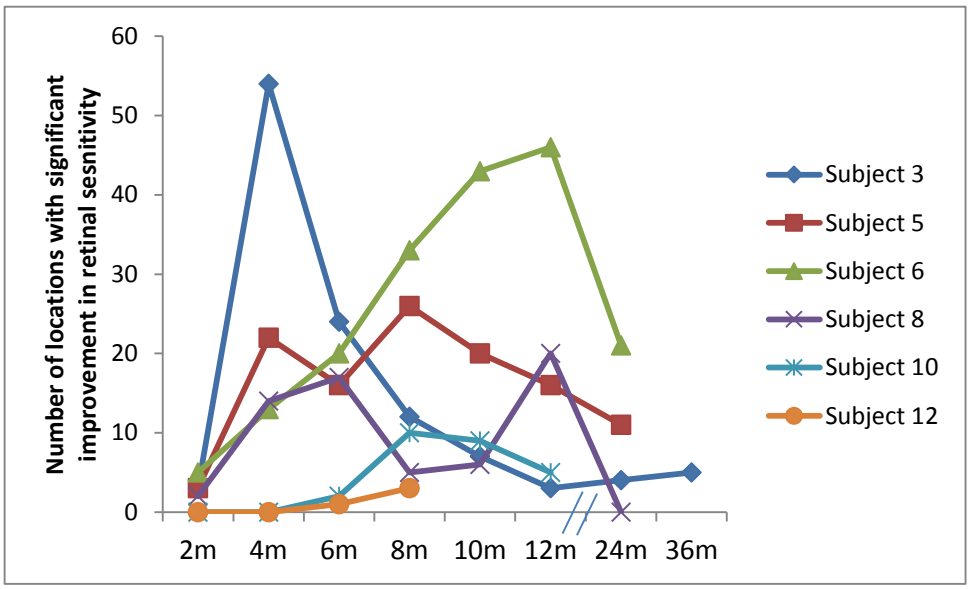

Fig. 16 – Graph of number of dark adapted perimetry locations with significant improvement in retinal sensitivity in study eye

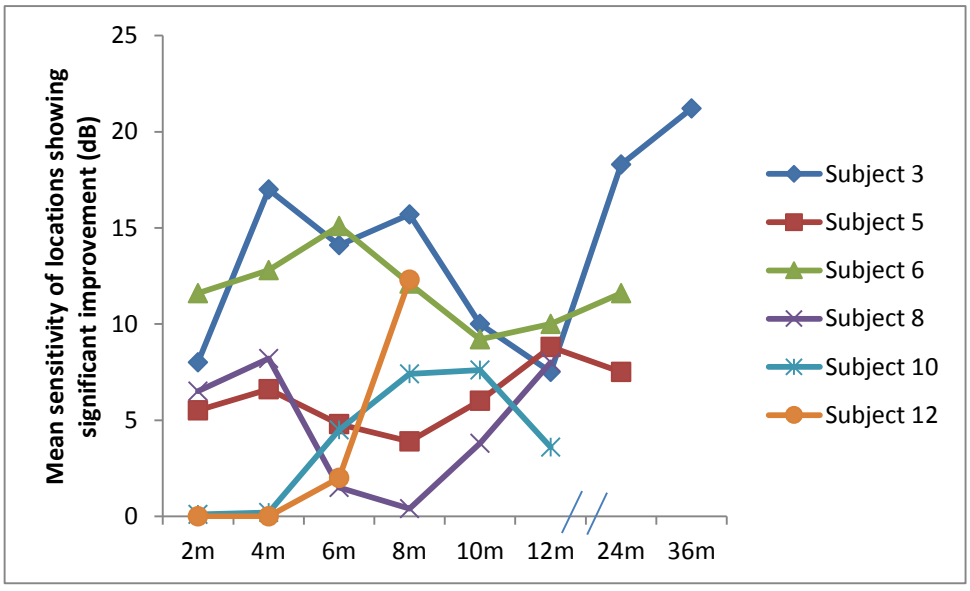

Fig. 17 – Graph of mean sensitivity of locations showing significant improvement in sensitivity (dB)

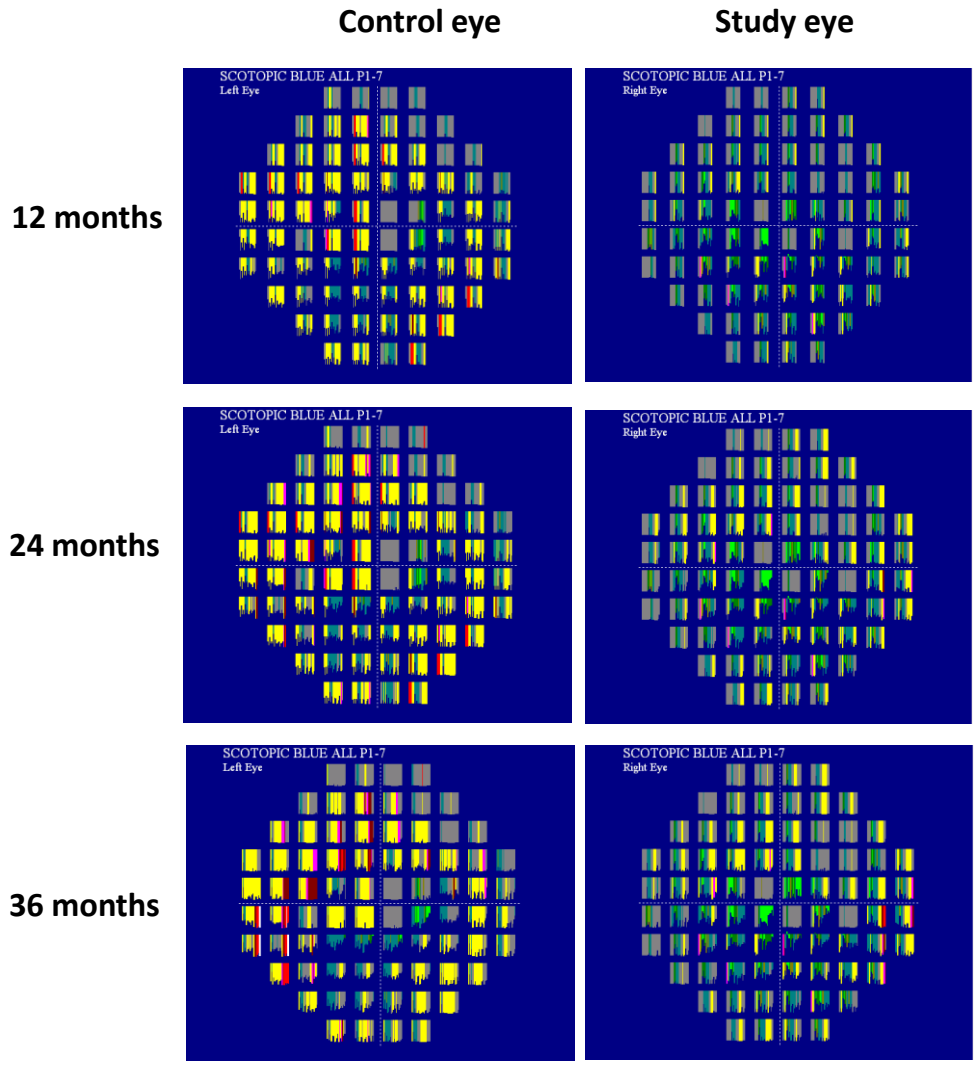

Fig. 18 – Dark-adapted perimetry Progressor plots for subject 3. Retinal sensitivity is represented by the lengths of the bars, with the long bars showing low sensitivity and the shorter bars showing improved sensitivity. Yellow indicates a decline in sensitivity that is not significant, red indicates a decline that is significant ($p<0.05$), and green indicates an improvement that is significant (<0.05). Several loci in the study eye continued to show significant improvement in sensitivity at 36 months follow-up, with high sensitivity (indicated by shorter green bars) maintained at central locations. There are many more loci in the control eye which show a significant reduction in sensitivity due to the natural progression of the disease from 12 to 36 months follow-up, compared to the study eye.

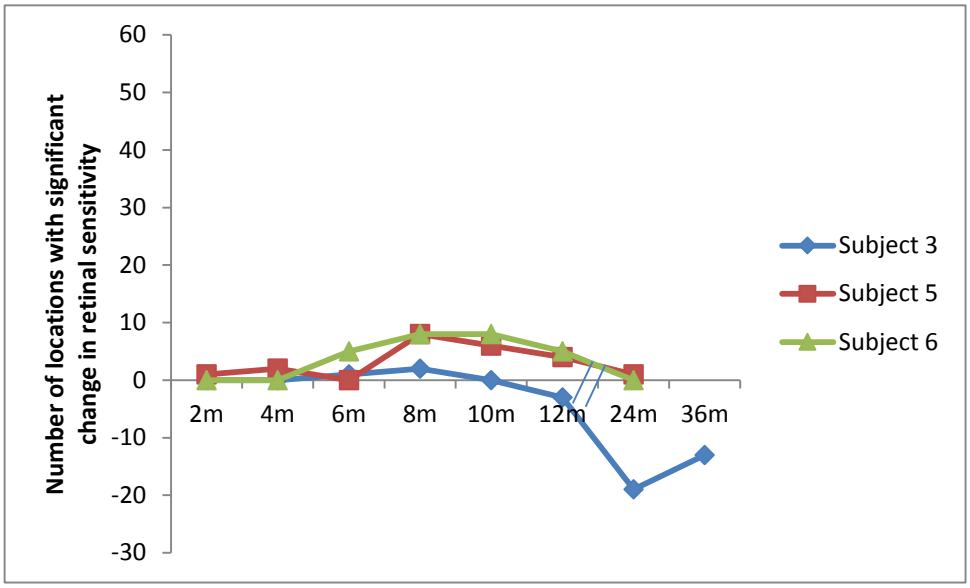

Fig. 19 – Graph of number of dark adapted perimetry locations with significant change in retinal sensitivity in control eye

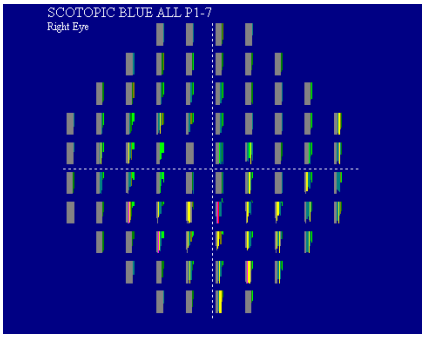

Subject 3 at 4 months

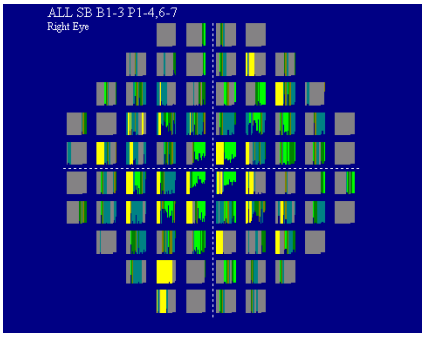

Subject 5 at 8 months

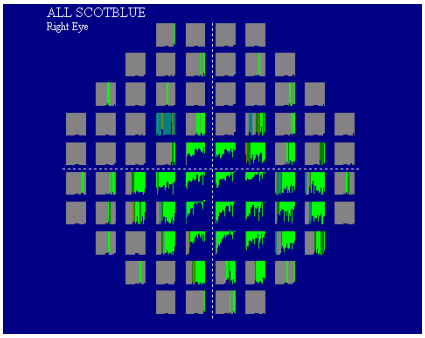

Subject 6 at 12 months

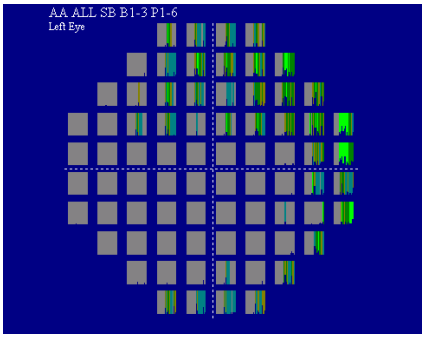

Subject 8 at 10 months

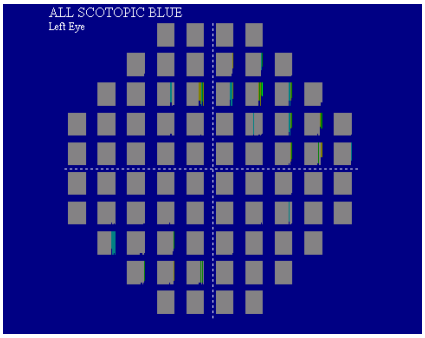

Subject 10 at 8 months

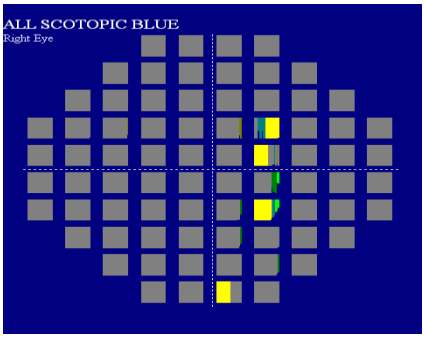

Subject 12 at 8 months

Fig. 20 – Plots of dark-adapted perimetry peak sensitivity improvement in subjects showing improvement

3.1.10 Microperimetry

The results of the microperimetry assessment of retinal sensitivity are shown in figure 21 to 24. Improvement in retinal sensitivity with microperimetry testing occurred in six subjects (subjects 3, 5, 6, 8, 10 and 12). The largest improvement in sensitivity occurred in subject 6, who achieved a 6.4dB improvement in mean sensitivity from baseline, at 6 months (Fig. 21). Peak sensitivity was not maintained with a decline in sensitivity to 2.09dB and 1.41dB at 12 and 24 months respectively (Fig. 21 and 22). Subject 5 achieved a peak improvement in mean sensitivity of 5.32dB at 8 months, and showed sustained improvement of over 5dB sensitivity at 24 months. Subject 3 achieved a peak mean sensitivity of 4.47dB at 12 months, with sensitivity reducing to 0dB at 36 months. As was observed with dark adapted perimetry testing, subject 8 had two peaks in retinal sensitivity, occurring at 2 months (2.31dB) and at 10 months (2.47dB), with retinal sensitivity declining to 0.14dB at 6 months. A more modest improvement in mean sensitivity from 0.09dB at baseline to 0.88dB at 6 months was seen in subject 10. Subject 12 achieved a maximum mean retinal sensitivity of 2dB at 6 months. Subject 7 had a reduction in mean sensitivity from 1.85 dB at baseline to 0.47dB at 6 months, with recovery to 1.08dB at 24 months. No significant changes in mean retinal sensitivity occurred in the control eye of the six subjects who showed improvements in their study eye, or in the study or control eyes of the other subjects (Fig. 23).

Plots of peak improvement in mean retinal sensitivity are depicted in Fig. 24.

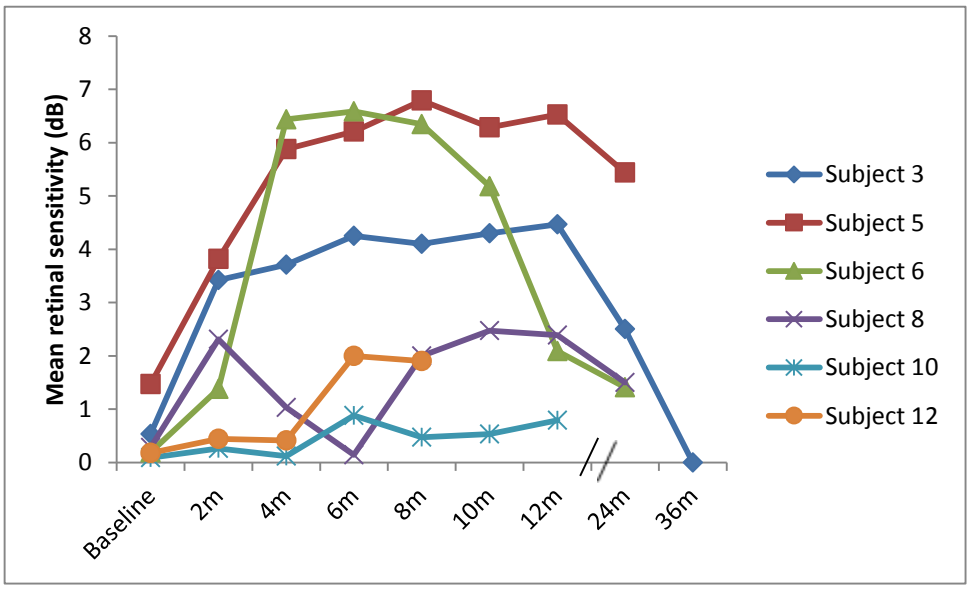

Fig. 21 – Graph of mean retinal sensitivity with microperimetry in subjects showing improvement

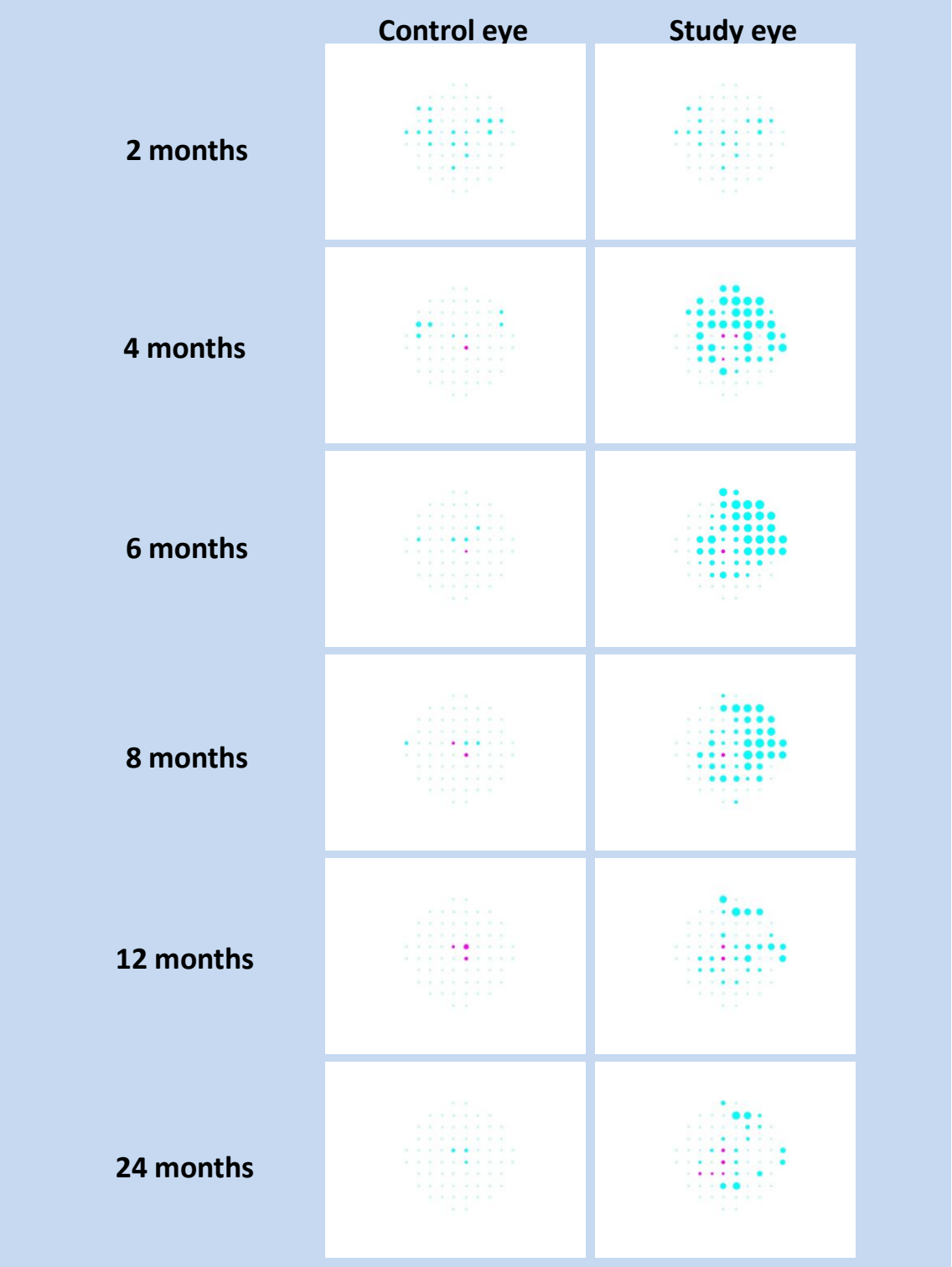

Fig. 22 – Plots of microperimetry retinal sensitivity in subject 6. Blue circles indicate locations of improved sensitivity, and red circles indicate locations of declined sensitivity. The size of the circles indicates retinal sensitivity on a scale of 0 to 14dB. There is a progressive improvement in sensitivity in the study eye until 8 months, after which overall sensitivity declines, although focal locations of improved sensitivity remain.

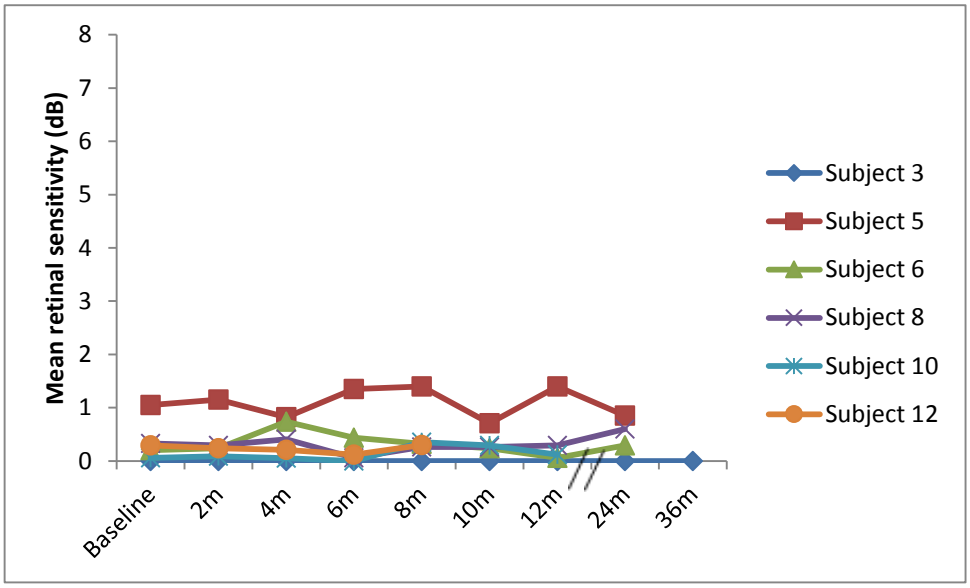

Fig. 23 – Graph of mean retinal sensitivity with microperimetry in control eye of subjects showing improvement with study eye

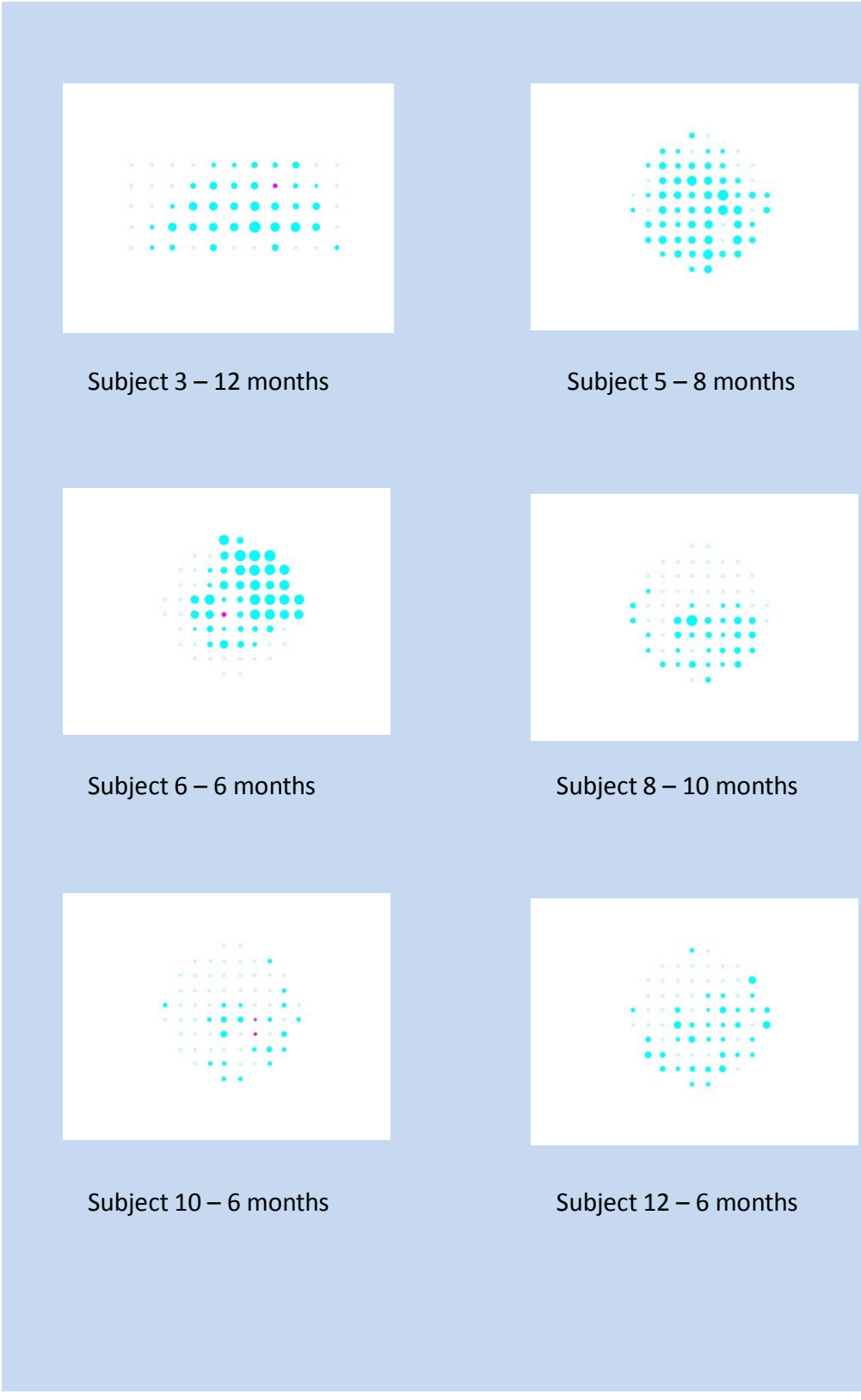

Fig. 24 – Plots of maximum retinal sensitivity in six subjects showing improvement with microperimetry testing.

3.1.11 Visual Mobility Assessment

Visual mobility is assessed in low light conditions by measuring the time taken by the subjects to navigate a simple maze and the number of navigation errors (loss of orientation or touching the barriers) made. Visual mobility improved in 5 subjects (subjects 3, 5, 6, 8 and 10) following treatment.

In subject 3, the travel time reduced from 77 seconds at baseline to 14 seconds at 6 months for the study eye when performed at 4 Lux light level. In addition, the number of mobility errors decreased from 8 to 0 during this period. In the control eye, travel time reduced by a smaller amount from 36 seconds at baseline to 12 seconds at 6 months, and mobility errors reduced from 1 to 0 at 4 Lux.

Subject 5 was unable to perform mobility testing preoperatively at the 2 Lux and 4 Lux levels, due to insufficient ability to see the maze at these low light levels. Postoperatively he was able to undergo assessment and made fewer errors in the study eye at both 2 Lux and 4 Lux compared to the control eye (Fig. 25a and b).

Subject 6 was unable to perform assessment at 2 Lux preoperatively, but postoperatively he was able to undergo testing and made zero errors in the study eye, compared to 4 errors with the control eye. At the 4 Lux level, there was a greater reduction in the errors made postoperatively in the study eye. In addition, travel time was less using the study eye at these light levels (Fig. 25c and d).

Subject 8 was unable to perform assessment at 2 Lux preoperatively, but postoperatively he was able to undergo testing and made zero errors in the study eye, compared to 8 errors with the control eye. At the 4 Lux level, there was a reduction in mobility errors from 5 to 0 after treatment using the study eye, with no decrease in errors made using the control eye. Travel times were also less when using the study eye at these light levels (Fig. 26a and b).

Subject 10 could only perform assessment at the 4 Lux level postoperatively, and made zero mobility errors using the study eye, compared to 7 errors with the control eye. In addition, the travel time was 10 seconds faster when using the study eye (Fig. 26c).

Subject 12 had an increase in the travel time at the 4 Lux level from 67 seconds to 136 seconds in the study eye, and from 80 seconds to 105 seconds. Mobility errors were similar at baseline and at 6 months for both eyes (Fig. 26d).

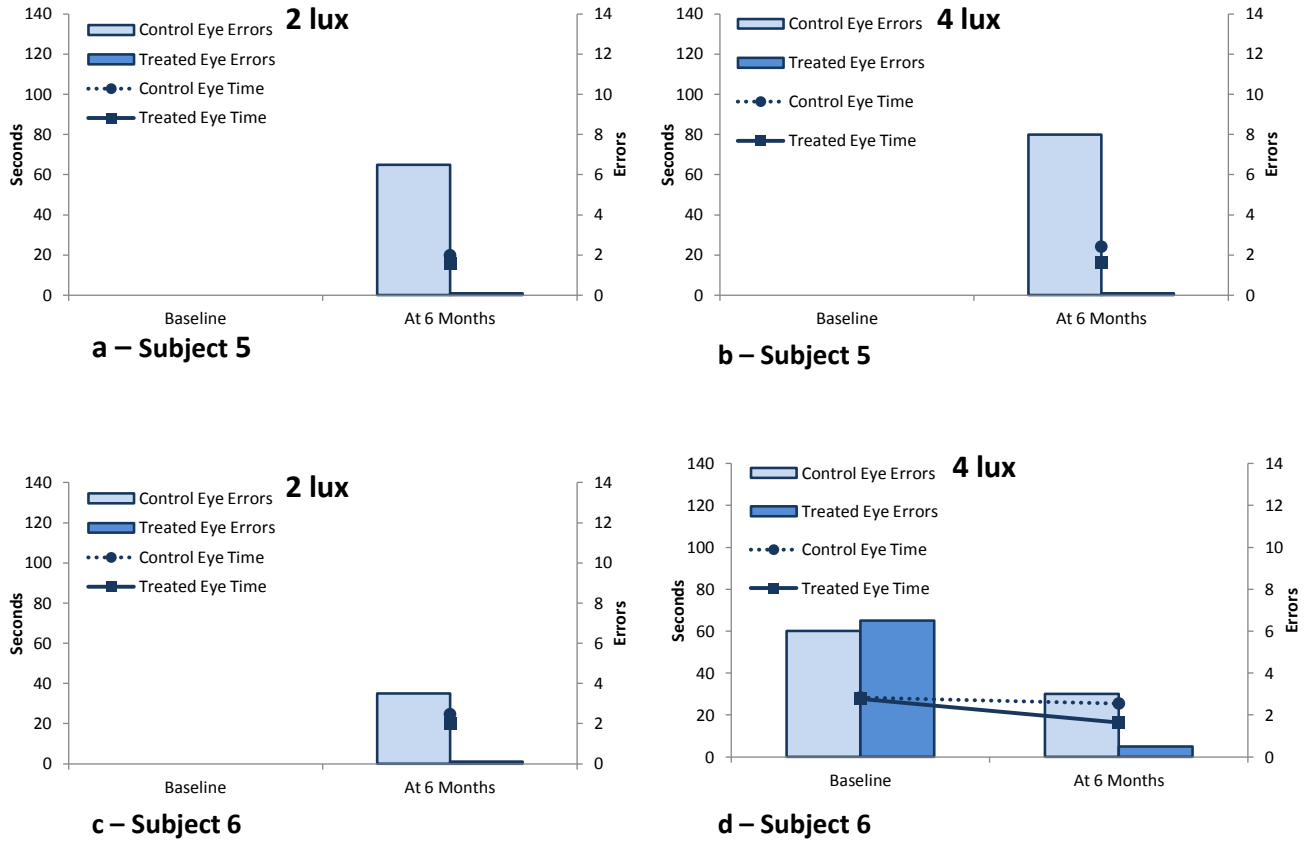

Fig. 25 – Visual mobility plots for subjects 5 and 6

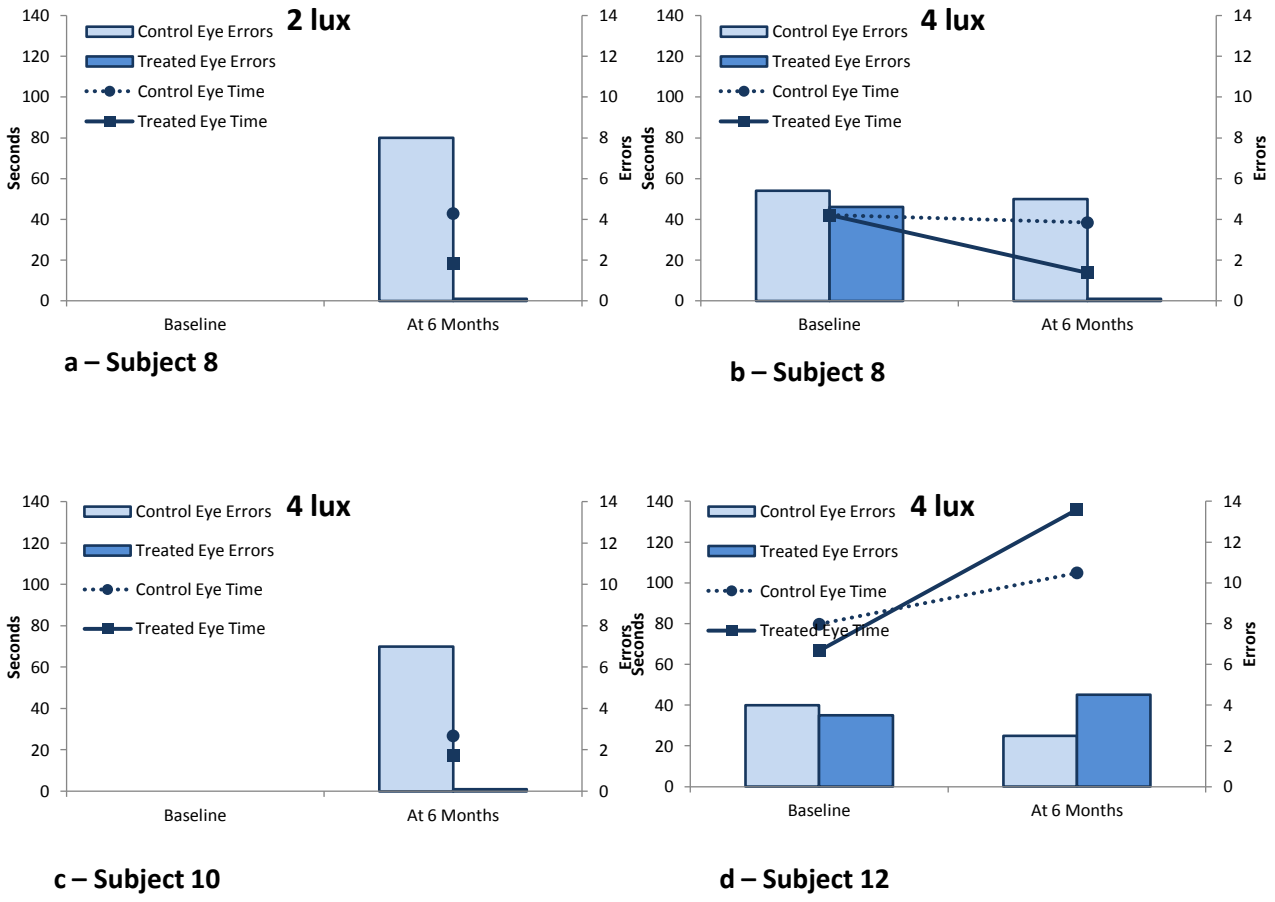

Fig. 26a-d - Visual mobility plots for subjects 8, 10 and 12

3.1.12 OCT Results

Pre-operative and post-operative SDOCT imaging was performed in eight subjects. Examples of the images obtained are shown in figure 28 and 29. Out of these eight subjects (subjects 5-12) five (subjects 5, 6, 7, 8 and 12) had a reduction in foveal thickness of over 15 µm (outside of test-retest variability) in their study eye at 6 months, with no control eye showing a similar reduction (Fig. 27a). In the six subjects (subjects 5-10) who underwent SDOCT and had at least 12 months follow-up, three subjects (subjects 5, 7, 8) had a reduction in foveal thickness of more than 15 µm (Fig. 27b) at final visit. At 24 months, the degree of retinal thinning in subject 6 had lessened to 14 µm, compared to 30 µm at their 6 month visit. The control eye of subject 5 also had a reduction in foveal thickness of more than 15 µm at 24 months. In all five subjects who showed a significant reduction in foveal thickness, thinning of the outer nuclear and photoreceptor layers were a common finding, with subjects 5, 6, 7 and 12 also showing disruption or disappearance of the IS/OS line. Subject 7 also had disruption of the ELM (Fig. 28a and 28b). No retinal thinning occurred in subject 10 (aged 6 years) who also underwent foveal injection (Fig. 29a and 29b).

In the four subjects (subjects 1-4) who only underwent time-domain OCT, retinal thinning outside of test-retest variability occurred in both the study and control eyes of subjects 1 and 3 at 6 months. At final follow-up visit of 36 months, significant retinal thinning had occurred in the study eye of subjects 3 and 4, and in the control eye of subjects 1 and 3.

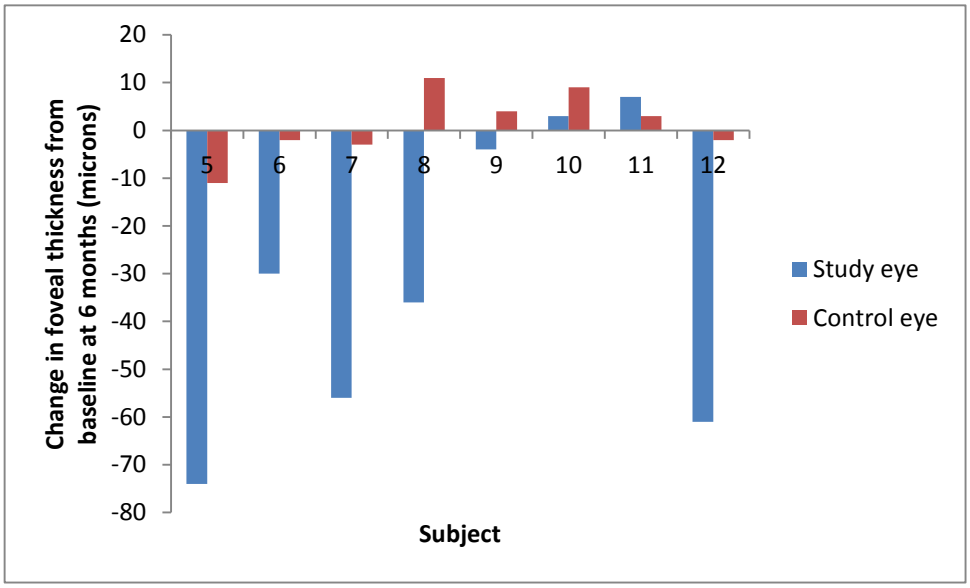

Fig. 27a – Graph showing change in foveal thickness from baseline at 6 months in subjects who underwent SDOCT imaging

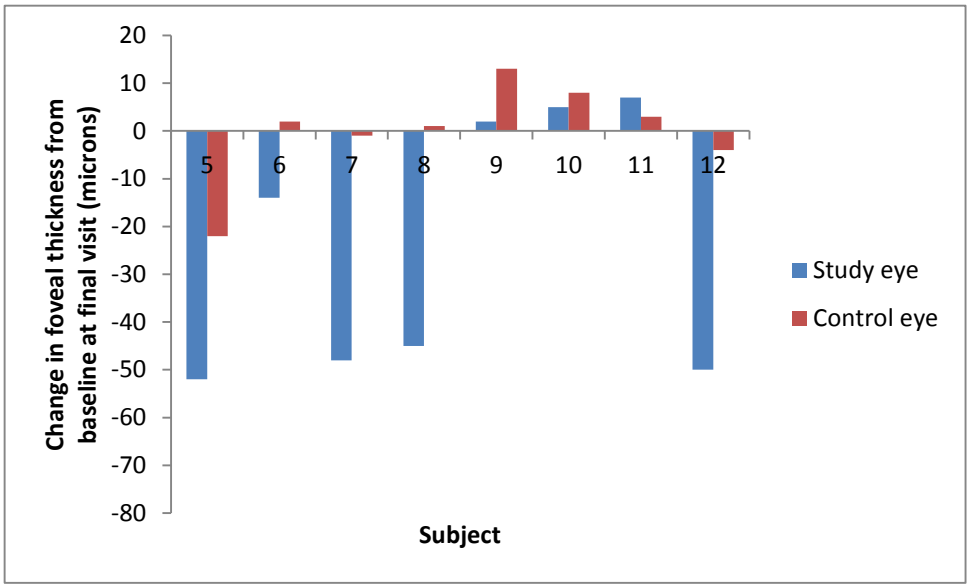

Fig.27b – Graph showing change in foveal thickness from baseline at final visit in subjects who underwent SDOCT imaging

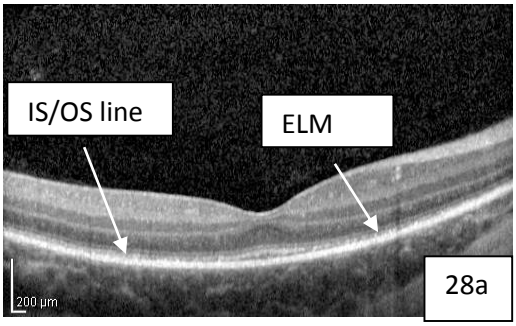

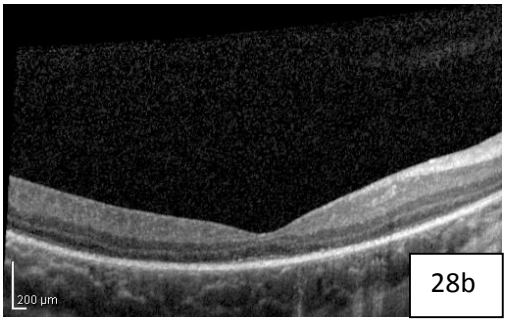

Fig. 28a – OCT at baseline of study eye in subject 7, showing intact IS/OS line and ELM. At 6 months (Fig. 228b), retinal thinning and disruption of the IS/OS line and ELM have occurred.

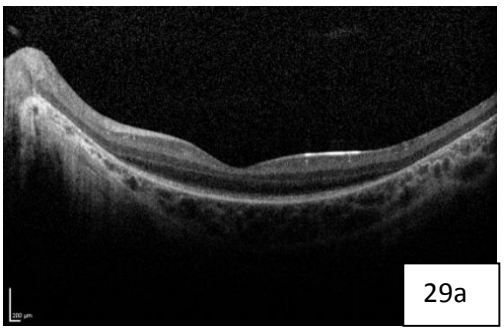

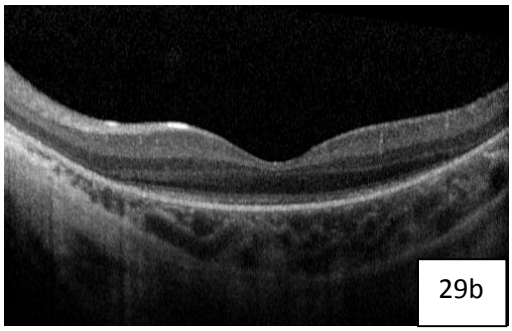

Fig. 29a – OCT at baseline of subject 10 (aged 6) study eye showing intact IS/OS line and ELM, with no retinal thinning or disruption to these layers occurring at 6 months (Fig. 29b).

Correlation of OCT changes with visual acuity

In the 5 subjects with evidence of retinal thinning and disruption on SDOCT imaging, 2 subjects (subjects 7 and 12) also experienced considerable reductions in visual acuity, contrast sensitivity and reading acuity. Both of these subjects showed disruption of the IS/OS junction, with involvement of the ELM in subject 7. Subject 6 showed disruption of the IS/OS junction and had a reduction in contrast sensitivity (of more than 0.2 logCS) but not in visual or reading acuity. Subjects 5 and 8 did not have any significant reduction in vision, nor show disruption in the IS/OS junction or ELM.

In the 5 subjects who showed foveal thinning of more than 20 microns at 6 months in their study eye, the greatest reduction in thickness occurred by 5 days after treatment in 4 out of the 5 subjects, and by 2 weeks in the remaining subject (Fig. 30a). No significant thinning occurred in the control eyes of these subjects at these time points (Fig. 30b).

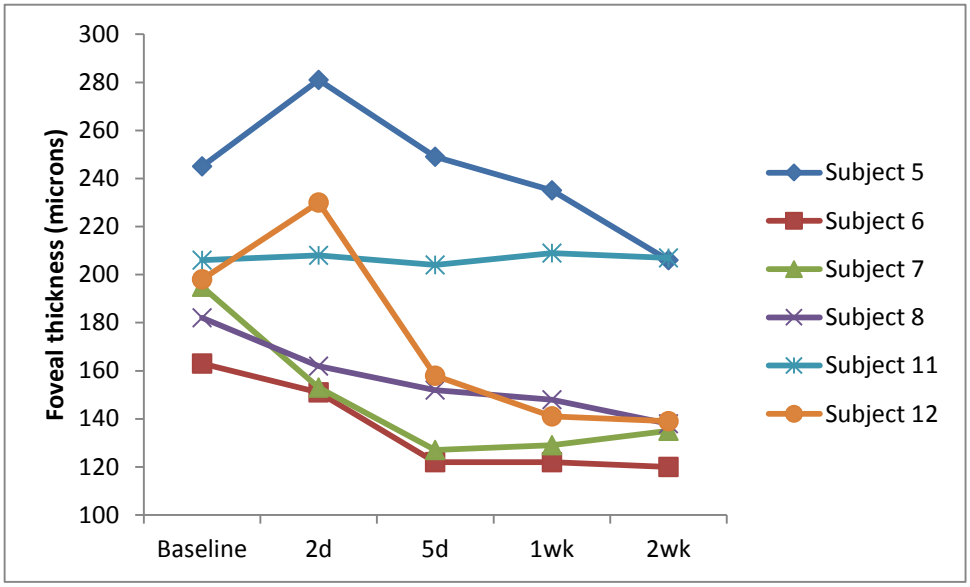

Fig. 30a – Graph showing foveal thickness in the early postoperative period in the study eye

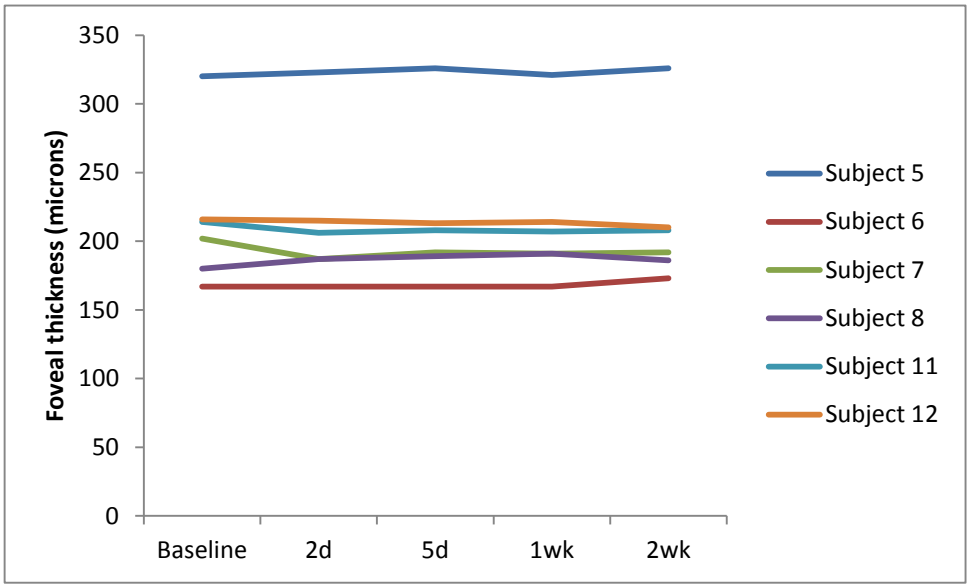

Fig. 30b – Graph showing foveal thickness in the early postoperative period in the control eye

3.2 Retinal structure and function in Achromatopsia: implications for gene therapy

3.2.1 Clinical examination

Twenty male and 20 female subjects with a mean age of 24.9 years (range 6 to 52) were included in this study (Table 8). Mean visual acuity was 0.92 logMAR (range 0.72 to 1.32), mean contrast sensitivity was 1.16 logCS (range 0.50 to 1.55), and mean reading acuity was 0.76 logMAR (range 0.5 to 1.32). There was no significant correlation between age and visual acuity (r=0.18, p=0.27, Fig. 31), contrast sensitivity (r= -0.27, p=0.09) or reading acuity (r=0.29, p=0.07).

All patients were able to read the Ishihara test plate, but were unable to read any subsequent plates, or correctly identify any of the HRR test plates.

Fundus examination revealed no evidence of macular retinal pigment epithelial (RPE) disturbance in 11 patients (mean age 19.5 years; range 6-33), RPE disturbance in 20 patients (mean age 27.5 years; range 12-52), and well-circumscribed macular atrophy in 9 patients (mean age 25.9 years; range 11 to 43) with no significant difference in mean age, visual acuity, contrast sensitivity or reading acuity between these three groups (Table 9).

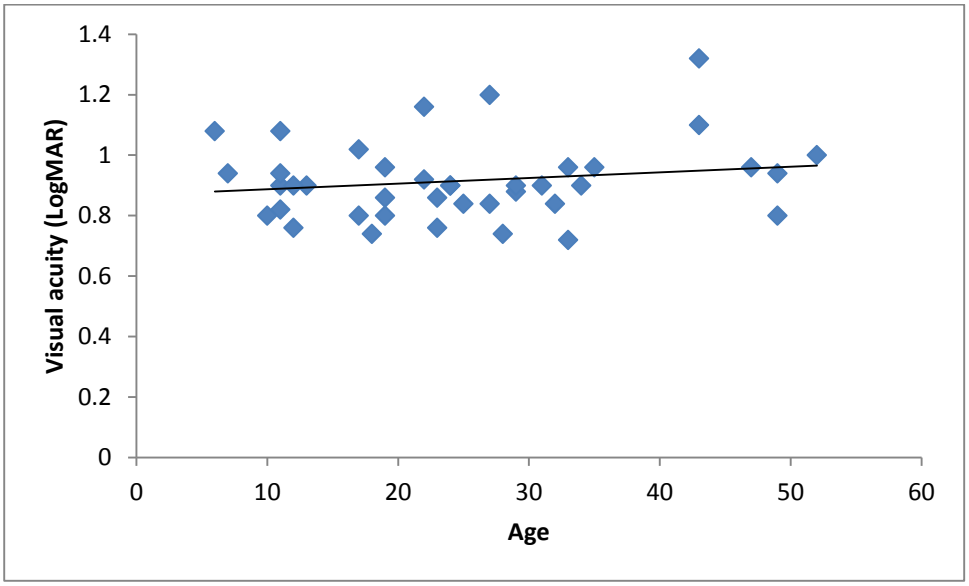

Fig. 31 – Graph showing no significant correlation between age and visual acuity (r=0.18, p=0.27)

Variable	Mean (SD)	Range	Median
Age (years)	24.9 (12.3)	6-52	23.5
Visual acuity (logMAR)	0.92 (0.13)	0.72-1.32	0.9
Contrast sensitivity (logCS)	1.16 (0.23)	0.50-1.55	1.2
Reading acuity (logMAR)	0.76 (0.19)	0.50-1.32	0.73
Retinal sensitivity (dB)	16.6 (3.4)	3.1-19.9	17.6
BCEA (degrees)	13.5 (13.5)	1.7-65	7.7
Genotype	**n (%)**		
CNGA3	17 (42.5)		
CNGB3	15 (37.5)		
GNAT2	4 (10)		
PDE6C	1 (2.5)		
Unknown	3 (7.5)		
OCT category	**n (%)**		
1	9 (22.5)		
2	13 (32.5)		
3	6 (15)		
4	9 (22.5)		
5	3 (7.5		
Foveal hypoplasia	N (%)		
No	16 (40%)		
Yes	21 (52.5)		
Unrecordable	3 (7.5)		
Fundus appearance category	**n (%)**		
1	11 (28)		
2	20 (50)		
3	9 (22)		

Table 8 – Clinical characteristics of patients. OCT category: 1=continuous ISe; 2=ISe disruption; 3=ISe absence; 4=Hyporeflective zone present; 5=Atrophic outer retina. Fundus appearance category: 1=no RPE disturbance; 2=RPE disturbance; 3=atrophy present

Fundus appearance category	**1**	**2**	**3**	
				p value
Age (years)				
Mean (SD)	19.5 (10.6)	27.5 (13.7)	25.9 (9.9)	
Range	6-33	12-52	11-43	
Median	22	23.5	25	0.22
Visual acuity (logMAR)				
Mean (SD)	0.92 (0.13)	0.90 (0.09)	0.94 (0.2)	
Range	0.72-1.16	0.74-1.1	0.8-1.32	
Median	0.9	0.9	0.84	0.68
Contrast sensitivity (logCS)				
Mean (SD)	1.22 (0.19)	1.18 (0.24)	1.06 (0.21)	
Range	0.90-1.45	0.70-1.55	0.50-0.9	
Median	1.25	1.2	0.7	0.25
Reading acuity (logMAR)				
Mean (SD)	0.77 (0.15)	0.77 (0.23)	0.72 (0.14)	
Range	0.58-1.00	0.54 -1.05	0.5-0.9	
Median	0.8	0.7	0.7	0.8
Retinal sensitivity (dB)				
Mean (SD)	16.9 (1.9)	17.3 (2.6)	14.5 (5.5)	
Range	14.9-19.8	12.8-19.9	3.1-19.7	
Median	17.6	18.4	16.7	0.38
BCEA (degrees)				
Mean (SD)	19.5 (20.9)	10.3 (8.6)	13.2 (9.7)	
Range	3.9-65	2.3-38.5	2.5-32.9	
Median	13.7	7.4	15.1	0.69

Table 9 - Mean, standard deviation, range and median values of testing parameters in different fundus appearance categories. 1=no RPE disturbance; 2=RPE disturbance; 3=atrophy present

3.2.2 Retinal morphology

On the basis of SDOCT imaging, subjects were placed into one of 5 OCT groups: (i) 9 patients (22.5%) had a continuous inner segment ellipsoid (ISe) layer at the fovea (mean age 26.8 years; range 6 to 52); (ii) 13 (32.5%) had ISe disruption (mean age 24.4 years; range 11 to 34); (iii) 6 (15%) had an absent ISe layer at the fovea (mean age 22.7 years; range 7 to 43); (iv) 9 (22.5%) had a hyporeflective zone (HRZ) (mean age 28.2; range 11 to 49); and (v) the remaining 3 subjects (7.5%) had evidence of outer retinal atrophy, including RPE loss (mean age 25 years; range 23 to 27) (Table 10).

There were no significant differences in the age ($p=0.54$), visual acuity ($p=0.14$) or contrast sensitivity ($p=0.42$) between patients in the five OCT categories; however intriguingly reading acuity was significantly lower ($p=0.09$) in patients with no ISe disruption compared to patients with a HRZ (Table 10). Figure 32 shows representative SDOCT images of patients of different ages.

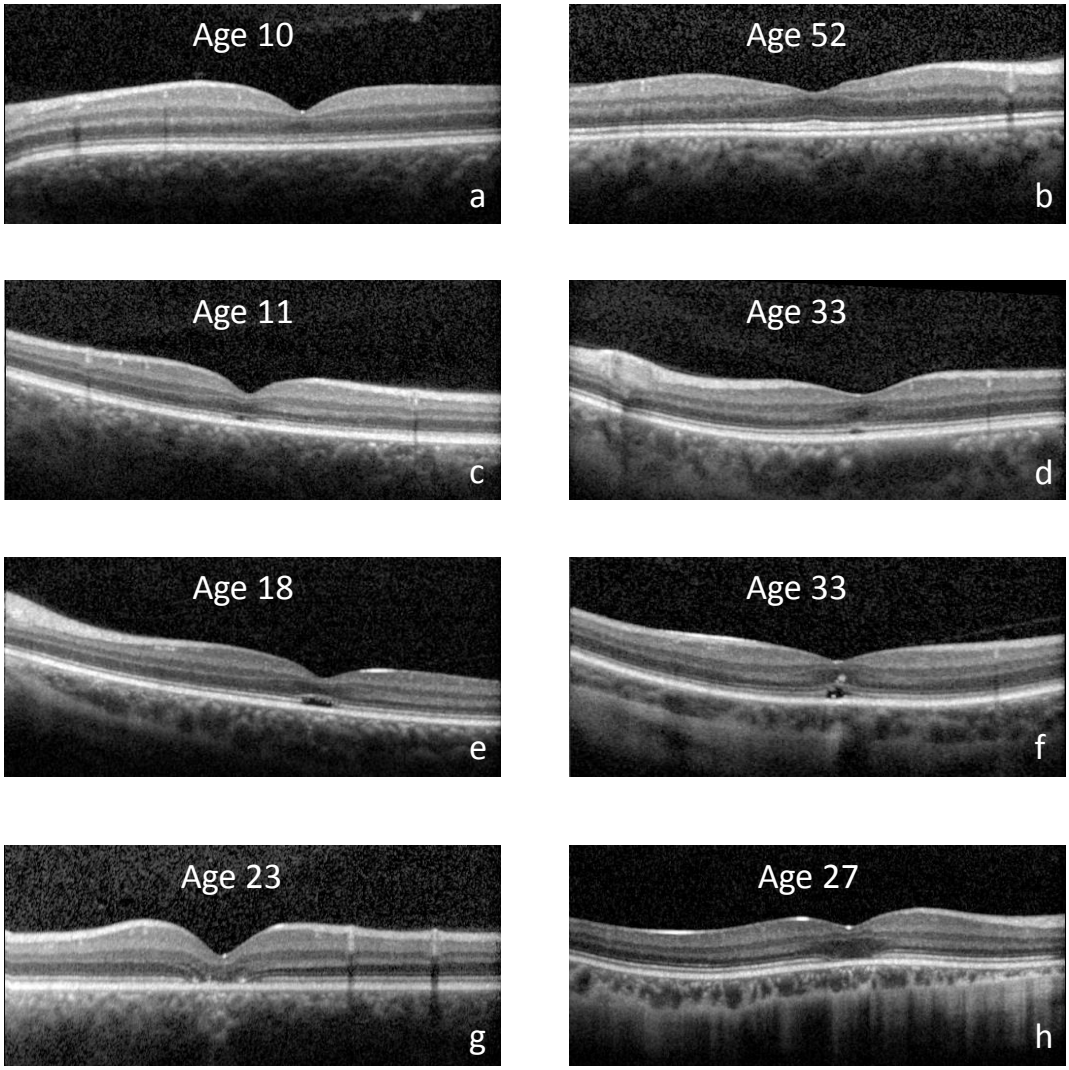

Fig. 32 – SDOCT appearance in patients of various ages. No IS/OS disruption is present in (a) or in (b), who is aged 52. IS/OS disruption is present in an 11 year old (c) and in (d). HRZ presence is shown in (e) and (f), with complete cone loss occurring in (g) and (h).

OCT Group	1 (n=9)	2 (n=13)	3 (n=6)	4 (n=9)	5 (n=3)	
						p value
Age (yrs)						
Mean (SD)	26.8 (18.0)	22.4 (9.4)	22.7 (12.0)	28.2 (12.8)	25 (2)	
Range	6-52	11-34	7-43	11-49	23-27	
Median	24	22	21	28	25	0.83
Visual acuity (logMAR)						
Mean (SD)	0.95 (0.13)	0.92 (0.10)	0.95 (0.19)	0.85 (0.08)	0.93 (0.23)	
Range	0.72-1.1	0.76-1.16	0.8-1.32	0.74-0.96	0.76-1.2	
Median	0.94	0.9	0.9	0.86	0.84	0.48
Contrast sensitivity (logCS)						
Mean (SD)	1.09 (0.33)	1.11 (0.23)	1.21 (0.15)	1.25 (0.13)	1.25 (0.1)	
Range	0.5-1.45	0.65-1.35	1.05-1.45	1.05-1.45	1.15-1.35	
Median	1.2	1.05	1.2	1.25	1.25	0.47
Reading acuity (logMAR)						
Mean (SD)	0.92 (0.25)	0.76 (0.13)	0.70 (0.16)	0.66 (0.13)	0.68 (0.11)	
Range	0.6-1.32	0.54-0.9	0.5-0.9	0.5-0.92	0.56-0.77	
Median	0.99	0.8	0.65	0.68	0.7	0.02∗
Retinal sensitivity (dB)						
Mean (SD)	16.1 (2.8)	17.4 (2.1)	16.3 (4.5)	17.4 (2.1)	12.3 (8.1)	
Range	12.8-19.8	13.6-19.8	7.8-19.9	14.3-19.7	3.1-18.4	
Median	14.9	17.6	18	17.8	15.4	0.70
BCEA (degrees)						
Mean (SD)	21.3 (19.7)	9.9 (4.9)	15.7 (14.8)	9.2 (11.9)	14.3 (11.6)	
Range	3.8-40.8	2.5-16.8	4.7-44	1.7-37.5	3.6-32.9	
Median	14.4	9.4	11.3	3.75	6.4	0.18

Table 10 – Mean, standard deviation, range and median values of testing parameters in different OCT categories. OCT category 1=continuous ISe; 2=ISe disruption; 3=ISe absence; 4=Hyporeflective zone present; 5=Atrophic outer retina. ∗Bonferroni post-hoc analysis shows a significant difference in reading acuity between OCT category 1 and 4

Foveal hypoplasia, defined as the persistence of one or more inner retinal layers (outer plexiform layer, inner nuclear layer, inner plexiform layer or ganglion cell layer) through the foveal centre, was found in 21 (52.5%) patients; with it not being possible to assess hypoplasia in 3 patients due to severe foveal atrophy. There was no significant difference in age, visual acuity, reading acuity or fixation stability between patients with or without foveal hypoplasia. Contrast sensitivity (p=0.02) and retinal sensitivity (p=0.03) were higher in patients with evidence of foveal hypoplasia compared to those without (Table 11).

Hypoplasia	**No (n=16)**	**Yes (n=21)**	
			p value
Age (yrs)			
Mean (SD)	27.5 (14.6)	22 (10.3)	
Range	6-52	7-49	
Median	26.5	22	0.08
Visual acuity (logMAR)			
Mean (SD)	0.96 (0.11)	0.85 (0.07)	
Range	0.72-1.16	0.74-0.96	
Median	0.95	0.86	0.14
Contrast sensitivity (logCS)			
Mean (SD)	1.07 (0.29)	1.23 (0.14)	
Range	0.5-1.55	0.9-1.45	
Median	1.05	1.25	0.02
Reading acuity (logMAR)			
Mean (SD)	0.90 (0.18)	0.65 (0.12)	
Range	0.6-1.32	0.5-0.9	
Median	0.86	0.62	0.19
Retinal sensitivity (dB)			
Mean (SD)	16.2 (2.4)	17.9 (1.86)	
Range	12.8-19.8	13.8-19.8	
Median	15.6	18.4	0.03
BCEA (degrees)			
Mean (SD)	15.0 (16.6)	11.7 (10.9)	
Range	1.7-40.7	3.7-37.4	
Median	8.6	7.3	0.56
Mutation	%	%	
CNGA3	31	52	
CNGB3	38	38	
GNAT2	25	0	
PDE6C	U	U	
Unknown	6	10	

Table 11 - Mean, standard deviation, range and median values of testing parameters in patients with and without foveal hypoplasia. The percentage of patients within genotypes is also shown. U=unclassifiable.

3.2.3 Microperimetry

All 40 patients underwent microperimetry testing on two occasions. There were significant correlations in mean retinal sensitivity and fixation stability between both eyes, and further analysis was performed using the left eye. No significant difference in mean retinal sensitivity or fixation stability was found between patients' first and second test, and the mean of these two tests was used for subsequent analysis. The mean retinal sensitivity of the group was 16.6 dB (range 3.1 to 19.9 dB) and significant negative correlations were found between retinal sensitivity and age (rho= -0.39, p=0.01, Fig. 33), visual acuity (rho= -0.44, p<0.01, Fig. 34) and reading acuity (rho= -0.55, p=<0.01). Surprisingly, a significant correlation was found between lower contrast sensitivity and a higher microperimetry score (rho=0.35, p=0.03). There was no significant difference in the retinal sensitivity or fixation stability (p=0.30) between OCT groups (p=0.24, Table 10). There was a significant correlation between fixation stability and visual acuity (rho=0.43, p<0.01), and unexpectedly, lower contrast sensitivity was significantly associated with a higher fixation stability (rho= -0.43, p<0.01).

Six patients had a scotoma (defined as 0 dB retinal sensitivity in at least any 1 location) with a mean retinal sensitivity in this group of 11.0 db (range 3.1 to 14.8 dB), and mean fixation stability of 12.8° (range 1.7° to 24°). The mean age of these patients was 40.2 years (range 25 to 52 years), and mean visual acuity was 1.01 logMAR (range 0.8 to 1.32). Four of these 6 patients had RPE disturbance on fundus examination, with the remaining 2 patients having macular atrophy. Variable macular structure was seen on SDOCT, with 3 of the 6 subjects having a normal ISe layer, and 1 patient having either an absent foveal ISe layer, or HRZ, or outer retinal atrophy respectively.

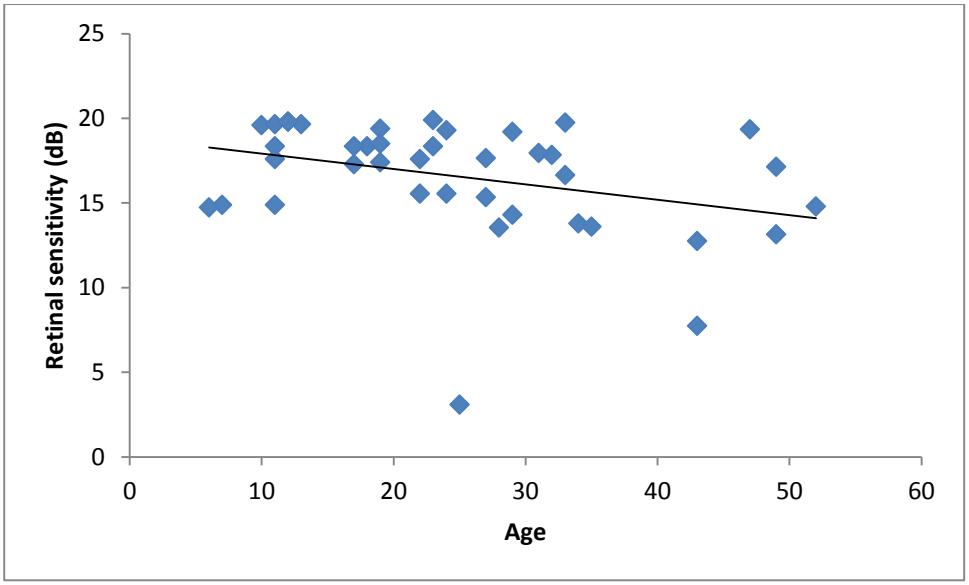

Fig. 33 – Graph showing a significant negative correlation between age and retinal sensitivity (rho= -0.39, p=0.01)

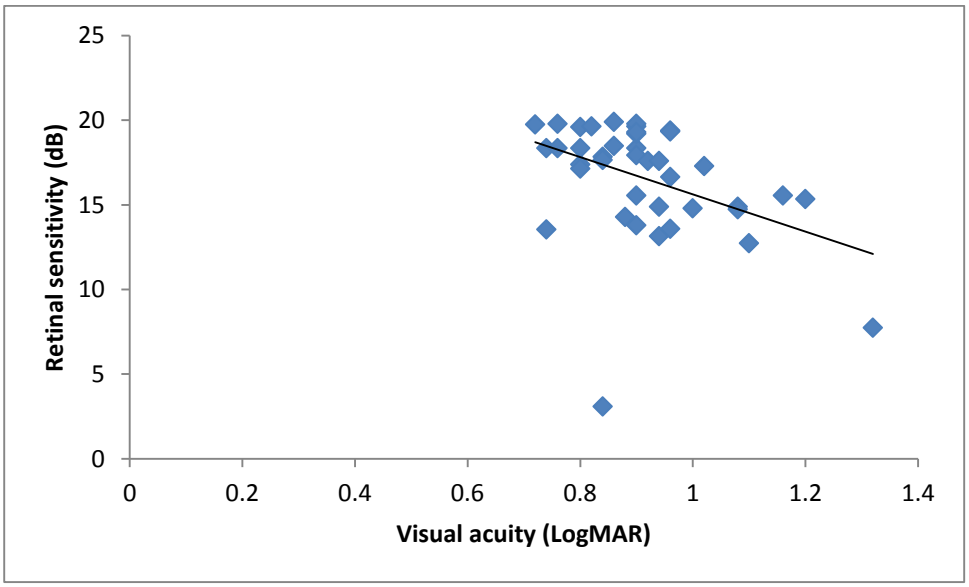

Fig. 34 – Graph showing a significant negative correlation between visual acuity and retinal sensitivity (rho= -0.44, p<0.01)

3.2.4 Molecular Genetics

Seventeen patients (42.5%) had *CNGA3* mutations (mean age 24.8 years; range 7-49), 15 (37.5%) had *CNGB3* mutations (mean age 20.4 years; range 6-47), 4 (10%) had *GNAT2* mutations (mean age 43.3 years; range 29-52), and 1 subject had a *PDE6C* mutation. No sequence variants were found in 3 individuals.

3.2.5 Genotype-phenotype correlation

The majority (80%) of patients in our study had either *CNGA3* or *CNGB3* mutations. Statistical analysis between the patients with these two genotypes showed no significant difference in terms of age, visual acuity, contrast sensitivity, reading acuity, or fixation stability (Table 12). However, retinal sensitivity was greater in the *CNGB3* group compared to the *CNGA3* group (18.1dB versus 16.1dB, p=0.04).

A comparison of the SDOCT images in the two genotype groups showed that 26.7% (n=4) of patients with *CNGB3* mutations had no ISe disruption, compared to 5.9% (n=1) with *CNGA3* sequence variants; and fewer (33.3%, n=5) patients harbouring *CNGB3* variants had ISe disruption compared to 47% (n=8) in the *CNGA3* group. The percentage of patients with a HRZ was similar in both groups - 23.5% (n=4; *CNGA3*) and 26.7% (n=4; *CNGB3*). An atrophic outer retina was observed in 13.3 % (n=2) of *CNGB3* patients compared to 5.9% (n=1) of *CNGA3* patients. In the *CNGA3* group, 69% (n=11) of patients had foveal hypoplasia, compared to 57% (n=8) of *CNGB3* patients. Foveal hyperplasia was not present in any patient with a *GNAT2* mutation (n=4), and the single *PDE6C* patient had severe foveal atrophy. On clinical examination, 41% (n=7) of *CNGA3* patients had a normal fundus appearance, compared to 20% (n=3) of patients in the *CNGB3* group, and also fewer (35%; n=6) *CNGA3* patients had RPE disturbance compared to subjects with *CNGB3* variants (53%; n=8). The percentage of patients with macular atrophy was similar in both groups (CNGA3 - 24%,n=4 and CNGB3 - 27%, n=4). Only one (*CNGA3* subject) of the six patients with a scotoma on microperimetry harboured variants in either of these two genes. The remaining 5 individuals had *GNAT2* mutations (n=4) and *PDE6C* variants (n=1). In addition, visual acuity, contrast sensitivity, reading acuity and mean retinal sensitivity were lower in these genotypes, compared to the *CNGA3* or *CNGB3* groups; however the mean age of patients with either *GNAT2* or *PDE6C* mutations was considerably higher than the *CNGA3*/*CNGB3* group and moreover reliable comparisons are limited by the relatively small number of patients harbouring these rarer genotypes (Table 12). Interestingly, 3 out of the 4 patients with *GNAT2* mutations had an intact ISe layer, despite a relatively low mean retinal sensitivity of 13.6dB and all of these patients having a central scotoma on microperimetry.

Genotype	***CNGA3* (n=17)**	***CNGB3* (n=15)**	***GNAT2* (n=4)**	***PDE6C* (n=1)**	
					p value
Age (yrs)					
Mean (SD)	24.8 (10.4)	20.4 (11.0)	43.3 (10.2)	43	
Range	7-49	6-47	29-52		
Median	25	18	46		0.21
Visual acuity (logMAR)					
Mean (SD)	0.88 (0.1)	0.90 (0.13)	0.98 (0.09)	1.32	
Range	0.74-1.16	0.72-1.2	0.88-1.1		
Median	0.9	0.9	0.97		0.76
Contrast sensitivity (logCS)					
Mean (SD)	1.19 (0.21)	1.21 (0.16)	0.86 (0.32)	1.05	
Range	0.65-1.55	0.9-1.45	0.5-1.2		
Median	1.2	1.25	0.88		0.91
Reading acuity (logMAR)					
Mean (SD)	0.72 (0.13)	0.73 (0.16)	1.12 (0.17)	0.9	
Range	0.5-0.9	0.54-1.00	0.92-1.32		
Median	0.7	0.7	1.13		0.96
Retinal sensitivity (dB)					
Mean (SD)	16.1 (3.9)	18.1 (1.76)	13.8 (0.96)	7.8	
Range	3.1-19.6	15.4-19.8	12.8-14.8		
Median	17.6	18.4	13.7		0.04
BCEA (degrees)					
Mean (SD)	12.1 (11.9)	13.2 (16.3)	14.0 (9.8)	17.1	
Range	2-44	3.7-65	1.7-24		
Median	7.7	7.3	15.1		0.82
OCT group	%	%	%		
1	5.9	26.7	75		
2	47	33.3	0		
3	17.6	0	0	100	
4	23.5	26.7	25		
5	5.9	13.3	0		
Fundus appearance	%	%	%		
1	41	20	0		
2	35	53	100		
3	24	27	0		

Table 12 - Mean, standard deviation, range and median values of testing parameters in different genotype categories. Statistical comparisons are between *CNGA3* and *CNGB3* groups only. The percentage of patients within genotypes with the various OCT and fundus changes is also shown.

3.2.6 Structure-Function Correlation using MMM

Five patients from each of the *CNGA3* and *CNGB3* groups, and 3 patients with *GNAT2* mutations, underwent MMM analysis, which allows co-registration of microperimetry with SDOCT imaging. A consistent correlation between retinal structure and function was not found, with 4 out of 5 *CNGB3* patients having either ISe absence or HRZ presence, still displaying at least 16dB retinal sensitivity in these areas of outer retinal change. In the 3 *CNGA3* patients with either ISe absence or HRZ presence, 2 patients had a reduction in retinal sensitivity to at least 10dB. All three of the GNAT2 patients had locations with 0dB sensitivity, with 2 of these patients having normal outer retinal structure. Fig. 35 shows MMM examples of inconsistent structure-function correlation.

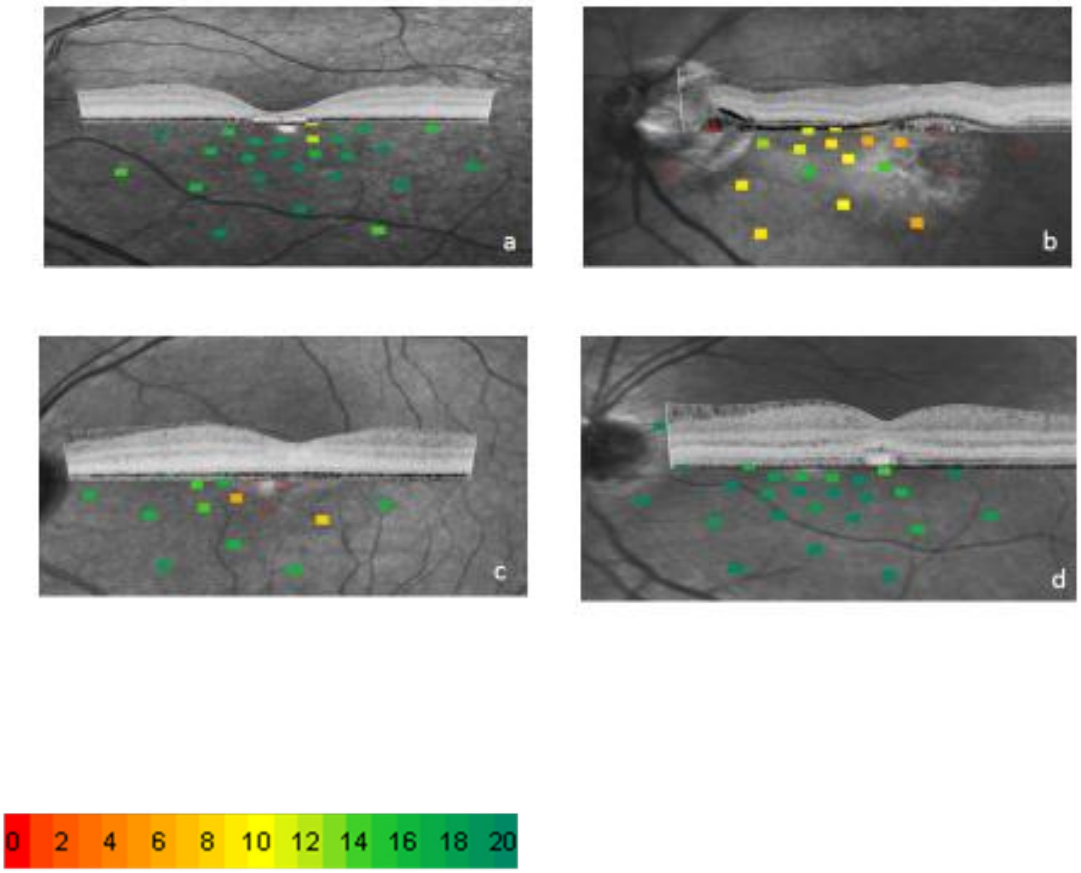

Fig. 35 – Overlay of SDOCT and Microperimetry, illustrating an inconsistent structure-function relationship. Retinal sensitivity derived from microperimetry is presented according to the scale panel in 2dB steps. Normal sensitivity is indicated by green colour and reduce sensitivity is indicated by red. Open red squares represent absolute defects.

In (a) Retinal sensitivity is reduced (red square) in a region corresponding with HRZ presence. In (b), reduced retinal sensitivity occurs in an area of complete cone loss with RPE involvement in a subject with a *CNGA3* mutation. The extent of foveal atrophy and photoreceptor loss in this patient was not typical of other *CNGA3* patients who had generally lesser degrees of retinal atrophy. However, in (c), retinal sensitivity is reduced despite there being no IS/OS disruption, and in (d), retinal sensitivity is high (green squares) in a region of HRZ presence in a *CNGB3* patient.

Discussion

4.1 RPE65 Trials

The commencement of 3 clinical gene therapy trials for RPE65 deficiency within a similar time period has given an opportunity to evaluate the results from a relatively large number of subjects, and to assess whether differences in treatment strategies have an impact on safety and efficacy. The results from each trial are individually discussed, followed by a collective summary of the pertinent results.

4.1.3 Bainbridge/Ali group

In this study, 12 subjects aged from 6 to 23 years underwent vitrectomy and subretinal rAAV2/2.hRPE65p.hRPE65 injection. A human *RPE65* promoter was used in this trial with the aim of limiting gene expression to RPE cells, instead of the more ubiquitous expression that occurs with the chicken β-actin promoter used in the two US trials (110, 111). Two different dose levels were used with the first 4 subjects receiving the lower dose of $1x10^{11}$ vector genomes, and the remaining 8 subjects receiving the higher dose of $1x10^{12}$ vector genomes. Foveal detachment was induced in 10 of the 12 eyes and follow-up ranged from 8 months to 3 years post treatment.

No significant adverse immune events occurred in this study. Subject 7 had a rise in neutralising antibodies and circulating antibodies to AAV2 between week 4 and month 8. This subject experienced mild anterior uveitis at week 6, and this responded to a further short period of topical steroid therapy. Tear samples were transiently positive at low levels for vector DNA sequences in 1 low dose subject and 2 high dose subjects (subjects 7 and 10) at 1 day after surgery only. No detection of vector DNA was found in peripheral blood or saliva in any subject.

Subjects 8 and 9 experienced mild and transient intraocular inflammatory episodes, which in both cases were asymptomatic, had no evidence of an adverse effect on visual function and resolved following a further course of oral corticosteroids. Both of these subjects had mild rises in neutralising antibodies to AAV2 which occurred at similar times to their periods of intraocular inflammation, suggesting that the inflammation may have arisen from an immune response to residual vector capsid.

One of these subjects showed improvement in both microperimetry and dark adapted perimetry, but their improvement was uniquely fluctuating with a temporary decline in retinal sensitivity with microperimetry between months 4 and 6, and occurring between months 8 and 10 with dark adapted perimetry testing. This patient had a mild degree of optic nerve head swelling 6 weeks following surgery, with the intraocular inflammation settling between months 2 and 3. The timing of

inflammation preceded the temporary reduction in retinal sensitivity improvement, and although the optic nerve inflammation was not associated with an adverse effect on visual acuity, it may have limited the improvement evident on perimetric testing. It is unclear why the decline in sensitivity occurred earlier with microperimetry, but may be due to the greater degree of cone involvement with this test and cone responses possibly being more susceptible than rod responses to optic nerve inflammation.

Reductions in reading acuity greater than 0.3 logMAR occurred in the study eye of 3 out of 8 subjects tested at 6 months. 1 further subject had a significant reduction in reading acuity at their final follow-up visit at 36 months, and no significant reductions occurred in the control eyes. Subject 7 was the only subject with significant reductions in both visual and reading acuity. 2 subjects had no significant reduction in visual acuity at 6 months (0.06 logMAR reduction in subject 2 and no change in subject 3), but both had a 0.32 logMAR visual acuity reduction at 36 months, possibly suggesting that continued disease progression may have accounted for this – although similar reductions in acuity were not observed in the control eyes. Subject 12 had a visual acuity reduction of 0.26 logMAR associated with a subjective deterioration in visual acuity . Subject 11 had more than a 0.3 logMAR improvement in acuity in both eyes at 6 months, but not at their last follow-up visit, suggesting that a learning effect may account for these changes.

A significant reduction in foveal thickness occurred in 5 out of the 8 subjects who underwent SDOCT, with a mean decrease of 51 microns in their study eye, compared to a mean decrease of 1 micron in the their control eye. All these subjects had subretinal injections involving the fovea. In the 4 subjects with at least 24 months of follow-up, foveal thickness remained significantly reduced compared to baseline in 3 subjects. The extent of foveal thinning recovered in subject 6, from 30 microns at 6 months to 14 microns at 24 months. Subject 10 (aged 6 years), who also underwent foveal detachment, did not develop foveal thinning. No foveal thinning was evident in the 2 subjects whose treatment area did not involve the fovea.

The reduction in foveal thickness seen in the 5 subjects was primarily attributable to changes in outer retinal structures. Thinning of the outer nuclear and photoreceptor layers were consistent findings. The IS/OS junction and the ELM structures were most well defined preoperatively in subject 7, and postoperatively there was significant disruption to both of these layers, with this subject also experiencing the largest reductions in visual acuity.

Structural changes reported to occur following rhegmatogenous retinal detachment include disruption of the inner segment/outer segment junction and the external limiting membrane (112,

113). Postoperative visual acuity has been correlated with the integrity of these layers following detachment repair and also, inner segment/outer segment disruption has only been reported to occur in macula-off detachments (112). The predictable adverse impact of retinal detachment on retinal structure and function may be dependent on the duration and height of the detachment. A shallower preoperative height of macula-off detachments has been shown to correlate with a better postoperative visual acuity (114, 115), in animal models of retinal detachment providing evidence that PR degeneration increases with the distance between the RPE and PR layers in experimental detachments. PR degeneration has been shown to be reduced by maintaining hyperoxic conditions during the period of detachment in a feline model of retinal detachment (116). This suggests that the loss of oxygen supply to the retina from the choriocapillaris is an important factor in the outer retinal disruption that can occur after detachment. In higher macula-off detachments, the greater amount of subretinal fluid present may make the diffusion of oxygen and other nutrients more difficult to the outer retina, therefore possibly contributing to the greater amount of PR degeneration and worse visual outcomes.

However, a significant degree of retinal thinning was observed in the treated eye of a number of subjects with fovea involving injections in both this study and that described by the Jacobson group, despite considerably less volume of fluid injected in the Jacobson study. These findings underline the importance of carefully weighing the balance of risk and when considering subfoveal vector injection for gene therapy. Eyes with good visual acuity at the time of intervention are more likely to sustain detachment-mediated deterioration in acuity than those with poor acuity at baseline

In 4 out of the 5 subjects with significant foveal thinning with SDOCT, the greatest reduction in thickness occurred within 1 week following surgery, and by 2 weeks in the remaining subject. Various animal models have shown that retinal detachment induces PR cell apoptosis which follows a consistent timeline of apoptotic PR cells seen within a few hours, peaks at 2 to 3 days and then reduces to a low level after day 7 following retinal detachment (117, 118). A similar pattern of PR apoptosis has also been found following retinal detachment in humans, with apoptosis occurring within 24 hours, peaking at day 2 and dropping to a low level after day 7 (119). The timing of the largest reductions in retinal thickness seen in our subjects is in keeping with the experimental evidence of PR death occurring relatively early following retinal detachment.

Significant improvements in retinal sensitivity with dark adapted perimetry using a blue light stimulus occurred in the study eye of 6 subjects. Subjects 3, 5 and 6 had the most number of locations showing significant improvements in retinal sensitivity. In subject 3, peak improvement occurred earlier than in other subjects at 4 months, with improvement declining considerably by 12

months. However, at 36 months follow-up, although the number of locations showing significant sensitivity improvement was considerably less than at 4 months, the mean decibel sensitivity of the locations with remaining improvement was maintained, indicating that focal improvements can be sustained. In addition, the number of locations with a reduction in sensitivity was greater in the control eye of subject 3 compared to their study eye, perhaps suggesting a protective effect on rod function following therapy. Subjects 5 and 6 also showed improvements in a few locations in their control eyes, with the timing of improvement and decline similar to their respective study eyes. The significance of these findings is uncertain and improvements in the control eyes have not been reported in the other trials.

The same 6 subjects also showed improvement in retinal sensitivity with microperimetry testing. Subjects 5 and 6 had the greatest improvements, however peak improvement was only maintained in subject 5 at 24 months follow-up. Although subject 3 showed evidence of maintained sensitivity improvement at specific loci with dark adapted perimetry, this was not the case with microperimetry testing with sensitivity declining to 0dB at 36 months. No significant improvements in sensitivity occurred in the control eye with microperimetry testing.

5 out of the 6 subjects who showed improvements with dark adapted perimetry and microperimetry testing, also showed improvements in visual mobility assessment. Postoperatively, 4 of these subjects were able to navigate the mobility maze at low light levels which they were unable to perform at prior to treatment, and made fewer errors when using the study eye.

Out of the 6 subjects who did not show improvement in any of the investigations, 3 of them had the lowest baseline visual acuities and received the lower treatment dose. The other 3 subjects who did not respond, received the higher dose but had the most severe predicted mutation effects as a result of either their homozygous nonsense or homozygous splice mutations. In contrast, the 2 subjects with the most pronounced improvements had mild predicted mutation effects from homozygous Y368H missense mutations, and received the higher dose. A surprising result was that in the 2 younger subjects aged 6 and 10 who showed some improvement, the degree of improvement was considerably less than in the older subjects who also received the higher treatment dose. This finding is in contrast to the results from the Maguire group which suggested that greater improvements occurred in younger subjects.

A limitation of this study is that by being a non-comparative interventional case series, there was not a sham treatment arm. However, it was decided that were subjects to undergo a vitrectomy and sham injection in the fellow eye, then this would involve an inappropriate level of risk – namely the

well reported potential complications of pars-plana vitrectomy which include infection, retinal tears, retinal detachment and cataract formation. In addition, as *RPE65* LCA is a relatively slowly progressive condition and that as subjects were to undergo repeated baseline assessments (and follow-up assessments), it was felt that any significant change in retinal function following treatment would be greater than that what would expected from natural disease progression or test-retest variability. Further support for the decision to not inject the contralateral eye is derived from animal studies which demonstrated that visual function in eyes that were treated with a sham injection, were similar to baseline measurements (120).

In summary, this trial provides support for the safe use of an AAV2 vector in retinal gene therapy with no serious immune related adverse events occurring. Fifty percent of subjects showed evidence of improved retinal function following treatment, although peak effects were generally not sustained. Retinal thinning in subjects undergoing foveal detachment was a consistent finding following surgery in keeping with the findings of the Jacobson group, and was associated with a reduction of visual acuity in the study eye. The number of subjects showing improvement in visual function is lower in our group than in the two US groups. This difference may reflect differences in the intervention and assessments of outcome. Although several differences in the treatment strategies exist between the 3 groups, one particular difference is the RPE specific promoter used in our trial. As this is primarily a safety study, it was considered appropriate in this initial trial to limit expression to RPE cells, rather than use a more ubiquitous promoter expected to drive expression inappropriately in additional cell types. There is a suggestion that mutation type and treatment dose had an effect on efficacy in our study, with subjects with the least severe predicted mutation effect and those receiving the higher dose having greater levels of improvement in retinal function. This finding was not consistent with the results of the other two groups, suggesting that mutation type and dose may only have an influence on efficacy when using a promoter which results in lower expression levels. This may also explain why older patients had greater improvements in our study, as the more extensive degree of retinal degeneration may consequently lessen the RPE65 requirement in older subjects. Putatively this is met by the level of expression achieved by a RPE65 specific promoter, which may not be the case in younger subjects who potentially have greater levels of RPE65 requirement.

4.1.2 Maguire/Bennett Group

One of the 3 initial RPE65 gene therapy trials was conducted at the Children's Hospital of Philadelphia by the Maguire/Bennett group (110). In this study, 12 subjects (aged from 8 – 44 years) underwent three-port pars plana vitrectomy and administration of subretinal AAV2-hRPE65v2, with foveal involvement in 9 subjects. This vector contained a chicken β-actin promoter for expression of the human RPE65 cDNA with an optimised Kozak sequence. Three different dose levels were used: 1) low dose of $1.5x10^{10}$ vector genomes in 150µL in 3 subjects; 2) medium dose of $4.8x10^{10}$ vector genomes in 150µL in 6 subjects; and 3) high dose of $1.5x10^{11}$ vector genomes in 300µL in 3 subjects. Follow-up for this study has been reported up to 2 years.

One subject was noted to have an outer lamellar cyst at day 5 on OCT imaging, which progressed to a full thickness macular hole at day 14. This subject already had a poor preoperative acuity and was not aware of any deterioration in acuity after development of the macular hole, and there has been no reported increase in the macular hole size since.

No serious adverse effects were reported in any subject. An increase in neutralising antibody (NAb) titre to AAV2 was observed during the first 30 days in 1 subject in both the low and medium dose groups, and in 2 subjects in the high dose group. At day 90, 1 subject in the low dose group, and 2 subjects in the medium dose group had elevated NAb, with levels remaining elevated in one of the medium dose subjects at 1 year follow up. Tear samples were transiently positive at low levels for vector DNA sequences in 1 low dose subject, 2 middle dose subjects and 2 high dose subjects, with no positive result detected after day 3. There was no reported evidence of systemic dissemination of the vector sequences in any of the low or middle dose subjects. However, in 2 of the 3 subjects in the high dose group, peripheral blood mononuclear cells were mildly positive for vector sequences up to day 3 postoperatively. There was no evidence of T cell responses to the AAV capsid.

Significant improvement in visual acuity was reported to occur in 7 out of 12 subjects, aged 10 to 26. These occurred in 3 subjects in each of the low and medium dose groups, and in 1 subject in the high dose group. The range of improvement was from 0.16 to 0.56 logMAR, with a mean improvement of 0.48 logMAR. However, the mean baseline acuity of the majority of patients with improved acuity following treatment was poor (1.46 logMAR), and the test-retest variability in such patients is underdetermined. Of note, the subject who developed a macular hole following surgery was also one of the subjects with a significant improvement in post-treatment visual acuity. This finding is not expected and illustrates the variation in visual acuity amongst patients with poor vision. One

subject experienced a worsening in visual acuity from 1.35 logMAR at baseline to 1.83 logMAR at 1 year follow-up.

Improvement in Goldmann Visual Field perimetry was reported in all 12 subjects. However, the actual amount of improvement in a substantial number of these subjects is marginal, with approximately only 5 subjects having clear demonstration of improvement – albeit without the details of the non-treated eye available for comparison.

One conclusion of this group's study is that the greatest improvements were seen in younger children – based on investigations including full-field dark adaptometry sensitivity threshold (FST) testing and pupillometry. With FST testing, 5 out of 7 subjects tested showed a significant improvement in sensitivity in their treated eye. In a comparison of younger (8-10 years) and older (20-24 years) subjects who both received the middle dose, greater improvements were seen in the younger subjects, in which one subject attained almost a 20dB interocular sensitivity difference post treatment, compared to a maximum 8dB difference in the older group. However, the greatest interocular sensitivity difference of approximately 30dB was attained in a 35 year old subject who received the higher dose, illustrating that significant improvements can also be obtained in older subjects. Of note, peak improvement in sensitivities were generally not maintained with 5 out of 7 subjects achieving their peak response within 100 days post-treatment, and only 2 subjects maintaining peak FST levels after 100 days. 11 out 11 subjects investigated with pupillometry testing showed significant improvement following treatment. Four younger subjects aged between 8 and 11 showed the greatest change of 2 to 3 log improvements in light sensitivity at 90 days post-treatment. However, significant improvements of 2 log light sensitivity were also seen in three older subjects with a mean age of 29 years, again questioning the conclusion that the treatment is more efficacious in younger subjects.

Four young subjects aged from 8 to 11 years are reported to have improvements in mobility testing following treatment. However, baseline details of the time taken to navigate the obstacle course and the numbers of errors made are not provided, making it difficult to evaluate the post operative results.

No differences in the degree of response to treatment were noted between the doses administered or by the subject's mutation type.

In summary, this trial has provided support for the safe use of AAV mediated gene transfer in humans, and subsequent improvement in visual function, particularly demonstrated by

improvements in FST and pupillometry. There is uncertainty as to the significance of visual acuity improvements reported and whether younger subjects responded more favourably to the therapy.

4.1.3 Jacobson Group

In another of the three initial RPE65 gene therapy trials conducted by the Jacobson group, 15 subjects age 11 to 30 years of age underwent vitrectomy and administration of subretinal AAV2-hRPE65v2 with a chicken β-actin promoter also used. 4 different doses with 2 injection strategies were used in 5 cohorts, each containing 3 subjects. Cohort 1 received $5.96x10^{10}$ vector genomes in 150µL; cohort 2 received $11.92x10^{10}$ vector genomes in 150µL; cohort 3 received $8.94x10^{10}$ vector genomes in 225µL and cohorts 4 and 5 both received $17.88x10^{10}$ vector genomes in 2x225 µL injections. Foveal involvement occurred in 5 of 15 subjects and follow up has been reported from 1 month to 3 years post-therapy (111).

No serious immune responses were detected following therapy. 2 subjects had elevated levels of circulating antibodies to AAV2, possibly consistent with a response to the vector, although coincidental exposure to wild-type AAV2 is also considered as an explanation of these rises. No vector genome copies were detected in peripheral blood samples.

Surgical complications included one subject having a retinal detachment one day after the retina was deemed attached – this subject required an uneventful secondary procedure, with no further problems reported. Another subject was noted to have choroidal effusions 3 days after surgery. Initial topical therapy with cycloplegics and steroids were unsuccessful, and oral steroids were administered, with final resolution of the choroidal effusion not occurring until day 238.

Visual acuity improvement of more than 0.3 logMAR occurred in 2 study eyes only, both of whom had preoperative extra-foveal fixation and also had the lowest baseline visual acuities. In both subjects the injection area included the extra-foveal fixation site. One subject had a reduction in acuity of over 0.3 logMAR.

Significant foveal thinning occurred in 4 study eyes, either at short-term or long-term follow-up. The largest reduction in foveal thickness of over 50 microns occurred in one subject with foveal involvement, with thinning noted during the early postoperative period and persisted at long-term follow-up. In another subject who also had foveal detachment, foveal thinning occurred in the short-term, but had resolved at long-term follow-up. Conversely, 2 other patients only had foveal thinning in the long-term, in one of whom the subretinal injection involved the fovea. Analysis of the retinal laminar architecture across the fovea showed that disturbance of the photoreceptor

inner and outer segments occurred in subjects with foveal detachment, and of note, the subject with the most significant visual acuity reduction after treatment also had the most prominent foveal abnormalities post therapy. In addition, the 2 subjects with the greatest reduction in foveal thickness had the greatest baseline foveal thickness, perhaps suggesting that greater foveal photoreceptor loss can occur in subjects with potentially the most photoreceptors to lose.

Using full-field stimulus testing with both blue and red flashes to stimulate rod and cone responses respectively, significant improvements were seen with both stimulus types. Post-treatment sensitivity to blue light was significantly greater in the study eye compared to the control eye, with 14 out 15 study eyes showing improvement in rod function with a mean increase of 1.59 $\log_{10.}$ All 15 of the study eyes showed an improvement in cone sensitivity with red stimuli, with mean improvement of 0.45 $\log_{10.}$ In the 9 subjects with over 12 months of follow-up, improvement from baseline was maintained in all 9 subjects with rod function testing, and in 5 subjects with cone testing. However, peak sensitivity in rod function occurred at final follow-up visit in only 2 of the 9 eyes, and in only 1 of the 5 eyes who showed cone function improvement, indicating that maximum treatment effect may not have been sustained.

Significant improvements were also found with pupillometry testing in the study eye, with this group showing a mean improvement of 1.17 $\log_{10}$, and 9 of 14 eyes tested having greater than 1 $\log_{10}$ improvement. No significant effect of age was found on the degree of pupillometry improvement, and similarly age did not appear to be associated with improvements in visual acuity of full-field stimulus testing.

Static dark-adapted visual field testing was performed to help identify the location of sensitivity improvements. In 11 of the 12 subjects investigated, the loci of visual field improvement corresponded with the subretinal injection site. In one subject, visual field improvement of more than 8dB sensitivity was only found in the temporal periphery, despite central-superior injection location. In several other subjects, the area of visual improvement extended outside that which would be predicted by the region covered by the injection.

Six subjects underwent both pre and postoperative mobility testing, and better performance post-treatment was observed in 3 study eyes, one of which was only apparent at the lowest illumination level of 0.2 Lux, whereas the other 2 subjects had improvements at 0.6, 2 and 4 Lux levels also.

In summary, this trial has provided further support for the safe use of AAV mediated gene transfer. Treatment can lead to improvements in both rod and cone function, with age, mutation or vector dose not appearing to have an effect on the degree of improvement that occurred. Some concerns

about the effect of foveal detachment are highlighted, with significant foveal thinning occurring in 2 out of 5 subjects with foveal involvement. In addition, significant visual acuity reduction occurred in 1 subject who also had the greatest degree of foveal thinning and adverse retinal structural changes after treatment. In view of the general lack of improvement in visual acuity, combined with the adverse visual acuity and foveal structural changes, the group suggest that the fovea should not be included in subretinal injections unless 1) there is OCT evidence of foveal atrophy or 2) extra-foveal fixation is determined preoperatively. This study was the only one to use more than a single injection site, with 6 subjects receiving both a superior retina and nasal retina located injection. In a modification of their injection strategy, they suggest that in cases where it is advisable to not involve the fovea, 150µL of the vector could be injected at 3 locations: superior retina, nasal-superior retina and temporal retina, to enhance the area of potential retinal function improvement.

4.1.4 Overall Results Discussion

Despite several differences in the study design of the 3 initial RPE65 gene therapy trials, it is possible to collectively assess the results, and draw some general conclusions to date. It appears that subretinal delivery of AAV2 carrying *RPE65* is immunologically safe, with no serious concerns raised in this aspect. There is evidence of improvement in retinal function in 33 out of the 39 patients treated. However, the level of improvement has not been sufficient to enhance ERG function, nor significantly and consistently improve visual acuity or subjective visual experience. Therefore, for RPE65 gene therapy it is reasonable to consider excluding the fovea in the treatment area until more substantive improvements can be obtained through the optimisation of vectors. Multiple injections of smaller vector volumes is one alternative approach to maximise the treatment area whilst minimising any possible photoreceptor degeneration from bullous retinal detachment, though this might increase the risk of intraoperative complications.

The use of a chicken β-actin promoter resulted in some degree of improved visual function in all the subjects that it was used, compared to half of subjects who received the RPE65 specific promoter. In view of the lack of significant immunological or clinical concern from using either of the promoter types, it could be proposed that a chicken β-actin promoter is a more effective promoter type to use in RPE65 deficiency – although the results obtained with this promoter in humans are still below those obtained in animal models which showed significant ERG improvements. Future vector optimisation work to obtain expression levels that result in ERG improvement will provide strong

support for foveal involvement as the benefits of visual function gain will most likely outweigh the risks from any potential iatrogenic adverse events.

The maximum levels of improvement in retinal sensitivity appear not to be sustained in all three trials, suggesting that the treatment effect may lose efficacy over time. It is possible that RPE65 expression levels are not maintained, or that continued natural disease progression negates any continued RPE65 expression. The fact that reductions in sensitivity from peak values can occur over a period of a few months suggests that expression levels not being maintained is the reason for declining improvement, rather than it being attributable to disease progression. Without performing histological analysis from treated subjects, it is difficult to be certain of levels of gene expression and whether they are maintained in the long term. The mechanism for a possible decline in gene expression is uncertain but possible explanations could include an as of yet undetected immune related form of down-regulation or disruption of the viral genome. It is too early to be certain whether the treatment is having an effect on the rate of slowing disease progression, with further follow-up required to address this important question.

In conclusion, the demonstration of improved visual function following vector administration represents significant proof of principle for gene therapy in inherited eye disease. There is considerable scope to build on these findings for the benefit of people with sight loss caused by defects in RPE65 and other genes

4.2 Retinal structure and function in Achromatopsia

In preparation for a gene therapy trial, the purpose of this study was to gain further understanding of the retinal structure and function in ACHM, and any association with age or genotype, thereby helping to identify potential patients who may benefit from intervention and time-points which this may be appropriate.

In contrast to recently reported case series (58, 59), our cross-sectional study (n=40) has not found an age-associated loss of cone structural integrity in patients with ACHM. No significant differences were found in the ages of patients with the aforementioned various SDOCT changes (section 3.2.2), and furthermore, patients without ISe disruption had the second highest mean age of the five SDOCT categories.

In a study involving 40 patients with ACHM, Thiadens et al. (55) reported that cone loss occurred in 42% (n=8) of patients who were under 30 years of age, with 95% (n=20) of patients over 30 years showing cone loss on SDOCT (58). In contrast, we found that cone loss (SDOCT categories 3 to 5) occurred in approximately 50% (14/27) of patients less than 30 years of age, but in only 30% (4/13) of patients aged over 30 years. In addition, we found that the proportion of patients with any disruption in cone structure (SDOCT categories 2 to 5) to be less than other studies, with 48% of patients having ISe disruption in our study, compared to 70% reported by Thiadens et al., 100% in the smaller Thomas et al. study (n=13) (59), and in 83% of patients in the Genead et al. study (n=12). Similarly, Thiadens et al. identified a HRZ in 60% of patients, with Thomas et al. reporting a HRZ in 54% and in 58% with Genead et al., compared to 23% in our study. One possible explanation for the difference in incidence of OCT changes and their severity across these studies includes a common feature of inherited retinal disease, namely the considerable phenotypic heterogeneity that is often characteristic. This is further illustrated by the family with *GNAT2* mutations in our study; with the youngest member aged 29 showing a HRZ, in contrast to his father aged 52 who had no ISe disruption.

Further evidence supporting the notion that an age-dependent deterioration in cone structure occurs in ACHM is provided by a longitudinal study which performed OCT imaging in 8 subjects on two occasions, with a mean follow-up of 16 months (121). In this study, all 5 of the younger subjects (aged less than 10 years) showed alterations in foveal cone morphology at the second visit, which included IS/OS disruption and HRZ development. This is in contrast to the 3 older subjects (aged between 42-45 years) who did not show changes in cone structure at the second visit.

In a further study, which utilised autofluorescene imaging in ACHM patients, age-dependent changes were found with younger patients exhibiting areas of foveal and parafoveal hyper autofluorescence, whereas older patients showed punch out regions of hypo autofluorescence which corresponded with areas of cavitation on OCT (122).

In view of these results however, it is important to state that progression does not imply that age alone should be the principle criterion for emerging trials; in other words different patients likely progress at different rates.

We did not identify any significant decline in visual acuity, contrast sensitivity or reading acuity with advancing age in our study, and to the best of our knowledge, this is the largest study to date reporting on any potential change in these parameters with age. We did however find a decline in retinal sensitivity with microperimetry with advancing age. A significant reduction in retinal sensitivity , determined by mesopic microperimetry, has been reported to occur in normal subjects with increasing age, with a 1dB lower retinal sensitivity found in subjects aged 70 to 75 years compared to those aged 20 to 29 years (123). A decline in retinal sensitivity of 3.1dB was observed in our study between patients less than 25 years of age (n=22) and those over 25 years (n=18), raising the possibility that the reduction was over and above that potentially attributable to natural age-related decline. In our cohort of patients with absent cone function (on the basis of electrophysiology and psychophysics), it is presumed that retinal sensitivity detected by mesopic microperimetry testing is a consequence of retained rod function. This raises the question as to whether rod function declines in patients with ACHM with age and if so, why? If there is no change in rod function, it remains a possibility that there is residual central cone function in some subjects, which may deteriorate over time. A future study is required to probe which class of photoreceptor(s) underlies the retinal sensitivity detected by mesopic microperimetry in patients with ACHM – for example determining the rate of recovery of retinal sensitivity using the aforementioned microperimeter following a full bleach might help to shed light on this intriguing issue. A mean retinal sensitivity of 16.6dB was found in our study, and this was higher than that reported by Genead et al. in which only 4 subjects underwent microperimetry testing and had a mean sensitivity of 12dB.

We did not observe a clear association between retinal structure and function, with no differences identified in visual acuity, contrast sensitivity, retinal sensitivity or fixation stability between patients with the various aforementioned SDOCT or fundus changes (section 3.2.1 and 3.2.2). This is in keeping with the lack of an association reported between the presence of an HRZ and visual acuity in previous studies (58, 59). Surprisingly, patients without ISe disruption had a significantly (p=0.02)

lower reading acuity compared to patients with SDOCT changes - however, a significant difference was not found in any other parameter, so this may be a spurious finding.

Foveal hypoplasia (defined as the persistence of one or more inner retinal layers through the foveal centre) was noted on SDOCT in 52.5% (n=21) of patients in our study. In contrast, foveal hypoplasia was defined as the presence of multiple ganglion cell layers by Thiadens et al. and noted in 80% of their patients (58). In the Thomas et al. study, foveal hypoplasia was defined as the continuation of the OPL and IPL at the fovea, and found in 69% of their patients (59), and if the same definition was used in our study, foveal hypoplasia would be present in 60% (n=24) of patients. Importantly, we did not find any significant differences in visual acuity, reading acuity or fixation stability in patients with or without foveal hypoplasia; however, significantly better contrast sensitivity and retinal sensitivity were found in patients with foveal hypoplasia.

In the majority of cases no definite correlations were observed between retinal structure or function and genotype. Mean retinal sensitivity was marginally, but significantly (p=0.04) higher amongst *CNGB3* compared to *CNGA3* patients. A similar number of *CNGA3* patients (n=9, 52.9%) and *CNGB3* patients (n=9, 60%) had milder outer retinal disturbance (grade 1 or 2) on SDOCT; with 1 patient in both of these groups also having the most severe grade of SDOCT structural damage. Visual acuity, reading acuity and retinal sensitivity were lower in patients with either *GNAT2* or *PDE6C* mutations, however the number of patients with either of these mutations was small, 4 and 1 respectively, and their ages generally higher than in the *CNGA3* or *CNGB3* groups, thereby limiting the ability to make reliable comparisons.

4.2.1 Implications for gene therapy

From our results, we propose that the potential window of opportunity for gene therapy intervention for patients with ACHM may be larger than recently suggested. We did not find an age-related association with disruption or loss of cone photoreceptors, with the age of patients with no ISe disruption ranging from 6 to 52 years of age.

As this was a cross-sectional study, it has not assessed whether patients who have any form of outer retinal change, continue to show progression, and if so, how variable is any rate of change. With respect to cone photoreceptor structure, we therefore suggest that patients who are being considered for potential gene therapy intervention are assessed on an individual basis, irrespective of age. In addition, we did not find that visual function was worse in patients with foveal hypoplasia, in fact significantly better contrast sensitivity and retinal sensitivity were found in patients with

foveal hypoplasia, suggesting that foveal hypoplasia per se should not be an exclusion criterion for potential therapy trials.

In addition to the integrity of cone photoreceptor architecture, another factor likely to influence the extent of a potential response to gene therapy is the ability of the higher visual system to respond to newly acquired cone activity. Functional magnetic resonance imaging has shown evidence of visual cortex reorganisation, with the area of visual cortex normally active following cone-derived foveal stimulation, being active instead following rod stimuli in ACHM patients (n=3) (124). To what degree and up to what age the visual cortex is able to adapt to and process input from cone photoreceptors, is an important consideration and will likely have bearing on the efficacy of gene replacement therapy.

Conclusions

5. Conclusions

The last decade has seen major advances in several key disciplines, including improvements in molecular genetics allowing identification of disease-causing mutations and viral vector gene transfer technology, which have enabled the commencement of the first human trials of gene replacement therapy for RPE65 deficient inherited retinal disease.

These trials have demonstrated the safety of AAV administration in the eye, with no serious immune-related consequences. These trials have also demonstrated that improvements in retinal function can be achieved and provide encouragement for the consideration of applying gene replacement therapy to other retinal dystrophies. The extent of species-specific differences is reinforced by the common finding that the impact of RPE65 gene therapy appears less strong in human subjects than in preclinical models.

In addition, although subretinal vector delivery is at present the most effective way of transducing outer retinal layers, a number of patients have experienced retinal thinning as a consequence, which in some cases has been associated with a decline in visual acuity when the fovea has been included in the injection region. To improve on the results of these current RPE65 trials, increased levels of expression by vector optimisation may provide therapeutic benefit to the fovea that can more than compensate for the predictable adverse effect of retinal detachment, as is evident outside the macula.

In contrast to LCA due to *RPE65* mutations in which the RPE is the primary site of dysfunction, ACHM is a disorder of purely cone photoreceptor function and as the highest concentration of cone cells is situated in the foveal region, for significant improvement following gene therapy to be achieved, it will be necessary to include the fovea in the subretinal treatment region. However, it is feasible that transduction of a significant proportion of cone cells can be achieved by delivery of a considerably smaller injection volume than that used in the RPE65 trial, thereby potentially minimising iatrogenic photoreceptor degeneration. In addition, foveal function is essentially non-existent in ACHM patients, therefore there is minimal scope for harm to function with sub-foveal injection. This ACHM study has also reiterated a common feature amongst inherited retinal diseases, namely the considerable phenotypic variability that can exist within conditions. With ACHM, a clear association between age and cone outer photoreceptor structure has not been demonstrated, with several patients in their third decade showing no disruption in cone structure. This implies that the window of opportunity for gene therapy intervention is potentially larger than has been suggested recently, and subjects need to be assessed on an individual basis, irrespective of their age.

With work progressing towards the development of gene vectors for a variety of other inherited retinal diseases, and studies helping to identify appropriate patients and time points for intervention, the next decade offers opportunity for significant advancement in the understanding and management of these debilitating and as of yet, untreatable conditions.

6. References

1. Smith AJ, Bainbridge JW, Ali RR. Prospects for retinal gene replacement therapy. Trends in Genetics. 2009;25(4):156-65.
2. Arshavsky V. Like night and day: rods and cones have different pigment regeneration pathways. Neuron. 2002 Sep 26;36(1):1-3.
3. Muniz A, Villazana-Espinoza ET, Hatch AL, Trevino SG, Allen DM, Tsin AT. A novel cone visual cycle in the cone-dominated retina. Exp Eye Res. 2007 Aug;85(2):175-84.
4. Berger W, Kloeckener-Gruissem B, Neidhardt J. The molecular basis of human retinal and vitreoretinal diseases. Prog Retin Eye Res. 2010 Sep;29(5):335-75.
5. Michaelides M, Hardcastle AJ, Hunt DM, Moore AT. Progressive cone and cone-rod dystrophies: phenotypes and underlying molecular genetic basis. Surv Ophthalmol. 2006 May-Jun;51(3):232-58.
6. Maugeri A, Klevering BJ, Rohrschneider K, Blankenagel A, Brunner HG, Deutman AF, et al. Mutations in the ABCA4 (ABCR) gene are the major cause of autosomal recessive cone-rod dystrophy. Am J Hum Genet. 2000 Oct;67(4):960-6.
7. Walia S, Fishman GA. Natural history of phenotypic changes in Stargardt macular dystrophy. Ophthalmic Genet. 2009 Jun;30(2):63-8.
8. Weingeist TA, Kobrin JL, Watzke RC. Histopathology of Best's macular dystrophy. Arch Ophthalmol. 1982 Jul;100(7):1108-14.
9. Petrukhin K, Koisti MJ, Bakall B, Li W, Xie G, Marknell T, et al. Identification of the gene responsible for Best macular dystrophy. Nat Genet. 1998 Jul;19(3):241-7.
10. Sun H, Tsunenari T, Yau KW, Nathans J. The vitelliform macular dystrophy protein defines a new family of chloride channels. Proc Natl Acad Sci U S A. 2002 Mar 19;99(6):4008-13.
11. Burgess R, Millar ID, Leroy BP, Urquhart JE, Fearon IM, De Baere E, et al. Biallelic mutation of BEST1 causes a distinct retinopathy in humans. Am J Hum Genet. 2008 Jan;82(1):19-31.
12. den Hollander AI, Black A, Bennett J, Cremers FPM. Lighting a candle in the dark: advances in genetics and gene therapy of recessive retinal dystrophies. Journal of Clinical Investigation. 2010;120(9):3042-53.
13. Doonan F, Donovan M, Cotter TG. Activation of multiple pathways during photoreceptor apoptosis in the rd mouse. Invest Ophthalmol Vis Sci. 2005 Oct;46(10):3530-8.
14. Bush RA, Kononen L, Machida S, Sieving PA. The effect of calcium channel blocker diltiazem on photoreceptor degeneration in the rhodopsin Pro213His rat. Invest Ophthalmol Vis Sci. 2000 Aug;41(9):2697-701.
15. Fain GL, Lisman JE. Photoreceptor degeneration in vitamin A deprivation and retinitis pigmentosa: the equivalent light hypothesis. Exp Eye Res. 1993 Sep;57(3):335-40.
16. Lisman J, Fain G. Support for the equivalent light hypothesis for RP. Nat Med. 1995 Dec;1(12):1254-5.
17. Woodruff ML, Wang Z, Chung HY, Redmond TM, Fain GL, Lem J. Spontaneous activity of opsin apoprotein is a cause of Leber congenital amaurosis. Nat Genet. 2003 Oct;35(2):158-64.
18. Harada T, Harada C, Kohsaka S, Wada E, Yoshida K, Ohno S, et al. Microglia-Muller glia cell interactions control neurotrophic factor production during light-induced retinal degeneration. J Neurosci. 2002 Nov 1;22(21):9228-36.
19. Stone EM. Leber congenital amaurosis - a model for efficient genetic testing of heterogeneous disorders: LXIV Edward Jackson Memorial Lecture. Am J Ophthalmol. 2007 Dec;144(6):791-811.
20. Mirdehghan SA, Dehghan MH, Mohammadpour M, Heidari K, Khosravi M. Causes of severe visual impairment and blindness in schools for visually handicapped children in Iran. Br J Ophthalmol. 2005 May;89(5):612-4.
21. Koenekoop R. An overview of leber congenital amaurosis: a model to understand human retinal development. Survey of Ophthalmology. 2004;49(4):379-98.

22. Denhollander A, Roepman R, Koenekoop R, Cremers F. Leber congenital amaurosis: Genes, proteins and disease mechanisms. Progress in Retinal and Eye Research. 2008;27(4):391-419.
23. Milam AH, Barakat MR, Gupta N, Rose L, Aleman TS, Pianta MJ, et al. Clinicopathologic effects of mutant GUCY2D in Leber congenital amaurosis. Ophthalmology. 2003 Mar;110(3):549-58.
24. Dyer MA, Donovan SL, Zhang J, Gray J, Ortiz A, Tenney R, et al. Retinal degeneration in Aipl1-deficient mice: a new genetic model of Leber congenital amaurosis. Brain Res Mol Brain Res. 2004 Dec 20;132(2):208-20.
25. Dharmaraj S, Leroy BP, Sohocki MM, Koenekoop RK, Perrault I, Anwar K, et al. The phenotype of Leber congenital amaurosis in patients with AIPL1 mutations. Arch Ophthalmol. 2004 Jul;122(7):1029-37.
26. Gerber S, Hanein S, Perrault I, Delphin N, Aboussair N, Leowski C, et al. Mutations in LCA5 are an uncommon cause of Leber congenital amaurosis (LCA) type II. Hum Mutat. 2007 Dec;28(12):1245.
27. Mohamed MD, Topping NC, Jafri H, Raashed Y, McKibbin MA, Inglehearn CF. Progression of phenotype in Leber's congenital amaurosis with a mutation at the LCA5 locus. Br J Ophthalmol. 2003 Apr;87(4):473-5.
28. Dharmaraj S, Li Y, Robitaille JM, Silva E, Zhu D, Mitchell TN, et al. A novel locus for Leber congenital amaurosis maps to chromosome 6q. Am J Hum Genet. 2000 Jan;66(1):319-26.
29. Boylan JP, Wright AF. Identification of a novel protein interacting with RPGR. Hum Mol Genet. 2000 Sep 1;9(14):2085-93.
30. Jacobson SG, Cideciyan AV, Aleman TS, Pianta MJ, Sumaroka A, Schwartz SB, et al. Crumbs homolog 1 (CRB1) mutations result in a thick human retina with abnormal lamination. Hum Mol Genet. 2003 May 1;12(9):1073-8.
31. Ahmed E, Loewenstein J. Leber congenital amaurosis: disease, genetics and therapy. Semin Ophthalmol. 2008 Jan-Feb;23(1):39-43.
32. Sohocki MM, Sullivan LS, Mintz-Hittner HA, Birch D, Heckenlively JR, Freund CL, et al. A range of clinical phenotypes associated with mutations in CRX, a photoreceptor transcription-factor gene. Am J Hum Genet. 1998 Nov;63(5):1307-15.
33. Traboulsi EI. The Marshall M. Parks memorial lecture: making sense of early-onset childhood retinal dystrophies--the clinical phenotype of Leber congenital amaurosis. Br J Ophthalmol. 2010 Oct;94(10):1281-7.
34. Belyaeva OV, Korkina OV, Stetsenko AV, Kim T, Nelson PS, Kedishvili NY. Biochemical properties of purified human retinol dehydrogenase 12 (RDH12): catalytic efficiency toward retinoids and C9 aldehydes and effects of cellular retinol-binding protein type I (CRBPI) and cellular retinaldehyde-binding protein (CRALBP) on the oxidation and reduction of retinoids. Biochemistry. 2005 May 10;44(18):7035-47.
35. Schuster A, Janecke AR, Wilke R, Schmid E, Thompson DA, Utermann G, et al. The phenotype of early-onset retinal degeneration in persons with RDH12 mutations. Invest Ophthalmol Vis Sci. 2007 Apr;48(4):1824-31.
36. Jacobson SG, Cideciyan AV, Aleman TS, Sumaroka A, Schwartz SB, Windsor EA, et al. RDH12 and RPE65, visual cycle genes causing leber congenital amaurosis, differ in disease expression. Invest Ophthalmol Vis Sci. 2007 Jan;48(1):332-8.
37. Chung DC, Traboulsi EI. Leber congenital amaurosis: Clinical correlations with genotypes, gene therapy trials update, and future directions. Journal of American Association for Pediatric Ophthalmology and Strabismus. 2009;13(6):587-92.
38. Hamel CP, Tsilou E, Harris E, Pfeffer BA, Hooks JJ, Detrick B, et al. A developmentally regulated microsomal protein specific for the pigment epithelium of the vertebrate retina. J Neurosci Res. 1993 Mar 1;34(4):414-25.
39. Gu SM, Thompson DA, Srikumari CR, Lorenz B, Finckh U, Nicoletti A, et al. Mutations in RPE65 cause autosomal recessive childhood-onset severe retinal dystrophy. Nat Genet. 1997 Oct;17(2):194-7.

40. Morimura H, Fishman GA, Grover SA, Fulton AB, Berson EL, Dryja TP. Mutations in the RPE65 gene in patients with autosomal recessive retinitis pigmentosa or leber congenital amaurosis. Proc Natl Acad Sci U S A. 1998 Mar 17;95(6):3088-93.
41. Bowne SJ, Humphries MM, Sullivan LS, Kenna PF, Tam LC, Kiang AS, et al. A dominant mutation in RPE65 identified by whole-exome sequencing causes retinitis pigmentosa with choroidal involvement. Eur J Hum Genet. 2011 Oct;19(10):1074-81.
42. Jin M, Yuan Q, Li S, Travis GH. Role of LRAT on the retinoid isomerase activity and membrane association of Rpe65. J Biol Chem. 2007 Jul 20;282(29):20915-24.
43. Moiseyev G, Chen Y, Takahashi Y, Wu BX, Ma JX. RPE65 is the isomerohydrolase in the retinoid visual cycle. Proc Natl Acad Sci U S A. 2005 Aug 30;102(35):12413-8.
44. Znoiko SL, Crouch RK, Moiseyev G, Ma JX. Identification of the RPE65 protein in mammalian cone photoreceptors. Invest Ophthalmol Vis Sci. 2002 May;43(5):1604-9.
45. Wang JS, Kefalov VJ. An alternative pathway mediates the mouse and human cone visual cycle. Curr Biol. 2009 Oct 13;19(19):1665-9.
46. Paunescu K, Wabbels B, Preising MN, Lorenz B. Longitudinal and cross-sectional study of patients with early-onset severe retinal dystrophy associated with RPE65 mutations. Graefe's Archive for Clinical and Experimental Ophthalmology. 2004;243(5):417-26.
47. Jacobson SG, Aleman TS, Cideciyan AV, Roman AJ, Sumaroka A, Windsor EAM, et al. Defining the Residual Vision in Leber Congenital Amaurosis Caused by RPE65 Mutations. Investigative Ophthalmology & Visual Science. 2008;50(5):2368-75.
48. Jacobson SG. Identifying photoreceptors in blind eyes caused by RPE65 mutations: Prerequisite for human gene therapy success. Proceedings of the National Academy of Sciences. 2005;102(17):6177-82.
49. Jacobson SG, Cideciyan AV, Aleman TS, Sumaroka A, Windsor EAM, Schwartz SB, et al. Photoreceptor Layer Topography in Children with Leber Congenital Amaurosis Caused by RPE65 Mutations. Investigative Ophthalmology & Visual Science. 2008;49(10):4573-7.
50. Lorenz B, Wabbels B, Wegscheider E, Hamel CP, Drexler W, Preising MN. Lack of fundus autofluorescence to 488 nanometers from childhood on in patients with early-onset severe retinal dystrophy associated with mutations in RPE65. Ophthalmology. 2004 Aug;111(8):1585-94.
51. Aguirre GK, Komaromy AM, Cideciyan AV, Brainard DH, Aleman TS, Roman AJ, et al. Canine and human visual cortex intact and responsive despite early retinal blindness from RPE65 mutation. PLoS Med. 2007 Jun;4(6):e230.
52. Cai X, Conley SM, Naash MI. RPE65: Role in the Visual Cycle, Human Retinal Disease, and Gene Therapy. Ophthalmic Genetics. 2009;30(2):57-62.
53. Rohrer B, Goletz P, Znoiko S, Ablonczy Z, Ma JX, Redmond TM, et al. Correlation of regenerable opsin with rod ERG signal in Rpe65-/- mice during development and aging. Invest Ophthalmol Vis Sci. 2003 Jan;44(1):310-5.
54. Znoiko SL, Rohrer B, Lu K, Lohr HR, Crouch RK, Ma JX. Downregulation of cone-specific gene expression and degeneration of cone photoreceptors in the Rpe65-/- mouse at early ages. Invest Ophthalmol Vis Sci. 2005 Apr;46(4):1473-9.
55. Samardzija M, von Lintig J, Tanimoto N, Oberhauser V, Thiersch M, Reme CE, et al. R91W mutation in Rpe65 leads to milder early-onset retinal dystrophy due to the generation of low levels of 11-cis-retinal. Hum Mol Genet. 2008 Jan 15;17(2):281-92.
56. Veske A, Nilsson SE, Narfstrom K, Gal A. Retinal dystrophy of Swedish briard/briard-beagle dogs is due to a 4-bp deletion in RPE65. Genomics. 1999 Apr 1;57(1):57-61.
57. Narfstrom K, Seeliger M, Lai CM, Vaegan, Katz M, Rakoczy EP, et al. Morphological aspects related to long-term functional improvement of the retina in the 4 years following rAAV-mediated gene transfer in the RPE65 null mutation dog. Adv Exp Med Biol. 2008;613:139-46.
58. Thiadens AA, Somervuo V, van den Born LI, Roosing S, van Schooneveld MJ, Kuijpers RW, et al. Progressive loss of cones in achromatopsia: an imaging study using spectral-domain optical coherence tomography. Invest Ophthalmol Vis Sci. 2010 Nov;51(11):5952-7.

59. Thomas MG, Kumar A, Kohl S, Proudlock FA, Gottlob I. High-resolution in vivo imaging in achromatopsia. Ophthalmology. 2011 May;118(5):882-7.
60. Genead MA, Fishman GA, Rha J, Dubis AM, Bonci DM, Dubra A, et al. Photoreceptor structure and function in patients with congenital achromatopsia. Invest Ophthalmol Vis Sci. 2011 Sep;52(10):7298-308.
61. Hood DC, Zhang X, Ramachandran R, Talamini CL, Raza A, Greenberg JP, et al. The inner segment/outer segment border seen on optical coherence tomography is less intense in patients with diminished cone function. Invest Ophthalmol Vis Sci. 2011 Dec;52(13):9703-9.
62. Spaide RF, Curcio CA. Anatomical correlates to the bands seen in the outer retina by optical coherence tomography: literature review and model. Retina. 2011 Sep;31(8):1609-19.
63. Fernandez EJ, Hermann B, Povazay B, Unterhuber A, Sattmann H, Hofer B, et al. Ultrahigh resolution optical coherence tomography and pancorrection for cellular imaging of the living human retina. Opt Express. 2008 Jul 21;16(15):11083-94.
64. Johnson S, Michaelides M, Aligianis IA, Ainsworth JR, Mollon JD, Maher ER, et al. Achromatopsia caused by novel mutations in both CNGA3 and CNGB3. J Med Genet. 2004 Feb;41(2):e20.
65. Kohl S, Baumann B, Rosenberg T, Kellner U, Lorenz B, Vadala M, et al. Mutations in the cone photoreceptor G-protein alpha-subunit gene GNAT2 in patients with achromatopsia. Am J Hum Genet. 2002 Aug;71(2):422-5.
66. Thiadens AA, den Hollander AI, Roosing S, Nabuurs SB, Zekveld-Vroon RC, Collin RW, et al. Homozygosity mapping reveals PDE6C mutations in patients with early-onset cone photoreceptor disorders. Am J Hum Genet. 2009 Aug;85(2):240-7.
67. Wissinger B, Gamer D, Jagle H, Giorda R, Marx T, Mayer S, et al. CNGA3 mutations in hereditary cone photoreceptor disorders. Am J Hum Genet. 2001 Oct;69(4):722-37.
68. Kohl S, Baumann B, Broghammer M, Jagle H, Sieving P, Kellner U, et al. Mutations in the CNGB3 gene encoding the beta-subunit of the cone photoreceptor cGMP-gated channel are responsible for achromatopsia (ACHM3) linked to chromosome 8q21. Hum Mol Genet. 2000 Sep 1;9(14):2107-16.
69. Michaelides M, Hunt DM, Moore AT. The cone dysfunction syndromes. Br J Ophthalmol. 2004 Feb;88(2):291-7.
70. Michaelides M, Aligianis IA, Holder GE, Simunovic M, Mollon JD, Maher ER, et al. Cone dystrophy phenotype associated with a frameshift mutation (M280fsX291) in the alpha-subunit of cone specific transducin (GNAT2). Br J Ophthalmol. 2003 Nov;87(11):1317-20.
71. Conley SM, Cai X, Naash MI. Nonviral ocular gene therapy: assessment and future directions. Curr Opin Mol Ther. 2008 Oct;10(5):456-63.
72. Weber M, Rabinowitz J, Provost N, Conrath H, Folliot S, Briot D, et al. Recombinant adeno-associated virus serotype 4 mediates unique and exclusive long-term transduction of retinal pigmented epithelium in rat, dog, and nonhuman primate after subretinal delivery. Mol Ther. 2003 Jun;7(6):774-81.
73. Bainbridge JW, Mistry A, Schlichtenbrede FC, Smith A, Broderick C, De Alwis M, et al. Stable rAAV-mediated transduction of rod and cone photoreceptors in the canine retina. Gene Ther. 2003 Aug;10(16):1336-44.
74. Allocca M, Doria M, Petrillo M, Colella P, Garcia-Hoyos M, Gibbs D, et al. Serotype-dependent packaging of large genes in adeno-associated viral vectors results in effective gene delivery in mice. J Clin Invest. 2008 May;118(5):1955-64.
75. Lai Y, Yue Y, Duan D. Evidence for the failure of adeno-associated virus serotype 5 to package a viral genome > or = 8.2 kb. Mol Ther. 2010 Jan;18(1):75-9.
76. Wu Z, Yang H, Colosi P. Effect of genome size on AAV vector packaging. Mol Ther. 2010 Jan;18(1):80-6.
77. Dong B, Nakai H, Xiao W. Characterization of genome integrity for oversized recombinant AAV vector. Mol Ther. 2010 Jan;18(1):87-92.

78. Pauwels K, Gijsbers R, Toelen J, Schambach A, Willard-Gallo K, Verheust C, et al. State-of-the-art lentiviral vectors for research use: risk assessment and biosafety recommendations. Curr Gene Ther. 2009 Dec;9(6):459-74.
79. Yanez-Munoz RJ, Balaggan KS, MacNeil A, Howe SJ, Schmidt M, Smith AJ, et al. Effective gene therapy with nonintegrating lentiviral vectors. Nat Med. 2006 Mar;12(3):348-53.
80. Reichel MB, Ali RR, Thrasher AJ, Hunt DM, Bhattacharya SS, Baker D. Immune responses limit adenovirally mediated gene expression in the adult mouse eye. Gene Ther. 1998 Aug;5(8):1038-46.
81. Rolling F. Recombinant AAV-mediated gene transfer to the retina: gene therapy perspectives. Gene Ther. 2004 Oct;11 Suppl 1:S26-32.
82. West EL, Pearson RA, MacLaren RE, Sowden JC, Ali RR. Cell transplantation strategies for retinal repair. Prog Brain Res. 2009;175:3-21.
83. Winter JO, Cogan SF, Rizzo JF, 3rd. Retinal prostheses: current challenges and future outlook. J Biomater Sci Polym Ed. 2007;18(8):1031-55.
84. Dejneka NS, Surace EM, Aleman TS, Cideciyan AV, Lyubarsky A, Savchenko A, et al. In utero gene therapy rescues vision in a murine model of congenital blindness. Mol Ther. 2004 Feb;9(2):182-8.
85. Pang JJ, Chang B, Kumar A, Nusinowitz S, Noorwez SM, Li J, et al. Gene therapy restores vision-dependent behavior as well as retinal structure and function in a mouse model of RPE65 Leber congenital amaurosis. Mol Ther. 2006 Mar;13(3):565-72.
86. Nusinowitz S, Ridder WH, 3rd, Pang JJ, Chang B, Noorwez SM, Kaushal S, et al. Cortical visual function in the rd12 mouse model of Leber Congenital Amarousis (LCA) after gene replacement therapy to restore retinal function. Vision Res. 2006 Oct;46(22):3926-34.
87. Bennicelli J, Wright JF, Komaromy A, Jacobs JB, Hauck B, Zelenaia O, et al. Reversal of blindness in animal models of leber congenital amaurosis using optimized AAV2-mediated gene transfer. Mol Ther. 2008 Mar;16(3):458-65.
88. Roman AJ, Boye SL, Aleman TS, Pang JJ, McDowell JH, Boye SE, et al. Electroretinographic analyses of Rpe65-mutant rd12 mice: developing an in vivo bioassay for human gene therapy trials of Leber congenital amaurosis. Mol Vis. 2007;13:1701-10.
89. Acland GM, Aguirre GD, Bennett J, Aleman TS, Cideciyan AV, Bennicelli J, et al. Long-term restoration of rod and cone vision by single dose rAAV-mediated gene transfer to the retina in a canine model of childhood blindness. Mol Ther. 2005 Dec;12(6):1072-82.
90. Jacobson SG, Acland GM, Aguirre GD, Aleman TS, Schwartz SB, Cideciyan AV, et al. Safety of recombinant adeno-associated virus type 2-RPE65 vector delivered by ocular subretinal injection. Mol Ther. 2006 Jun;13(6):1074-84.
91. Annear MJ, Bartoe JT, Barker SE, Smith AJ, Curran PG, Bainbridge JW, et al. Gene therapy in the second eye of RPE65-deficient dogs improves retinal function. Gene Ther. 2011 Jan;18(1):53-61.
92. Le Meur G, Stieger K, Smith AJ, Weber M, Deschamps JY, Nivard D, et al. Restoration of vision in RPE65-deficient Briard dogs using an AAV serotype 4 vector that specifically targets the retinal pigmented epithelium. Gene Ther. 2007 Feb;14(4):292-303.
93. Bennett J, Maguire AM, Cideciyan AV, Schnell M, Glover E, Anand V, et al. Stable transgene expression in rod photoreceptors after recombinant adeno-associated virus-mediated gene transfer to monkey retina. Proc Natl Acad Sci U S A. 1999 Aug 17;96(17):9920-5.
94. Jacobson SG, Boye SL, Aleman TS, Conlon TJ, Zeiss CJ, Roman AJ, et al. Safety in nonhuman primates of ocular AAV2-RPE65, a candidate treatment for blindness in Leber congenital amaurosis. Hum Gene Ther. 2006 Aug;17(8):845-58.
95. Alexander JJ, Umino Y, Everhart D, Chang B, Min SH, Li Q, et al. Restoration of cone vision in a mouse model of achromatopsia. Nat Med. 2007 Jun;13(6):685-7.
96. Michalakis S, Muhlfriedel R, Tanimoto N, Krishnamoorthy V, Koch S, Fischer MD, et al. Restoration of cone vision in the CNGA3-/- mouse model of congenital complete lack of cone photoreceptor function. Mol Ther. 2010 Dec;18(12):2057-63.

97. Pang JJ, Alexander J, Lei B, Deng W, Zhang K, Li Q, et al. Achromatopsia as a potential candidate for gene therapy. Adv Exp Med Biol. 2010;664:639-46.
98. Carvalho LS, Xu J, Pearson RA, Smith AJ, Bainbridge JW, Morris LM, et al. Long-term and age-dependent restoration of visual function in a mouse model of CNGB3-associated achromatopsia following gene therapy. Hum Mol Genet. 2011 Aug 15;20(16):3161-75.
99. Komaromy AM, Alexander JJ, Rowlan JS, Garcia MM, Chiodo VA, Kaya A, et al. Gene therapy rescues cone function in congenital achromatopsia. Hum Mol Genet. 2010 Jul 1;19(13):2581-93.
100. Mantyjarvi M, Laitinen T. Normal values for the Pelli-Robson contrast sensitivity test. J Cataract Refract Surg. 2001 Feb;27(2):261-6.
101. Marmor MF, Fulton AB, Holder GE, Miyake Y, Brigell M, Bach M. ISCEV Standard for full-field clinical electroretinography (2008 update). Doc Ophthalmol. 2009 Feb;118(1):69-77.
102. Haimovici R, Owens SL, Fitzke FW, Bird AC. Dark adaptation in age-related macular degeneration: relationship to the fellow eye. Graefes Arch Clin Exp Ophthalmol. 2002 Feb;240(2):90-5.
103. Sieving PA, Caruso RC, Tao W, Coleman HR, Thompson DJ, Fullmer KR, et al. Ciliary neurotrophic factor (CNTF) for human retinal degeneration: phase I trial of CNTF delivered by encapsulated cell intraocular implants. Proc Natl Acad Sci U S A. 2006 Mar 7;103(10):3896-901.
104. Thayaparan K, Crossland MD, Rubin GS. Clinical assessment of two new contrast sensitivity charts. Br J Ophthalmol. 2007 Jun;91(6):749-52.
105. Patel PJ, Chen FK, Da Cruz L, Rubin GS, Tufail A. Test-retest variability of reading performance metrics using MNREAD in patients with age-related macular degeneration. Invest Ophthalmol Vis Sci. 2011 May;52(6):3854-9.
106. Fitzke FW, Hitchings RA, Poinoosawmy D, McNaught AI, Crabb DP. Analysis of visual field progression in glaucoma. Br J Ophthalmol. 1996 Jan;80(1):40-8.
107. McNaught AI, Crabb DP, Fitzke FW, Hitchings RA. Visual field progression: comparison of Humphrey Statpac2 and pointwise linear regression analysis. Graefes Arch Clin Exp Ophthalmol. 1996 Jul;234(7):411-8.
108. Crossland MD, Dunbar HM, Rubin GS. Fixation stability measurement using the MP1 microperimeter. Retina. 2009 May;29(5):651-6.
109. Charbel Issa P, Troeger E, Finger R, Holz FG, Wilke R, Scholl HP. Structure-function correlation of the human central retina. PLoS One. 2010;5(9):e12864.
110. Maguire AM, High KA, Auricchio A, Wright JF, Pierce EA, Testa F, et al. Age-dependent effects of RPE65 gene therapy for Leber's congenital amaurosis: a phase 1 dose-escalation trial. The Lancet. 2009;374(9701):1597-605.
111. Jacobson SG, Cideciyan AV, Ratnakaram R, Heon E, Schwartz SB, Roman AJ, et al. Gene therapy for leber congenital amaurosis caused by RPE65 mutations: safety and efficacy in 15 children and adults followed up to 3 years. Arch Ophthalmol. 2012 Jan;130(1):9-24.
112. Wakabayashi T, Oshima Y, Fujimoto H, Murakami Y, Sakaguchi H, Kusaka S, et al. Foveal microstructure and visual acuity after retinal detachment repair: imaging analysis by Fourier-domain optical coherence tomography. Ophthalmology. 2009 Mar;116(3):519-28.
113. Delolme MP, Dugas B, Nicot F, Muselier A, Bron AM, Creuzot-Garcher C. Anatomical and functional macular changes after rhegmatogenous retinal detachment with macula off. Am J Ophthalmol. 2012 Jan;153(1):128-36.
114. Ross W, Lavina A, Russell M, Maberley D. The correlation between height of macular detachment and visual outcome in macula-off retinal detachments of < or = 7 days' duration. Ophthalmology. 2005 Jul;112(7):1213-7.
115. Mowatt L, Tarin S, Nair RG, Menon J, Price NJ. Correlation of visual recovery with macular height in macula-off retinal detachments. Eye (Lond). 2010 Feb;24(2):323-7.
116. Mervin K, Valter K, Maslim J, Lewis G, Fisher S, Stone J. Limiting photoreceptor death and deconstruction during experimental retinal detachment: the value of oxygen supplementation. Am J Ophthalmol. 1999 Aug;128(2):155-64.

117. Cook B, Lewis GP, Fisher SK, Adler R. Apoptotic photoreceptor degeneration in experimental retinal detachment. Invest Ophthalmol Vis Sci. 1995 May;36(6):990-6.
118. Lewis GP, Charteris DG, Sethi CS, Fisher SK. Animal models of retinal detachment and reattachment: identifying cellular events that may affect visual recovery. Eye (Lond). 2002 Jul;16(4):375-87.
119. Arroyo JG, Yang L, Bula D, Chen DF. Photoreceptor apoptosis in human retinal detachment. Am J Ophthalmol. 2005 Apr;139(4):605-10.
120. Narfstrom K, Katz ML, Ford M, Redmond TM, Rakoczy E, Bragadottir R. In vivo gene therapy in young and adult RPE65-/- dogs produces long-term visual improvement. J Hered. 2003 Jan-Feb;94(1):31-7.
121. Thomas MG, McLean RJ, Kohl S, Sheth V, Gottlob I. Early signs of longitudinal progressive cone photoreceptor degeneration in achromatopsia. Br J Ophthalmol. 2012 Sep;96(9):1232-6.
122. Fahim AT, Khan NW, Zahid S, Schachar IH, Branham K, Kohl S, et al. Diagnostic Fundus Autofluorescence Patterns in Achromatopsia. Am J Ophthalmol. 2013 Aug 20.
123. Midena E, Vujosevic S, Cavarzeran F. Normal values for fundus perimetry with the microperimeter MP1. Ophthalmology. 2010 Aug;117(8):1571-6, 6 e1.
124. Baseler HA, Brewer AA, Sharpe LT, Morland AB, Jagle H, Wandell BA. Reorganization of human cortical maps caused by inherited photoreceptor abnormalities. Nat Neurosci. 2002 Apr;5(4):364-70.